. . . . . contributing to man's understanding of the environment World

TECHNICAL REPORT NO. 84-7

SEISMIC OBSERVATION OF INFRASONIC SIGNALS

FINAL REPORT

by

JACK G. SWANSON and J. CRAIG WOERPEL

The views and conclusions contained in this document are those of the authors and should not be interpreted as necessarily representing the official policies, either expressed or implied, of the Defense Advanced Research Projects Agency or the U.S. Government.

Sponsored by

Advanced Research Projects Agency (DOD)
DARPA Order No. 4246/03
Monitored by AFOSR/NP under Contract #F49620-83-C-0136

TELEDYNE GEOTECH
3401 Shiloh Road
Garland, Texas 75041

TELEDYNE GEOTECH

Unclassified

SECURITY CLASSIFICATION OF THIS PAGE

REPORT DOCUMENTATION PAGE

1a. REPORT SECURITY CLASSIFICATION: Unclassified	1b. RESTRICTIVE MARKINGS
2a. SECURITY CLASSIFICATION AUTHORITY	3. DISTRIBUTION/AVAILABILITY OF REPORT: Approved for public release; distribution unlimited.
2b. DECLASSIFICATION/DOWNGRADING SCHEDULE	
4. PERFORMING ORGANIZATION REPORT NUMBER(S): TR 84-7	5. MONITORING ORGANIZATION REPORT NUMBER(S): AFOSR-TR- 84-1206
6a. NAME OF PERFORMING ORGANIZATION: Teledyne Geotech; 6b. OFFICE SYMBOL (If applicable)	7a. NAME OF MONITORING ORGANIZATION: AFOSR/NP
6c. ADDRESS (City, State and ZIP Code): Garland, Texas 75041	7b. ADDRESS (City, State and ZIP Code): Bolling AFB, D.C. 20332
8a. NAME OF FUNDING/SPONSORING ORGANIZATION: Defense Advanced Research Projects Agency (DOD); 8b. OFFICE SYMBOL (If applicable)	9. PROCUREMENT INSTRUMENT IDENTIFICATION NUMBER: F49620-83-C-0136 DARPA
8c. ADDRESS (City, State and ZIP Code): Bolling AFB, D.C. 20332	10. SOURCE OF FUNDING NOS.

PROGRAM ELEMENT NO.	PROJECT NO.	TASK NO.	WORK UNIT NO.
61101E	A.O. 4346 4		

11. TITLE (Include Security Classification): Seismic Observation of Infrasonic Signals (U)

12. PERSONAL AUTHOR(S): Swanson, Jack G.; Woerpel, J. Craig

13a. TYPE OF REPORT	13b. TIME COVERED	14. DATE OF REPORT (Yr., Mo., Day)	15. PAGE COUNT
Final	FROM 83/07/15 TO 84/07/14	84/11/1	132

16. SUPPLEMENTARY NOTATION: The views and conclusions contained in this document are those of the authors and should not be interpreted as necessarily representing the official policies, either expressed or implied, of the Defense Advanced Res. Proj. Agen. or the U.S. Government

17 COSATI CODES		
FIELD	GROUP	SUB. GR

18. SUBJECT TERMS (Continue on reverse if necessary and identify by block number): Infrasonic, Seismic, Microseisms, Volcano, El Chichon, Pure State Filter, Polarization Filter, State Vector

19. ABSTRACT (Continue on reverse if necessary and identify by block number)

A sliding pure-state filter attenuated wind-induced noise recorded by individual elements of a four-element microbarograph array an average of 22 dB. Summation of the processed microbarograms yielded an additional 5 dB attenuation, whereas summation of the unprocessed microbarograms attenuated the noise 6 dB relative to the individual microbarograms. A sliding pure-state filter yielding separate estimates of linearly and elliptically polarized arrivals, applied to the outputs of three-component, long-period inertial seismographs at a site near McKinney, Texas, and at Seismic Research Observatories ANMO, BOCO, and GRFO detected infrasonic signals from five eruptive sequences of El Chichon volcano. Application of the pure-state filter improved the signal-to-noise ratio of the seismically detected infrasonic signals an average of 14 dB. A combination of adaptive beam forming and pure-state filtering applied to the outputs of the seven elements of the NORSAR three-component, long-period array marginally detected an infrasonic signal from the largest El Chichon eruption. Adaptive beam forming and pure-state filtering applied to the NORSAR data failed

20 DISTRIBUTION/AVAILABILITY OF ABSTRACT	21. ABSTRACT SECURITY CLASSIFICATION
UNCLASSIFIED/UNLIMITED ☒ SAME AS RPT. ☐ DTIC USERS ☐	Unclassified

22a. NAME OF RESPONSIBLE INDIVIDUAL	22b TELEPHONE NUMBER (Include Area Code)	22c OFFICE SYMBOL

DTIC ELECTE JAN 24 1985 S E

DD FORM 1473, 83 APR EDITION OF 1 JAN 73 IS OBSOLETE.

Unclassified

SECURITY CLASSIFICATION OF THIS PAGE

18. Subject Terms (Continued)

Array Processing, Adaptive Beam Forming, SRO, NORSAR

19. Abstract (Continued)

to detect infrasonic signals from any of a set of industrial explosions of Soviet Project MARSA. With one possible exception, no infrasonic signals within the 6-14 second microseism band were seismically detected by the pure-state filter, although the microbarometric data in this period band were highly polarized during the higher-mode acoustic arrivals for all five El Chichon events. A technique to remove the effects of the polarized microseismic noise before estimating the degree of polarization, by conditioning the spectral matrix of each filter block with an estimate of the noise spectral matrix obtained from a signal-free time interval, was less effective in attenuating the microseismic noise at McKinney than was the pure-state filter without noise conditioning. The lower effectiveness of the noise conditioning technique is attributed to nonstationarity of the microseismic noise at McKinney.

Observed character of seismically recorded infrasonic signals, after pure-state filtering, together with arrival time differences at stations of the SRO network, should be sufficient to discriminate infrasonic signals from seismic surface wave signals. In order to understand differences in observed signal character among the different sites, accurate atmospheric pressure-ground displacement transfer functions are needed for each SRO.

TECHNICAL REPORT NO. 84-7

SEISMIC OBSERVATION OF INFRASONIC SIGNALS

FINAL REPORT

by

JACK G. SWANSON AND J. CRAIG WOERPEL

The views and conclusions contained in this document are those of the authors and should not be interpreted as necessarily representing the official policies, either expressed or implied, of the Defense Advanced Research Projects Agency or the U.S. Government.

Sponsored by

Advanced Research Projects Agency (DOD)
DARPA Order No. 4246/03
Monitored by AFOSR/NP under Contract #F49620-83-C-0136

TELEDYNE GEOTECH
3401 Shiloh Road
Garland, Texas 75041

1 November 1984

TABLE OF CONTENTS

LIST OF ILLUSTRATIONS

LIST OF ILLUSTRATIONS, Continued

LIST OF ILLUSTRATIONS, Continued

LIST OF ILLUSTRATIONS, Continued

LIST OF ILLUSTRATIONS, Continued

TABLES

1. SUMMARY

This report presents final results of the research on seismic observation of infrasonic signals conducted by Teledyne Geotech for DARPA/AFOSR under Contract F49620-83-C-0136, covering work conducted during 15 July 1983 through 14 July 1984. The work is a continuation of the research reported on by Mauk, et al (1982) and employed the data base developed under that research program as well as additional data. The goals of the research are to investigate the usefulness of polarization state filters and long-period array processing techniques in discriminating between infrasonic signals and seismic surface waves and in improving seismically observed infrasonic signal-to-noise ratios, particularly in the oceanic microseism band (0.05 - 0.25 Hz).

During the investigation, a sliding pure-state filter, yielding separate estimates of linearly and elliptically polarized arrivals, was applied to the outputs of three-component, long-period borehole inertial seismographs at a temporary site near McKinney, Texas, and at Seismic Research Observatories ANMO, BOCO, and GRFO, for infrasonic signals generated by five eruptive sequences of El Chichon volcano, located in the state of Chiapas, Mexico. A pure-state filter was also applied to the outputs of a five-element microbarograph array installed at the McKinney site. Both adaptive beam forming and pure-state filtering were applied to the outputs of the NORSAR seven-element array of three-component, long-period seismographs for infrasonic signals from the El Chichon eruptions as well as for infrasonic signals possibly generated by a set of industrial explosions of Soviet project MARSA. The sequence of explosive eruptions of El Chichon occurred during 29 March through 6 April 1982. In addition, the pure-state filter was applied to a sample of wind-induced noise recorded by the microbarograph array at McKinney. To help understand the polarization states of seismically recorded infrasonic signals and seismic noise, parameters defining the polarization state vector were estimated for each filter block. Methods used to estimate the degree of polarization and state vector parameters and the technique developed to apply the pure-state filters are described in section 3.3

Results of the research are fully described in section 3.4. Application of the pure-state filter to outputs of the microbarograph array attenuated wind-induced noise recorded by individual microbarographs an average of 22 dB. Summation of four processed microbarograms yielded an additional 5 dB noise attenuation, whereas summation of four unprocessed microbarograms attenuated the noise 6 dB relative to the individual microbarograms. Application of the pure-state filter to the three-component, inertial seismograph at McKinney attenuated the seismic noise 16-23 dB. At this site, the microseismic noise in the 6-14 second period band remaining after pure-state filtering occurs in bursts of three to ten minutes duration and is elliptically polarized.

Application of a pure-state filter to the outputs of individual three-component elements or to the seven vertical elements of the NORSAR long-period array failed to detect infrasonic signals from any of the El Chichon eruptions. Application of adaptive beam forming separately to the vertical, radial, and transverse components of the array, followed by application of a pure-state filter to the resulting three-component system, marginally detected an infrasonic signal from the largest El Chichon eruption. Combinations of adaptive beam forming and pure-state filtering applied to the outputs of the NORSAR long-period array failed to detect infrasonic signals from any of the MARSA explosions.

The character of the seismically recorded infrasonic signals varied significantly among the different sites, presumably because of differences in the atmospheric pressure-ground displacement transfer functions at the various sites. For the McKinney data, the processed seismograms for all five El Chichon eruptive sequences show a linearly polarized, narrow-band arrival, with a period of about 30 seconds, during the higher-mode acoustic arrival evident on the microbarograph beam. The state vector is oriented within 15 degrees of vertical for all five events. The dominant frequency of this arrival (0.03 Hz) falls on a null in the atmospheric pressure-horizontal ground displacement transfer function for the McKinney site, probably accounting for the lack of horizontal ground motion at this site. In contrast, the infrasonic signals recorded at the SRO's were of lower frequency and, typically, had elliptically polarized components showing complex

dispersion. Infrasonic signals from the El Chichon eruptions were undetectable to marginally detectable at McKinney and the SRO's before processing, and were clearly detectable at these sites after processing, except that ANMO failed to detect signals from the two weakest eruptions. The average improvement in signal-to-noise ratio achieved by pure-state filtering was 14 dB.

With one possible exception, no infrasonic signals within the 6-14 second microseismic band were seismically detected by the pure-state filter, although the microbarometric data in this period band were highly polarized during the higher-mode acoustic arrivals for all five El Chichon events. This may be explained by the fact that, because the infrasonic signal and microseismic noise have different polarization states, the degree of polarization estimated from the spectral matrix will be low, and the pure-state filter will attenuate both infrasonic signal and microseismic noise in this frequency band. A technique to remove the effects of the polarized microseismic noise before estimating the degree of polarization, by conditioning the spectral matrix of each filter block with an estimate of the noise spectral matrix obtained from a signal-free time interval, was ineffective in attenuating the microseismic noise at McKinney. The noise conditioning technique attenuated the 6-8 second microseismic noise only 11 dB, compared to 14 dB noise attenuation in this period band achieved by the pure-state filter without noise conditioning. The lower effectiveness of the noise conditioning technique is attributed to nonstationarity of the microseismic noise at McKinney.

Observed character of seismically recorded infrasonic signals, after pure-state filtering, together with arrival time differences at stations of the SRO network, should be sufficient to discriminate infrasonic signals from seismic surface-wave signals. In order to understand differences in observed signal character among the different sites, accurate atmospheric pressure-ground displacement transfer functions are needed for each SRO.

2. BACKGROUND

2.1 RATIONALE

It is reasonable to expect that a number of new nations will acquire a nuclear weapons capability within the next few years. Moreover, it is likely that their initial tests of this capability will be carried out in the atmosphere. A need therefore exists for additional, independent data sources and techniques to corroborate the information provided by current atmospheric nuclear test monitoring systems. This need can readily be met by providing a means for detecting and identifying infrasonic signals generated by atmospheric nuclear explosions.

2.2 PREVIOUS WORK

In the past, small microbarograph arrays were used to monitor for infrasonic signals generated by atmospheric nuclear explosions. These arrays were capable of detecting atmospheric pressure variations of a few tenths of a microbar in the frequency range 0.001 to 1 Hz. Therefore, under conditions of ambient noise, these arrays had the potential for detecting infrasonic signals generated by atmospheric nuclear explosions in the low kiloton range at distances up to a few thousand kilometers. This potential was not realized because of atmospheric pressure fluctuations created by local surface winds, which can be a few tens to a few hundred microbars. Pipe arrays were attached to the inlet ports of the microbarograms to reduce the wind noise, but were effective only for frequencies greater than 0.1 Hz, because of the small dimensions of the arrays. Greater noise suppression at low frequencies would have required much larger-scaled arrays of microbarographs. This approach was abandoned because of the development of a different type of system to monitor for atmospheric nuclear tests.

Research sponsored by DARPA/AFOSR during the early 1970's demonstrated that the earth movement created by the passage of an infrasonic wave could be detected by a long-peiod seismograph installed at a depth of approximately 100 meters (Sorrells et al, 1971). The results of this research showed that, at moderately shallow depths, the shorter wavelength earth movements

caused by the local atmospheric pressure field would be attenuated relative to the longer wavelength components. Therefore, the infrasonic signal to wind-generated noise ratio (SNR) should be substantially greater at the output of a long-period vertical seismometer installed at a depth of 100 meters than at the output of a microbarograph installed at the surface. In addition, the research predicted that the speed and direction of approach of an infrasonic signal could be determined from the outputs of a three-component, long-period seismograph. The implication of these results is that an infrasonic monitoring capability already exists in the current seismic network and could be reduced to practice for a much lower cost and in a much shorter period of time than could the fabrication and deployment of a new network of microbarograph arrays.

A preliminary research program was sponsored by DARPA/AFOSR to investigate the technical feasibility of utilizing combinations of microbarometric and seismic observations to detect and identify infrasonic signals. This program involved the collection and analysis of data from a small array of microbarographs and a three-component, long-period seismograph installed at a depth of 150 meters near McKinney, Texas. Results of this research, reported by Mauk et al (1982), showed that, under moderate to high wind conditions, the infrasonic SNR over the frequency band 0.005 to 0.1 Hz can be greater on the output of a long-period vertical seismograph buried at moderate depth than on the output of a microbarograph installed at the surface, the upper frequency limit being fixed by oceanic microseisms recorded by the seismograph. These authors concluded that infrasonic signals generated by sources with yields in the low to moderate kiloton range should be seismically observable. In addition, Mauk et al, presented evidence that seismically recorded infrasonic signals are strongly polarized in a vertical plane parallel to the direction of propagation, and concluded that determination of polarization state should be sufficient to discriminate seismically recorded infrasonic waves from seismic surface waves.

3. RESEARCH PROGRAM

3.1 OBJECTIVES

The current research program is a continuation of the research reported on by Mauk et al, investigating the usefulness of a three-component, long-period seismograph for detecting and identifying infrasonic signals. The research program is divided into two tasks, as described in the following paragraphs.

3.1.1 Task 1. Investigate Methods for Discriminating Between Seismically Observed Infrasonic Signals and Seismic Surface Waves

Analysis of infrasonic signals recorded at McKinney, Texas, (Mauk et al) has confirmed theoretical predictions that determination of the polarization state of the observed signal is probably sufficient to discriminate between seismically observed infrasonic waves and seismic surface waves. A quantifiable measure of the degree of polarzation can be calculated from the 3 X 3 spectral matrix S derived from the outputs of a three-component seismograph (Samson and Olson, 1981). In addition, for frequencies for which the degree of polarization is high, the state vector defining the polarization state can also be computed from elements of the spectral matrix of an orthogonal, three-component seismograph (Samson and Olson, 1980). An objective under Task 1 is to investigate the usefulness of these measures of the degree of polarization and parameters defining the state vector, obtained from the outputs of a three-component, long-period seismograph, in discriminating between infrasonic signals and seismic surface waves.

Because of the large difference in horizontal phase velocity between infrasonic and seismic signals, array observations should provide an independent discrimination technique. Therefore, another objective under Task 1 is to investigate the usefulness of existing long-period seismic arrays in discriminating between seismically observed infrasonic signals and seismic surface waves. This objective includes investigation of the usefulness of filters based on the degree of polarization applied to three-component elements of a long-period seismic array in conjunction with array processing techniques.

3.1.2 Task 2. Investigate Methods for Enhancing Seismically Observed Infrasonic SNR's

Detection of seismically recorded infrasonic signals at frequencies greater than 0.1 Hz is primarily inhibited by the strong earth noise in the oceanic microseism band (0.05-0.25 Hz). The objective under Task 2 is to investigate the effectiveness of polarization state filters and various array processing techniques in improving seismically observed infrasonic SNR's, particularly in the oceanic microseism band. The data base developed under Task 1 was used in this investigation.

3.2 DATA BASE

The data base used in this research includes long-period seismograms of infrasonic signals from five eruptive sequences of El Chichon volcano recorded at a temporary site near McKinney, Texas, at selected Seismic Research Observatories (SRO's), and by the NORSAR seven-element array of three-component, long-period seismographs. Microbarograms recorded by a five-element array of microbarographs at the McKinney site were also used. The El Chichon data recorded at McKinney consist of the data base developed by Mauk et al (1982) in their investigation of seismic methods of infrasonic signal detection. Locations of the sites used are shown in figure 1. The instrumentation at McKinney consisted of a three-component, long-period borehole seismograph (Teledyne Geotech Model KS-36000), five model M-4 microbarographs, and a high-resolution anemometer. The spatial configuration of the instrumentation is shown in figure 2. The KS-36000 seismograph was located at 33°14'54"N latitude, 96°36'07"W longitude at a depth of 152 meters below the surface. Microbarographs MKB3, MKB4, and MKB5 were installed in shallow vaults; MKB1 and MKB2 were located at the surface. Each microbarograph was fitted at the inlet port with a 15-meter length of garden hose (19 mm ID) perforated at one-meter intervals to attenuate high-frequency atmospheric turbulence effects. The SRO seismographs consist of a three-component borehole seismograph (Teledyne Geotech Model KS-36000) installed at a depth of 100 meters. The configuration of the NORSAR three-component, long-period seismograph array is shown in figure 3. Locations of the array

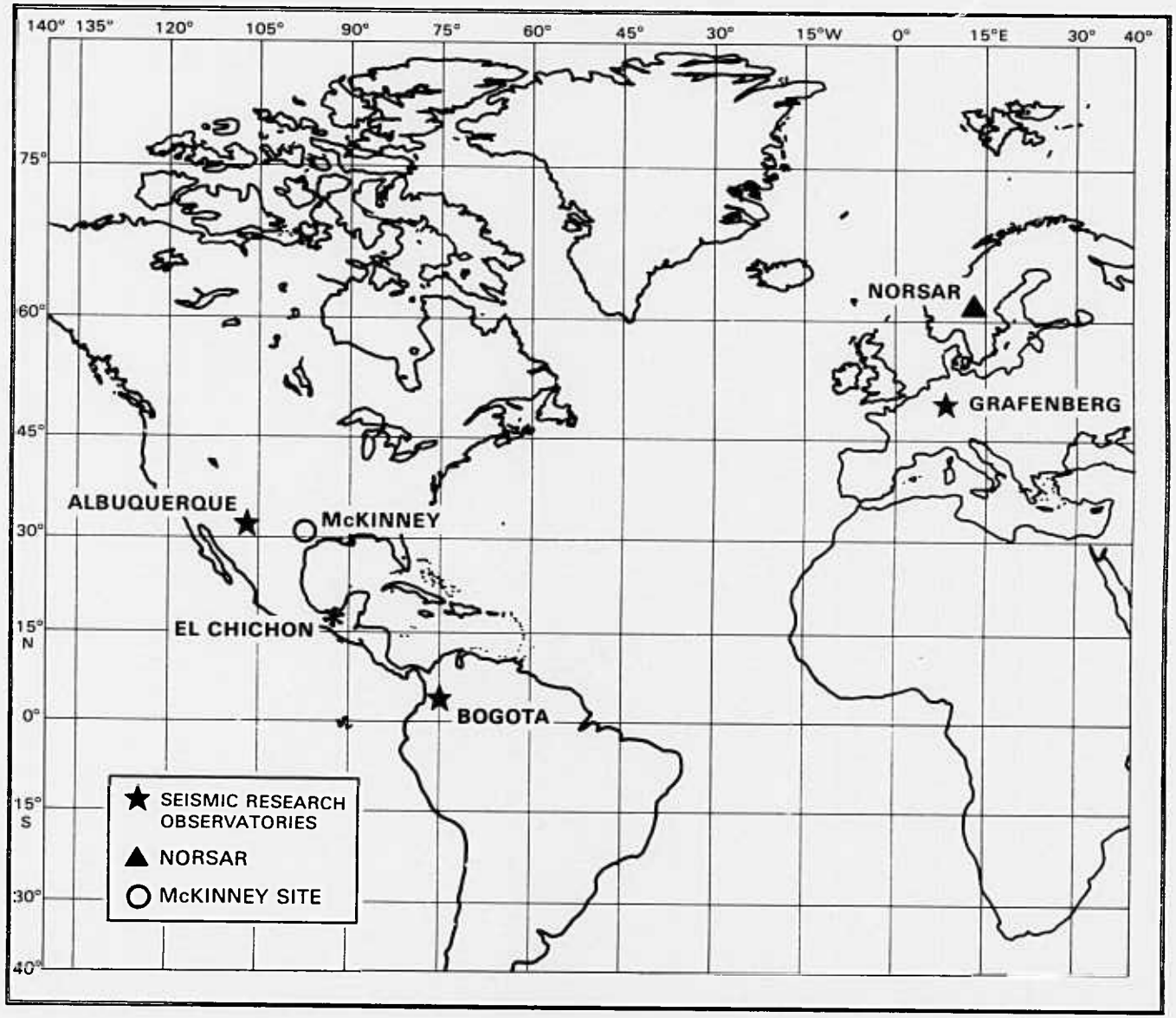

FIGURE 1. LOCATIONS OF EL CHICHON VOLCANO AND SITES USED IN THE INVESTIGATION.

G15368

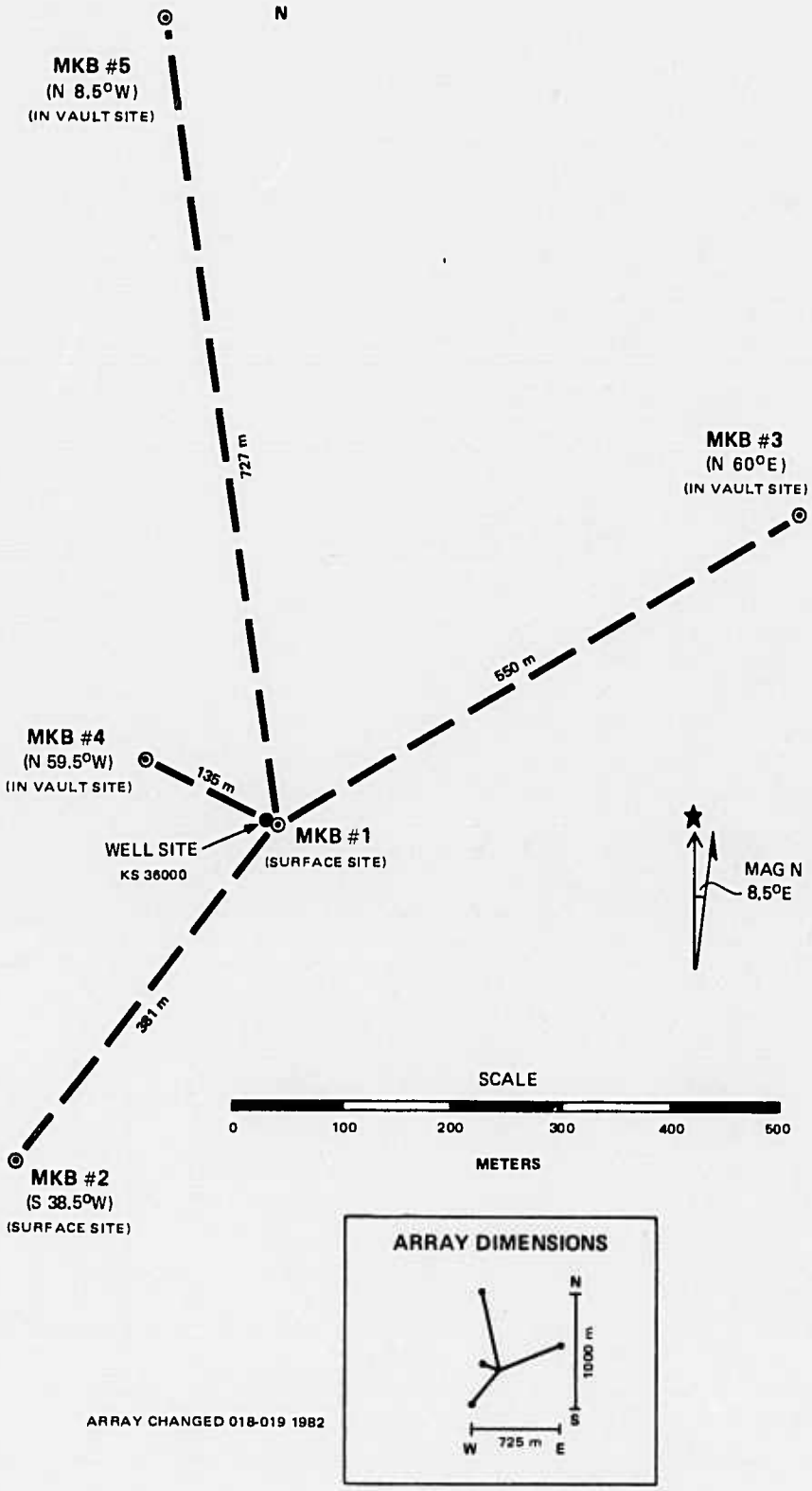

FIGURE 2. McKINNEY, TEXAS, MICROBAROGRAPH/SEISMOGRAPH EXPERIMENT LAYOUT.

G 12929

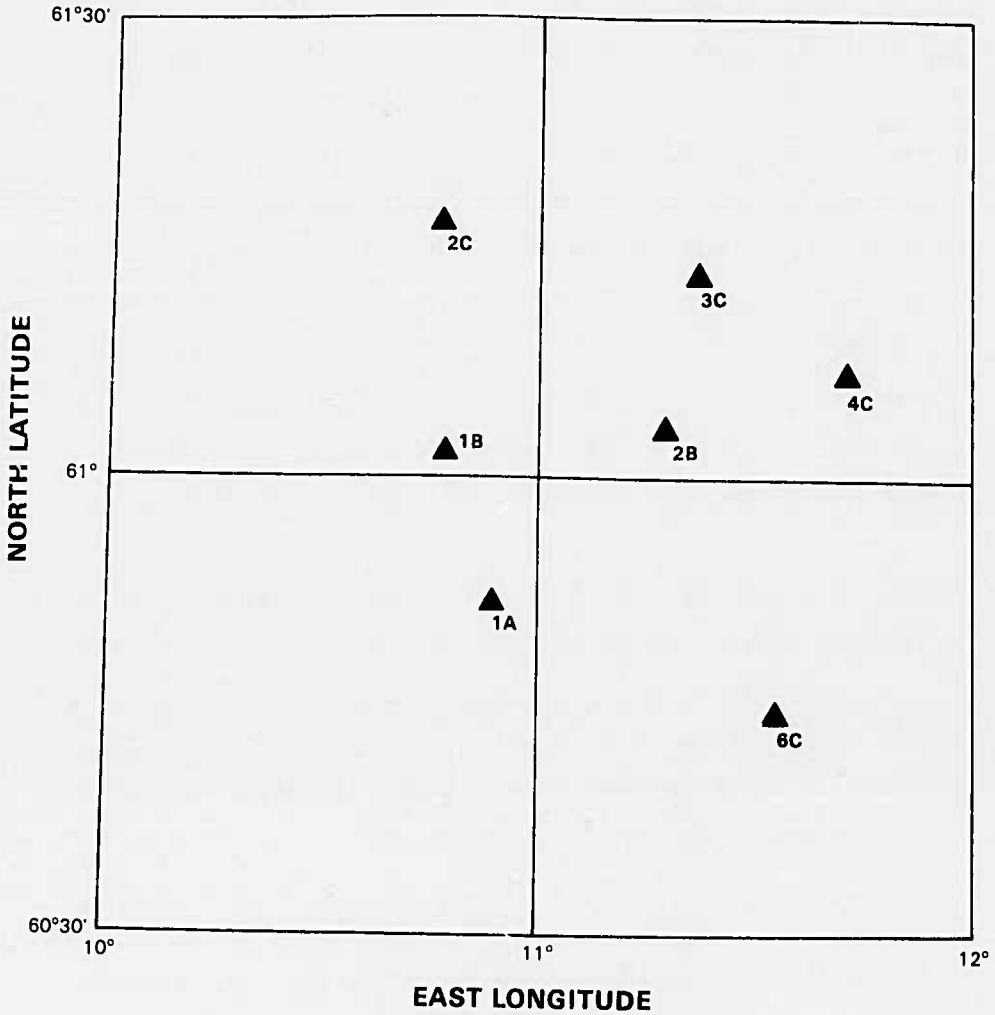

FIGURE 3. CONFIGURATION OF NORSAR THREE-COMPONENT, LONG-PERIOD ARRAY.

elements are given in table 1. The NORSAR long-period instruments are Geotech model 7505B (vertical) and model 8700C (horizontal), which are moving-coil, velocity-type seismometers. Displacement amplitude frequency responses for the long-period seismographs at McKinney, the SRO's, and NORSAR and the pressure amplitude frequency response for the microbarograph at McKinney are shown in figure 4. The microbarograph response is flat for barometric pressure changes from 0.06 Hz to 0.4 Hz. The high-frequency attenuation rate is 36 dB/octave, and the low-frequency attenution rate is 6 dB/octave. The McKinney seismograph ground displacement response peaks at 0.033 Hz with both high- and low-frequency attenuation rates of 18 dB/octave. The standard SRO long-period response is identical to that used at McKinney. For the data used in this investigation, a 6-second notch filter had been applied to the SRO data. The NORSAR long-period seismograph response peaks at a frequency of 0.05 Hz with both low- and high-frequency attenuation rates of 18 dB/octave.

Transfer functions relating infrasonic atmospheric pressure variations to vertical and horizontal ground displacement for the McKinney site are shown in figure 5. These theoretical transfer functions were computed using a seventeen-layer earth model by means of the technique described by Sorrells and Goforth (1973). Note the sharp null in the apparent horizontal transfer function, which includes the effect of tilt, at a frequency of 0.03 Hz.

The El Chichon volcanic complex is located at 17.33°N 93.20°W in the state of Chiapas, Mexico. The sequence of explosive eruptions occurred during 29 March through 6 April 1982. Individual events in the sequence had energy releases which varied over several orders of magnitude. Distances and azimuths from the principal volcano to each of the recording sites are given in table 2.

In addition to the El Chichon data, seismograms of the NORSAR three-component, long-period array covering expected arrival times of infrasonic signals possibly generated by twenty large, industrial explosions of Soviet Project MARSA were used in the investigation. Origin times and epicenters of the MARSA explosions were provided to us by AFOSR.

TABLE 1. LOCATIONS OF NORSAR LONG-PERIOD ARRAY ELEMENTS

Site	North Latitude Degrees	East Longitude Degrees
1A	60.8580	10.8903
1B	61.0217	10.8117
2B	61.0418	11.2760
2C	61.2722	10.7672
3C	61.2185	11.3567
4C	61.1062	11.7057
6C	60.7372	11.5352

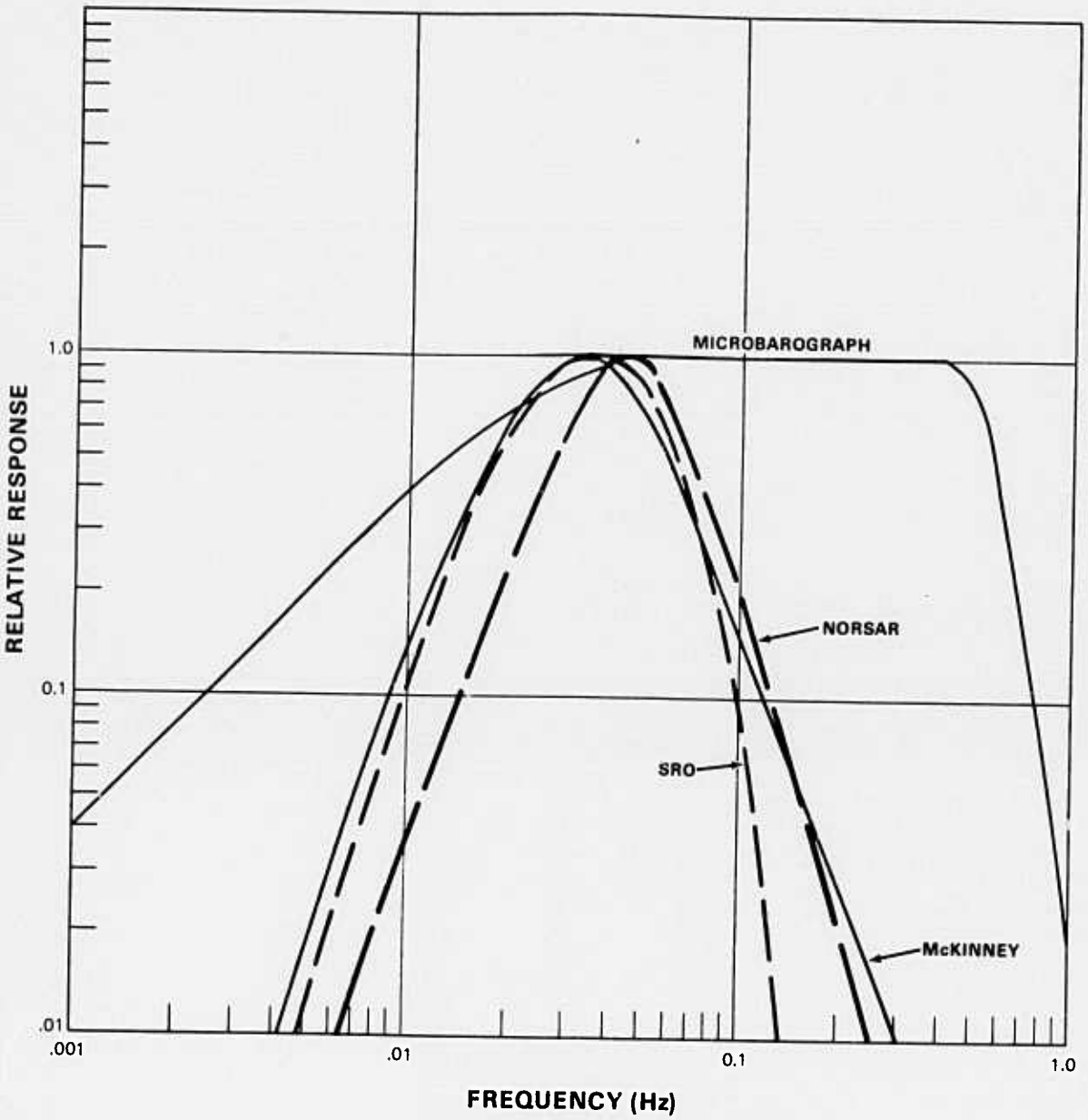

FIGURE 4. RELATIVE RESPONSES OF SEISMOGRAPH CHANNELS TO DISPLACEMENT AND MICROBAROGRAPH CHANNELS TO PRESSURE.

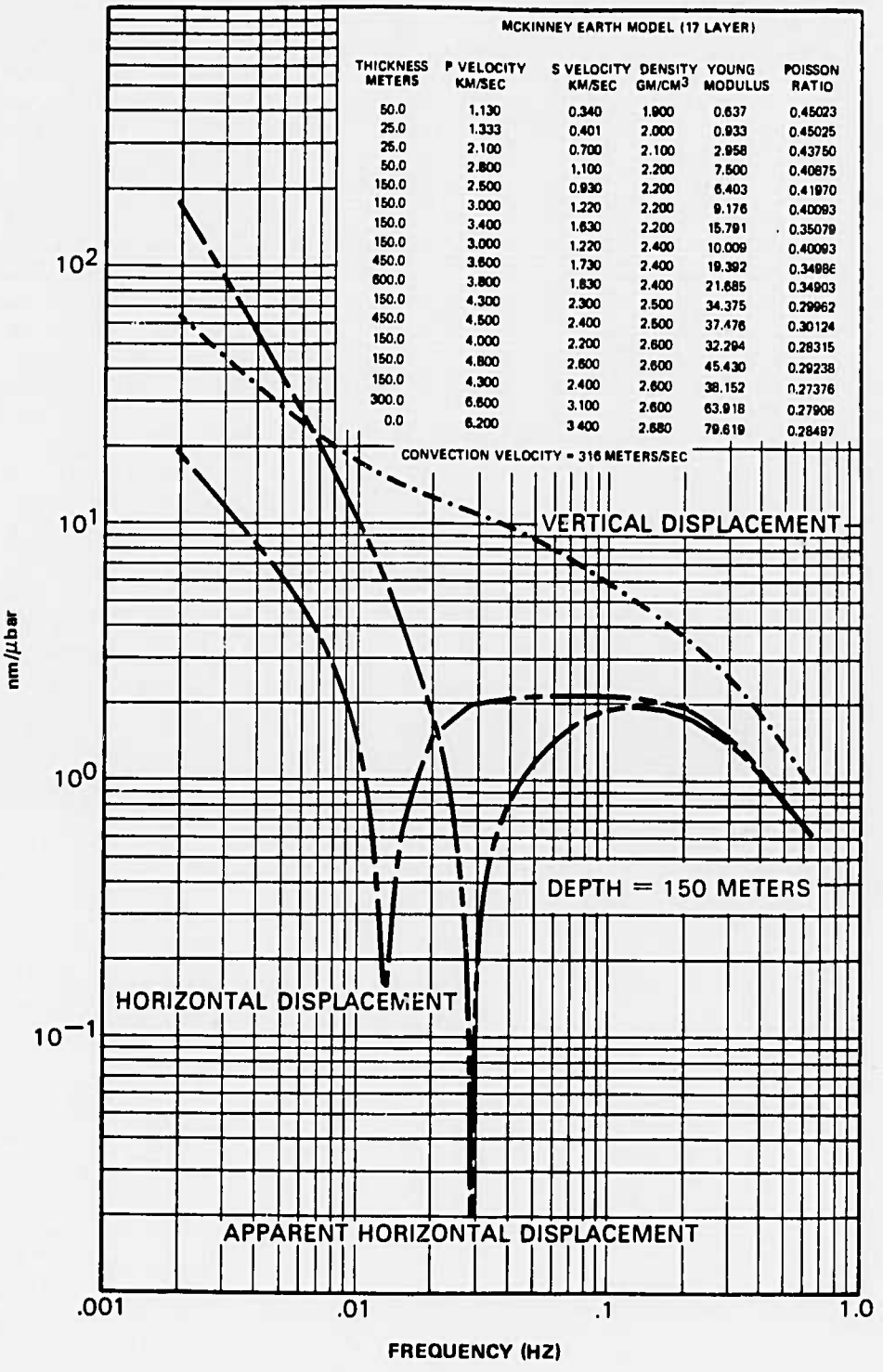

FIGURE 5. THEORETICAL RESPONSE OF AN ELASTIC LAYERED HALF SPACE TO ATMOSPHERIC LOADING, McKINNEY, TEXAS.

G 12349

TABLE 2. DISTANCES AND AZIMUTHS OF RECORDING SITES FROM EL CHICHON

Site	Distance		Azimuth
	Degrees	km	Degrees
McKinney	16.15	1796.12	349.55
ANMO	21.82	2426.39	329.04
BOCO	27.38	2489.11	121.01
NORSAR	81.81	9097.30	28.42
GRFO	85.87	9547.98	38.62

3.3 PROCESSING METHODS

A useful measure of the degree of polarization of a multicomponent time series has been developed by Samson and Olson (1981) and is given by:

$$P = \frac{n(\mathrm{Tr}\underline{S}^2) - (\mathrm{Tr}\underline{S})^2}{(n-1)\,(\mathrm{Tr}\underline{S})^2} \qquad (1)$$

Where P is estimated degree of polarization; n is number of components of the time series; $\mathrm{Tr}\underline{S}$ is trace of the n X n spectral matrix $\underline{S}$ of the input time series.

A sliding pure-state filter based on this measure of the degree of polarization was developed and appplied to the El Chichon infrasonic data recorded at at each of the sites. The pure-state filter, applied in the frequency domain, is defined as P^g, where P is the estimated degree of polarization computed from the spectral matrix of a segment of the vector time series, and the exponent g typically is assigned a value of 3 or 4. To obtain reliable estimates of P, elements of the spectral matrix were averaged over seven adjacent frequencies. For the El Chichon infrasonic data, a filter length of ten minutes was used. Some overlapping of the filters is necessary to minimize discontinuities in the filtered time series at the boundaries between successive filters resulting from changes in polarization. Initial tests of the algorithm, updating the filter each sample point, proved to be excessively slow. Therefore, the following technique was developed and applied to the El Chichon infrasonic data. The filter blocks were overlapped 50 percent, and a cosine window was applied to each data segment before processing. The filtered time series of successive segments were added in the overlap zone, thereby effectively applying a weighted mean of the filters computed for successive segments. This technique has virtually eliminated discontinuities at boundaries between filter segments in the filtered time series.

Sampson (1983b) developed an estimator of the bias in the estimated degree of polarization, given by

$$\text{bias}\ (P) = \frac{2n}{\nu(n-1)} \left[1 + \frac{3(\mathrm{Tr}\underline{S}^2)^2}{(\mathrm{Tr}\underline{S})^4} - \frac{4\ \mathrm{TR}\underline{S}^3}{(\mathrm{Tr}\underline{S})^3} \right] \qquad (2)$$

Where n is number of components of the time series;
ν is the degrees of freedom of the spectral estimator;
$\mathrm{Tr}\underline{S}$ is trace of the nxn spectral matrix $\underline{S}$ of the input time series.

This estimator was applied to the estimated degree of polarization P (equation 1) to provide unbiased estimates of the degree of polarization computed from the SRO and NORSAR data.

Samson and Olson (1980) showed that, under the assumption that the data represent a pure state, i.e., the spectral matrix has only one nonzero eigenvalue, the state vector defining the polarization state can be computed from the spectral matrix. These authors showed that 2n-1 parameters are required to define the state vector, where n is the number of components of the vector time series. For data recorded by a three-component seismograph, five parameters are needed to specify the state vector, which can be represented by a vector rotating in a plane embedded in the three-dimensional real space defined by the three seismograph components. An algorithm embodying this technique for a three-component, orthogonal system was developed and incorporated into the pure-state filter program. State vector parameters calculated include strike and dip of the plane of polarization, ellipticity (ratio of lengths of minor to major axes) of the polarization ellipse, and length, trend, and plunge of the major axis, each as a function of frequency for each filter block. The trend of the major axis is defined as the azimuth, relative to the radial direction, of the vertical projection of the major axis onto the horizontal plane. For an upward-travelling, compressional

wave, the trend represents the horizontal component of the direction of wave propagation. The plunge of the major axis is defined as the angle of the major axis from the vertical (upward) axis. Although only five parameters are needed to specify the state vector for a three-component system, interpretation of the physical meaning of the state vector is facilitated by determining these six parameters. The state vector calculations are based on the assumption that the arrival is a pure state and, therefore, have meaning only if the estimated degree of polarization is high.

An additional option was added to the pure-state filter program to provide separate estimates of linearly polarized and elliptically polarized arrivals. If this option is selected, the filter (P^g) is multiplied by a weight (W) based on the estimated ellipticity, obtained from the state vector calculation. The weight W is set to a value of 0.0 for ellipticities less than a specified value e_l and to a value of 1.0 for ellipticities greater than a specified value e_h, with a linear transition for ellipticities greater than e_l and less than e_h. Therefore, the filters yielding estimates of elliptically and linearly polarized arrivals are given by:

$F_e = WP^g$ emphasizes elliptically polarized arrivals.

$F_l = (1-W)P^g$ emphasizes linearly polarized arrivals.

For the McKinney data, values of 0.1 and 0.6 were specified for e_l and e_h, respectively, while values of 0.2 and 0.4 were used for the SRO and NORSAR data.

Uncorrelated (diagonal spectral matrix) noise will appear to the pure-state processor to be polarized if the power levels on the different components are not nearly equal. Such uncorrelated, but nonisotropic, noise can be made isotropic by normalizing the data of each component to unit variance. This was done for the data processed during this investigation. A limitation of this technique is that error may be introduced into the orientation of the state vector. Preliminary results of applying a pure-state filter to the

outputs of a three-component seismograph indicated that performance of the pure-state filter in the oceanic microseism band (0.05-0.25 Hz) is limited by polarized seismic noise in this frequency band (Swanson, 1984). If polarized noise is stationary, an estimate of the noise obtained from a signal-free time interval may be used to condition the spectral matrix for the time period being processed (Samson, 1983a, 1983b):

$$\underline{S}' = \underline{N}^{-1/2} \; \underline{S} \; \underline{N}^{-1/2} \qquad (3)$$

Where $\underline{S}'$ is the conditioned spectral matrix
$\underline{S}$ is the spectral matrix
$\underline{N}^{-1/2}$ is the square root of the inverse of the noise matrix.

The degree of polarization is then estimated from the conditioned spectral matrix. This technique will only be effective if the noise is stationary over the time interval being processed. This technique projects the spectral matrix onto a subspace in which the noise is unpolarized. It can happen that the signal is orthogonal to this subspace, in which case the signal will be rejected by the pure-state filter. An algorithm implementing this technique was incororated into the pure-state filter program and was applied to the three-component seismic data for two of the El Chichon events recorded at the McKinney site.

For processing the NORSAR LP array data, both adaptive beam forming and pure-state filtering were employed. The adaptive beam forming program implements the constrained least-mean-squares algorithm described by Frost (1972). The Frost algorithm is a gradient-descent algorithm which requires only that the signal arrival direction and the frequency band of interest be specified *a priori*. The algorithm progressively adapts to the noise field and rejects organized noise arriving from directions other than the beamed direction. A major advantage of the Frost algorithm over nonconstrained, gradient-descent techniques is that the Frost algorithm continuously corrects for roundoff or truncation errors so that the algorithm does not deviate from its constraints over long periods of time.

Before processing, the horizontal seismograms for each of the recording sites were computationally rotated from a NS, EW orthogonal pair to an orthogonal pair oriented radial and transverse to the direction from the recording site to the source. For the McKinney microbarograph array, appropriate time delays were applied to the outputs of the five microbarographs, and the outputs were summed to form an array beam for the location of MKB1 oriented at an azimuth of 168° (the great circle back azimuth from McKinney to El Chichon).

3.4 RESULTS

3.4.1 Discrimination

Results of processing the El Chichon infrasonic signals recorded at McKinney and at selected SRO's are presented in the following paragraphs. For each of the five El Chichon infrasonic events, figures are given showing the unprocessed three-component seismograms recorded at each of the SRO's and at McKinney and the unprocessed beamed output of the microbarograph array at McKinney. Additional figures are given showing, for each recording site, inertial seismograms displaying estimates of linearly and elliptically polarized arrivals obtained by application of the ten-minute, sliding, pure-state filter. For the McKinney data, the beamed output of the microbarograph array with a ten-minute, sliding, pure-state filter applied to the array before beaming is included. No band-pass filtering was applied to the seismograms in any of these figures. In addition, for each event, a figure is given showing the pure-state filters (P^3, where P is the estimated degree of polarization) for selected filter blocks. The filter block selected for each site is indicated on the figure showing the processed seismograms for that site. In order to estimate expected arrival times of the infrasonic signals, event origin times were estimated from arrival times of direct Rayleigh waves, which preceded each infrasonic signal. In the case of event 094B, five separate peaks were identified in the direct Rayleigh wave arrival during the 66-minute eruptive sequence. These peaks are interpreted to result from distinct explosions within the eruptive sequence. Origin times of the five separate explosions were computed from arrival times of these

Rayleigh wave peaks. These origin times were then used to compute group velocities of seismically observed infrasonic arrivals. Origin times of the five El Chichon eruptive sequences, together with origin times estimated from peak amplitudes within the direct Rayleigh waves are presented in table 3, together with values of the Volcanic Explosivity Index (VEI) assigned by the Smithsonian Institution or estimated by Mauk, et al (1982). Infrasonic group velocities, for the observed periods, are indicated on the figures showing the processed seismograms. Results of processing data from SRO's ANMO and BOCO are included for all five El Chichon eruptions. In addition, results of processing data from GRFO are included for the two eruptions on day 094. Application of a pure-state filter to individual three-component elements or to the seven vertical elements of the NORSAR long-period array failed to detect infrasonic signals from any of the five El Chichon eruptions. For the largest El Chichon eruption (094B), adaptive beam forming was applied separately to the vertical, radial, and transverse components of the seven-element array. A sliding pure-state filter, with a filter length of ten minutes, was then applied to the resulting three-component system of beamed components. Results of this processing are included for eruption 094B. Application of adaptive beam forming and pure-state filtering to the NORSAR three-component, long-period array data failed to detect infrasonic signals from any of the MARSA explosions.

Results for the event on day 088 are presented in figures 6 through 12. This eruptive sequence was complex with repeated injections into the plinian column. This complexity is clearly evident on the microbarograph beams recorded at McKinney (figures 6 and 9). The character of the processed seismograms is quite different for the differnt sites. The seismograms recorded at McKinney (figure 9) show a narrow-band, linearly polarized wave train with a period of thirty seconds that begins during the earliest higher-mode acoustic arrival as evidenced by the microbarograph beam and persists throughout the infrasonic arrival. The pure-state filters (P^3) computed from the inertial data and from the microbarometric data for the filter block beginning at 07:35:28 (figure 12) show that the barometric data are highly polarized over a much wider frequency band than are the seismic data. The

TABLE 3. EL CHICHON ERUPTION TIMES

Date	Julian Date	Time UTC hr:min Start	End	Peaks	VEI
29 March 1982	088	05:32	06:22	05:50 06:15	4
02 April 1982	093	08:40	08:45	08:41	2-3+
03 April 1982	093	10:03	10:08	10:07	2-3+
04 April 1982	094	01:49	02:05	02:00	U
04 April 1982	094	11:16	12:22	11:21 11:33 11:43 12:05 12:17	4

\+ Estimated by Mauk

U Unassigned VEI

state vector parameters computed for this block indicate that the 0.03-0.04 Hz arrival at McKinney is linearly polarized and that the state vector is oriented within 15 degrees of vertical. The infrasonic arrival at ANMO (figure 10) is elliptically polarized with a dominant period of about sixty seconds, showing little or no dispersion. The pure-state filter for the filter block beginning at 08:05:00 is shown in figure 12. The state vector parameters for this block indicate that the 60-second arrival at ANMO is elliptically polarized, the plane of polarization having a strike of 160 degrees relative to the radial direction to El Chichon and a dip of 80 degrees. The motion is retrograde elliptical for a wave traveling from El Chichon to ANMO. The infrasonic arrival at BOCO (figure 11) has both an elliptically polarized component showing negative dispersion for periods of 60 to 75 seconds and a narrow-band, linearly polarized component with a period of 35 seconds. The pure-state filter for the filter block beginning at 08:00:00 is given in figure 12. The state vector parameters for this block show the 60-70 second arrival to be elliptically polarized, the plane of polarization having a strike of 10 degrees relative to the radial direction to El Chichon and a dip of 80 degrees. The motion is retrograde for a wave traveling from El Chichon to BOCO. The 35-second arrival is linearly polarized, and the state vector is oriented within 10 degrees of vertical.

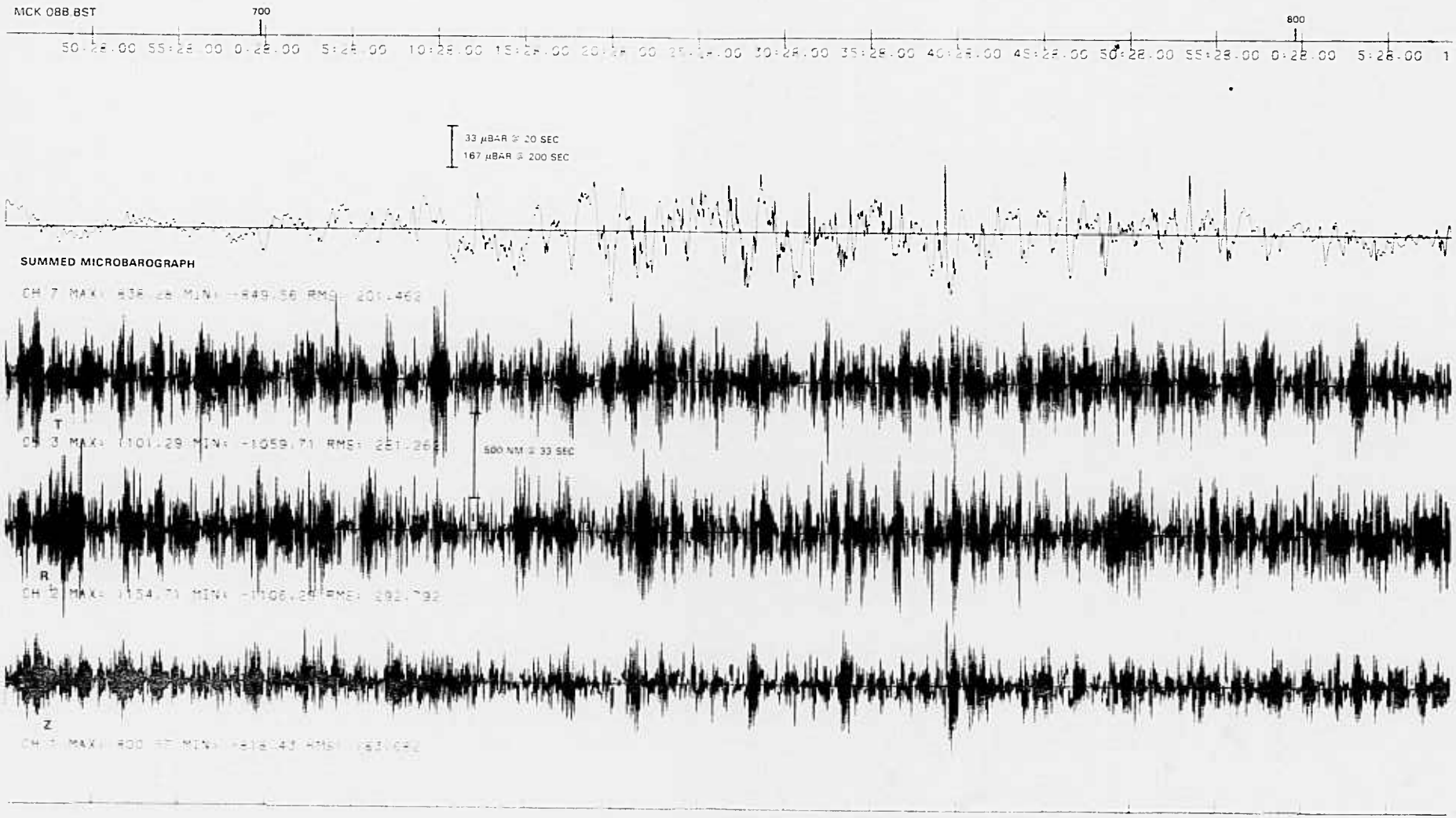

FIGURE 6 EL CHICHON ERUPTION 088 ORIGIN TIME ~ 05:32
THREE-COMPONENT INERTIAL SEISMOGRAMS AND MICROBAROGRAPH BEAM BEFORE PURE-STATE FILTERING.
RECORDED AT McKINNEY

3-19/20

TR 84-7

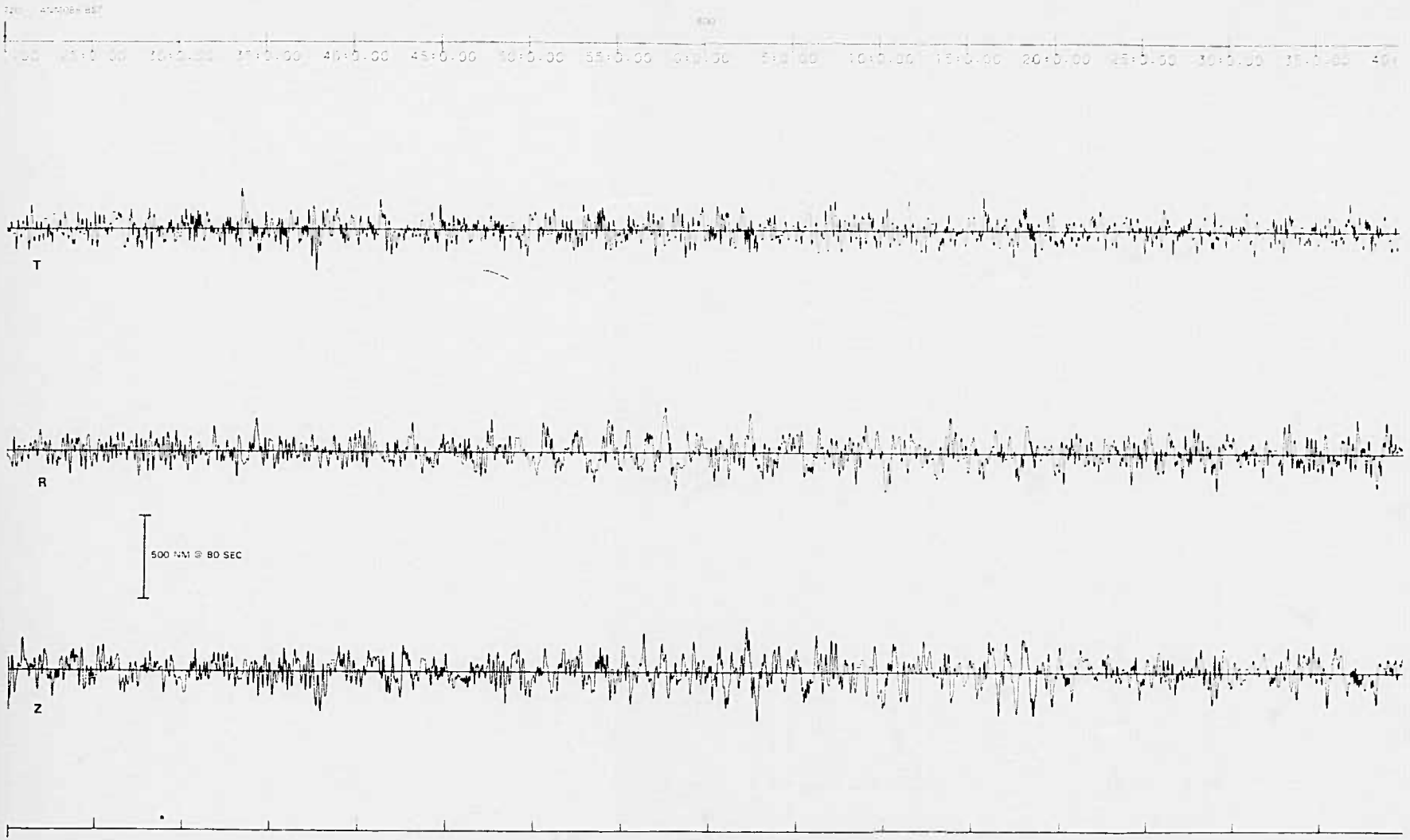

FIGURE 7. EL CHICHON ERUPTION 088 ORIGIN TIME ~ 05:32.
THREE-COMPONENT INERTIAL SEISMOGRAMS BEFORE PURE-STATE FILTERING. RECORDED AT ANMO.

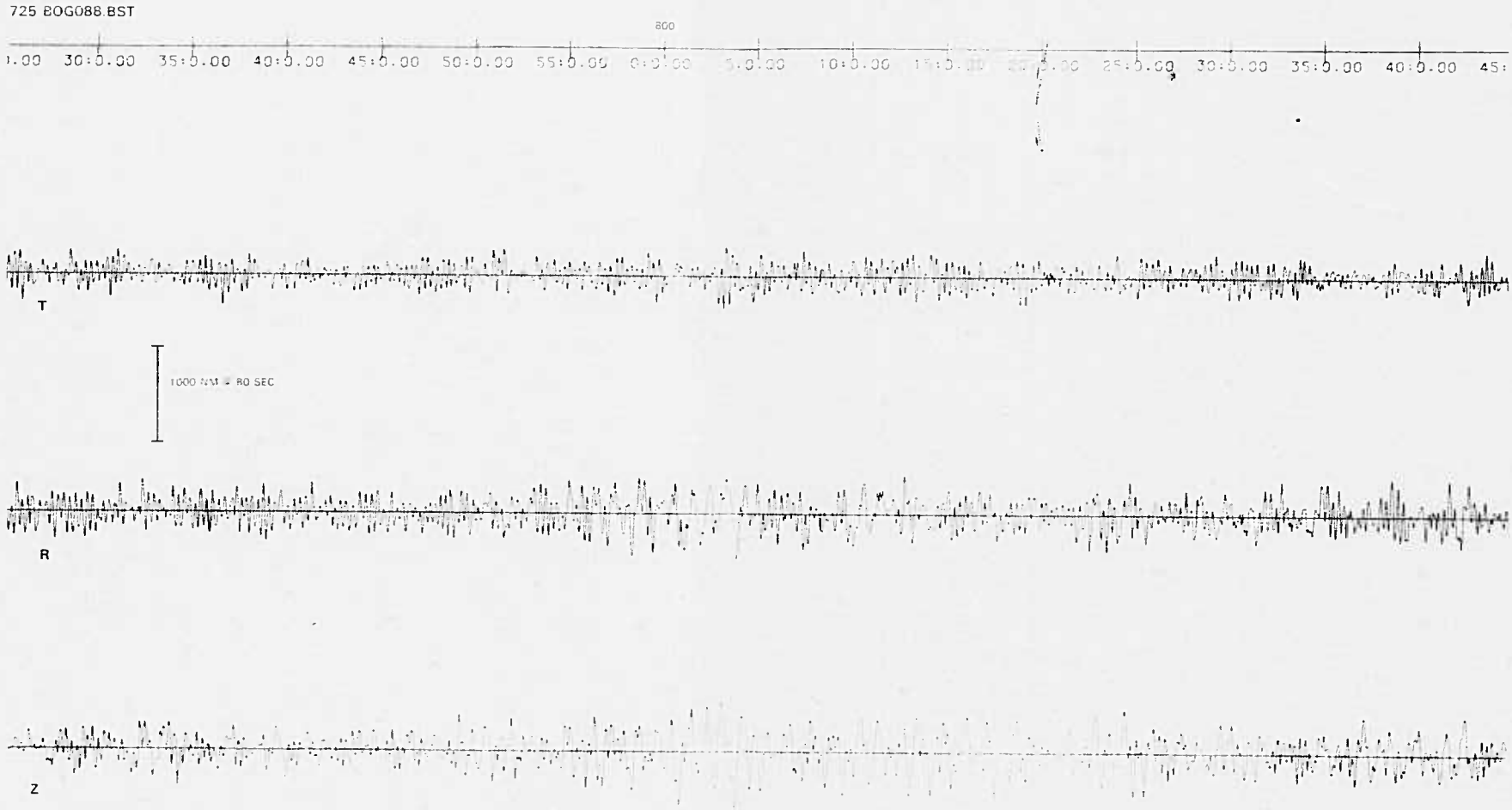

FIGURE 8 EL CHICHON ERUPTION 1982 ORIGIN TIME 05:32
THREE COMPONENT HORIZONTAL SEISMOGRAMS BEFORE PURE STATE FILTERING, RECORDED AT BOGO

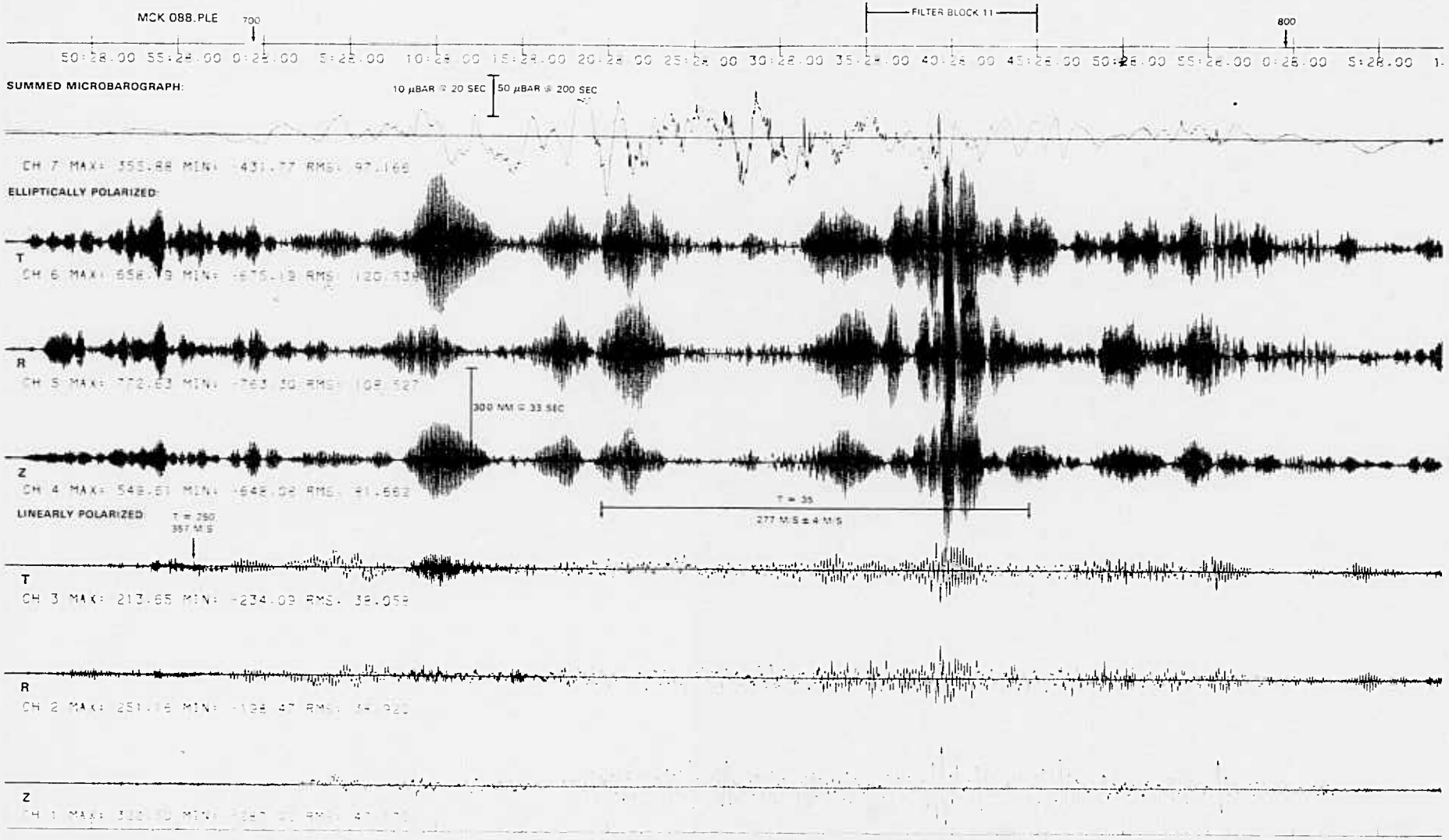

FIGURE 9 EL CHICHON ERUPTION 088 ORIGIN TIME ~ 05 32
THREE-COMPONENT INERTIAL SEISMOGRAMS AND MICROBAROGRAPH BEAM AFTER PURE-STATE FILTERING.
RECORDED AT McKINNEY

3-25/26

TR 84-7

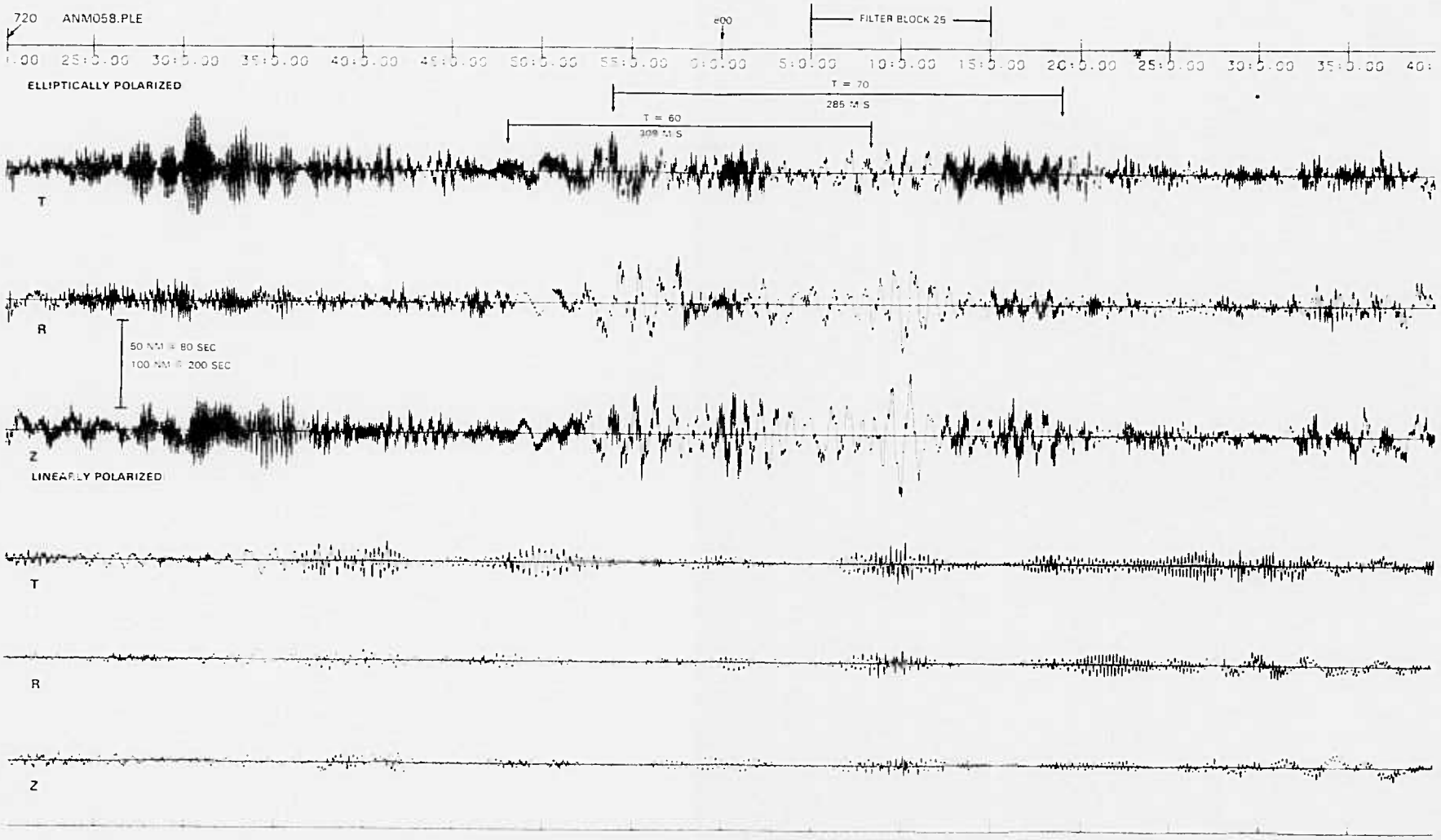

FIGURE 10 EL CHICHON ERUPTION 083 ORIGIN TIME ~ 05:32
THREE-COMPONENT INERTIAL SEISMOGRAMS AFTER PURE-STATE FILTERING RECORDED AT ANMO

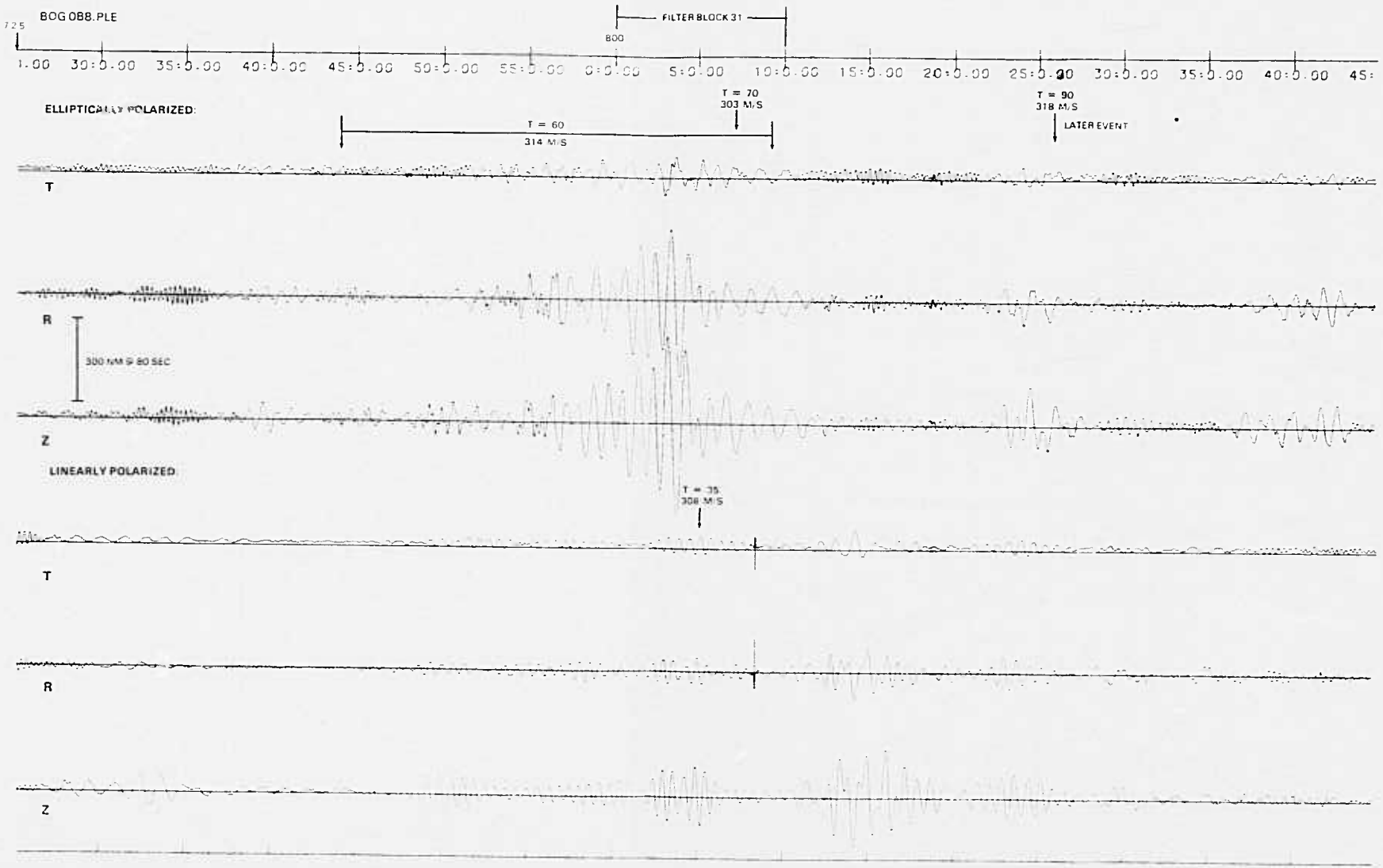

FIGURE 11 EL CHICHON ERUPTION 088 ORIGIN TIME ~ 05:32
THREE-COMPONENT INERTIAL SEISMOGRAMS AFTER PURE-STATE FILTERING RECORDED AT BOCO

3-29/30

TR 84-7

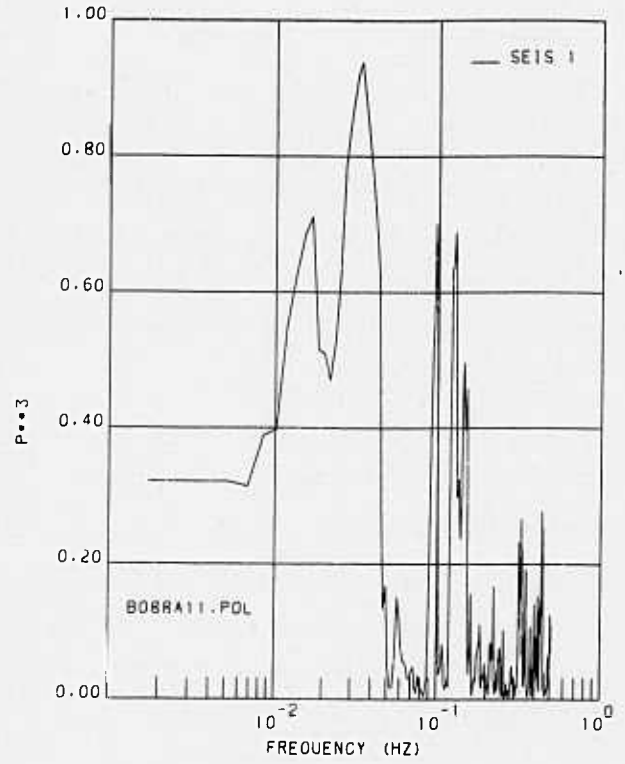

BLK 11 088 MC KINNEY

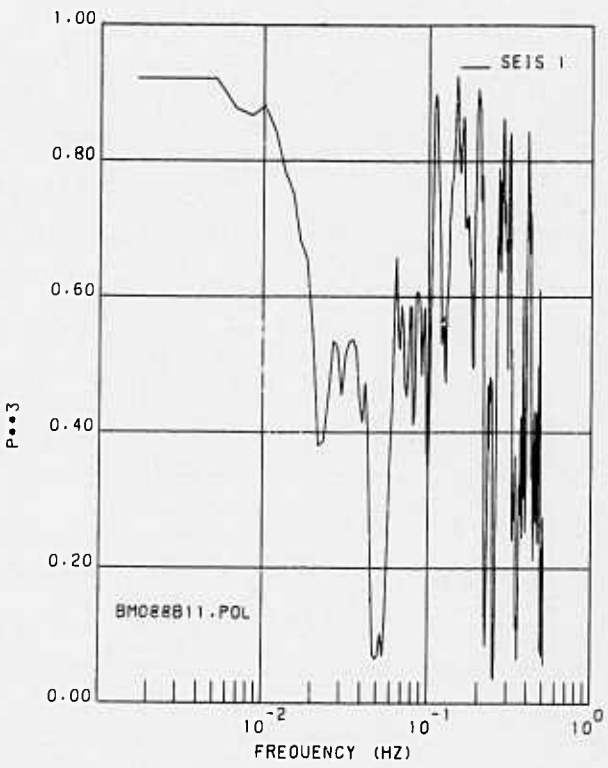

BLK 11 088 MC KINNEY MICROBAROGRAPHS

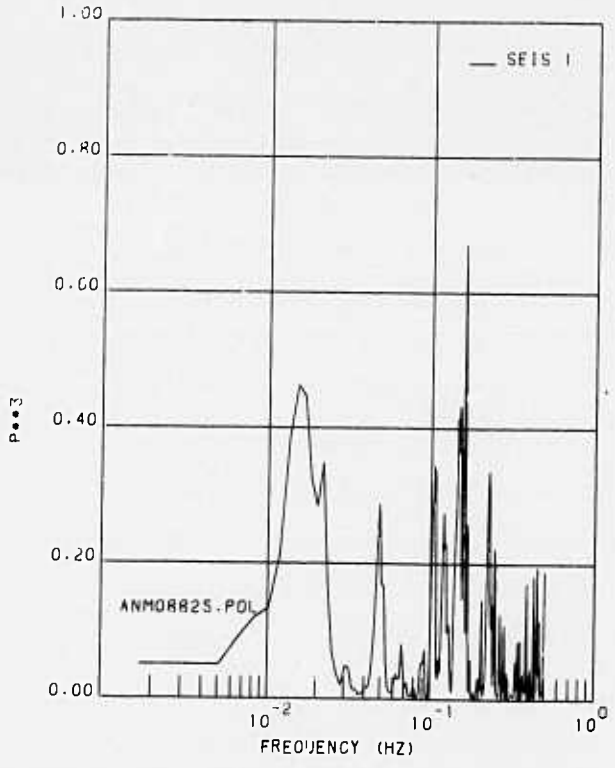

BLK 25 088 ANM

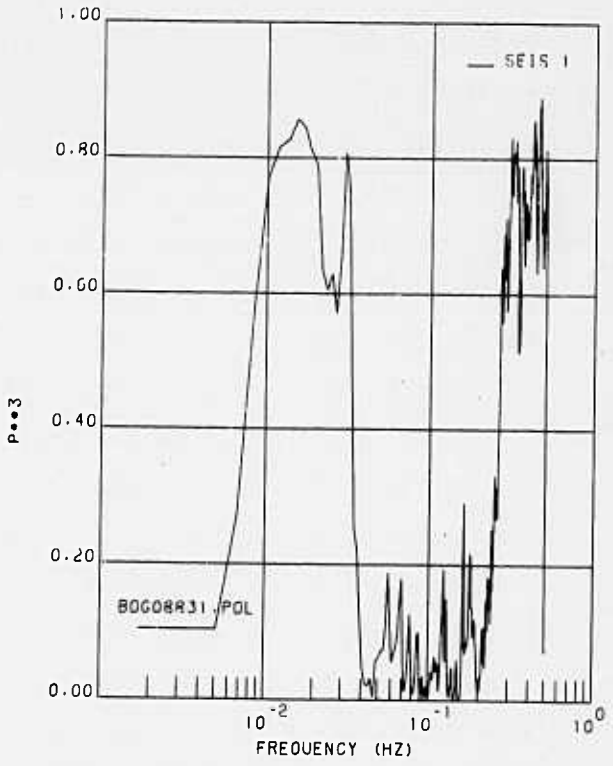

BLK 31 088 BOG

FIGURE 12. EL CHICHON ERUPTION 088 ORIGIN TIME ~ 05:32.
SEISMIC AND MICROBAROMETRIC PURE-STATE FILTERS (P^3) FOR SELECTED FILTER BLOCKS.
McKINNEY, ANMO, AND BOCO.

G15375

The two infrasonic signals on day 093 were weaker than the 088 event and resulted from simpler eruptive sequences. Processing results for the earlier of these events with origin time about 08:40 (event 093A) are presented in figures 13 through 19. The infrasonic signal recorded by the microbarographs at McKinney (figure 16) is relatively simple, with a clear gravity mode arrival having a period of about five minutes followed by higher-mode acoustic arrivals exhibiting periods as short as two seconds. Application of the pure-state filter to the outputs of the microbarograph array substantially improved the SNR. The processed seismograms from McKinney (figure 16) show a weak, narrow-band arrival with a dominant period of about 33 seconds during the higher-mode acoustic arrival evident on the microbarograph beam. The state vector parameters for this arrival indicate this arrival to be linearly polarized with a near-vertical orientation of the state vector; however, the degree of polarization estimated from the microbarographic data for this time interval (figure 19) was very low for frequencies less than 0.07 Hz. The elliptically polarized arrival beginning at about 10:10:20 is not traveling in the radial direction and is probably not associated with the El Chichon eruption. The ANMO processed seismograms (figure 17) show a linearly polarized arrival with a period of about 170 seconds within the expected infrasonic arrival time window for this event; however, the degree of polarization at this period for the filter block beginning at 10:43:30 is low (figure 19). Also, other very long-period pulses occur on the vertical component outside the expected infrasoic arrival time window; therefore, this arrival cannot definitely be identified as an infrasonic signal generated by this El Chichon eruption. The processed seismograms from BOCO (figure 18) show a large-amplitude, narrow-bnad, linearly polarized arrival with a dominant period of about 70 seconds within the expected arrival time window. This arrival is followed by a weaker, elliptically polarized arrival with a a period of about 90 seconds. Pure-state filters for these two arrivals are presented in figure 19. The state vector for the 70-second, linearly polarized arrival is oriented within 15 degrees of the radial direction and 25 degrees from vertical. For the 90-second, elliptically polarized arrival, the plane of polarization strikes 10 degrees relative to the radial direction with a dip of 80 degrees. The motion is retrograde elliptical for a wave traveling from El Chichon toward BOCO.

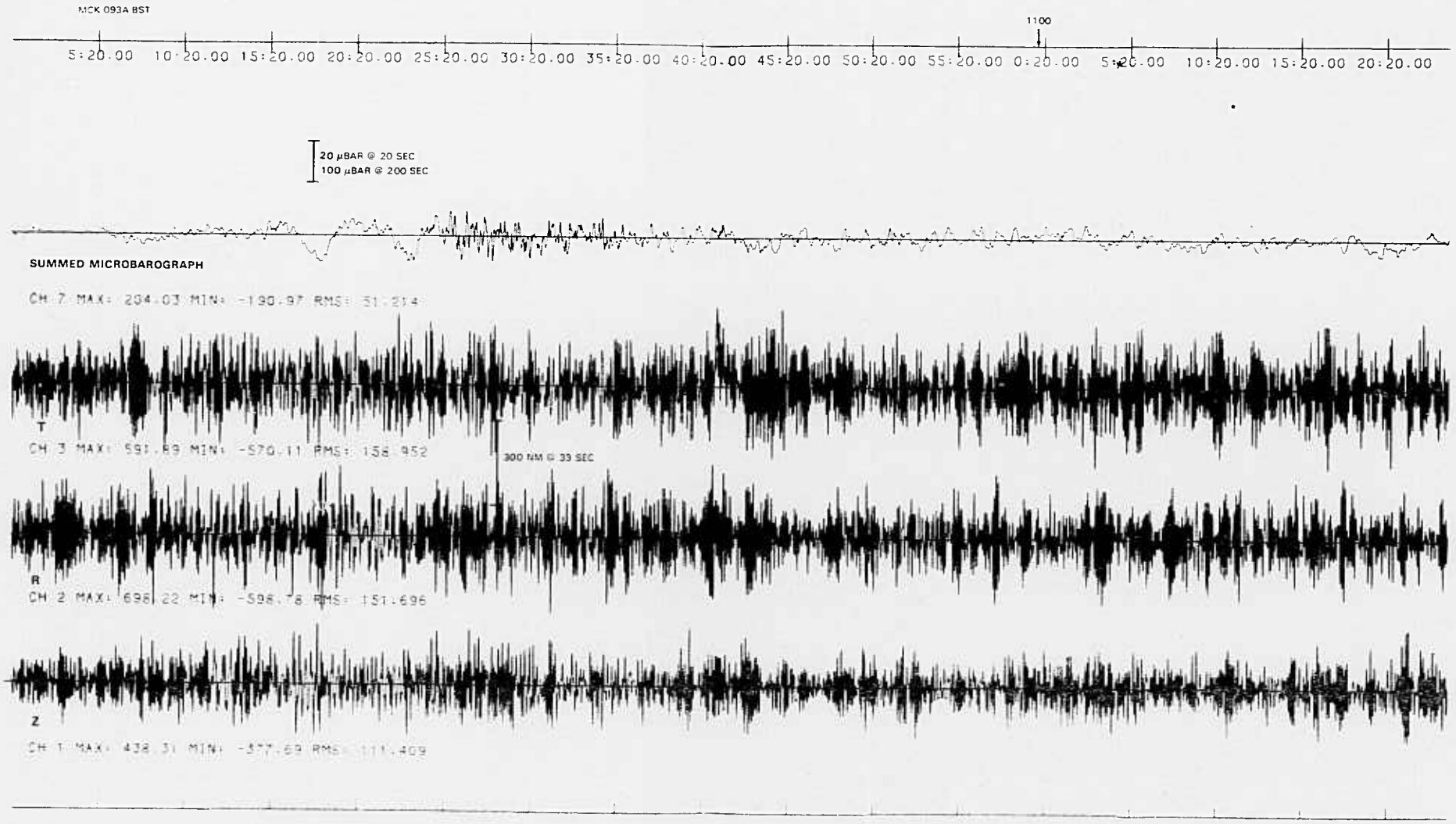

FIGURE 13. EL CHICHON ERUPTION 093A ORIGIN TIME ~ 08:50.
THREE-COMPONENT INERTIAL SEISMOGRAMS AND MICROBAROGRAPH BEAM BEFORE PURE-STATE FILTERING.
RECORDED AT McKINNEY.

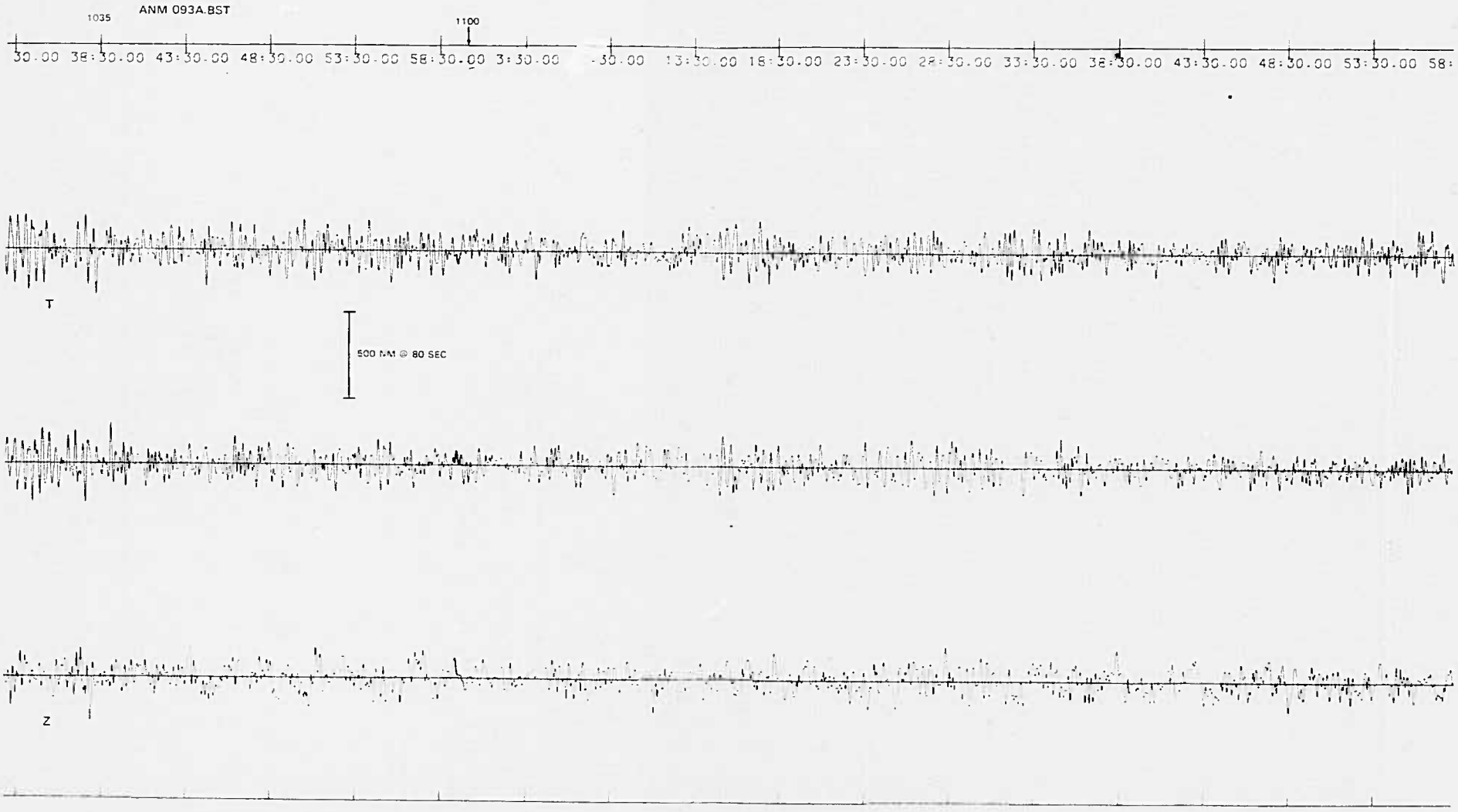

FIGURE 14. EL CHICHON ERUPTION 093A ORIGIN TIME ~ 08:50
THREE-COMPONENT INERTIAL SEISMOGRAMS BEFORE PURE-STATE FILTERING, RECORDED AT ANMO

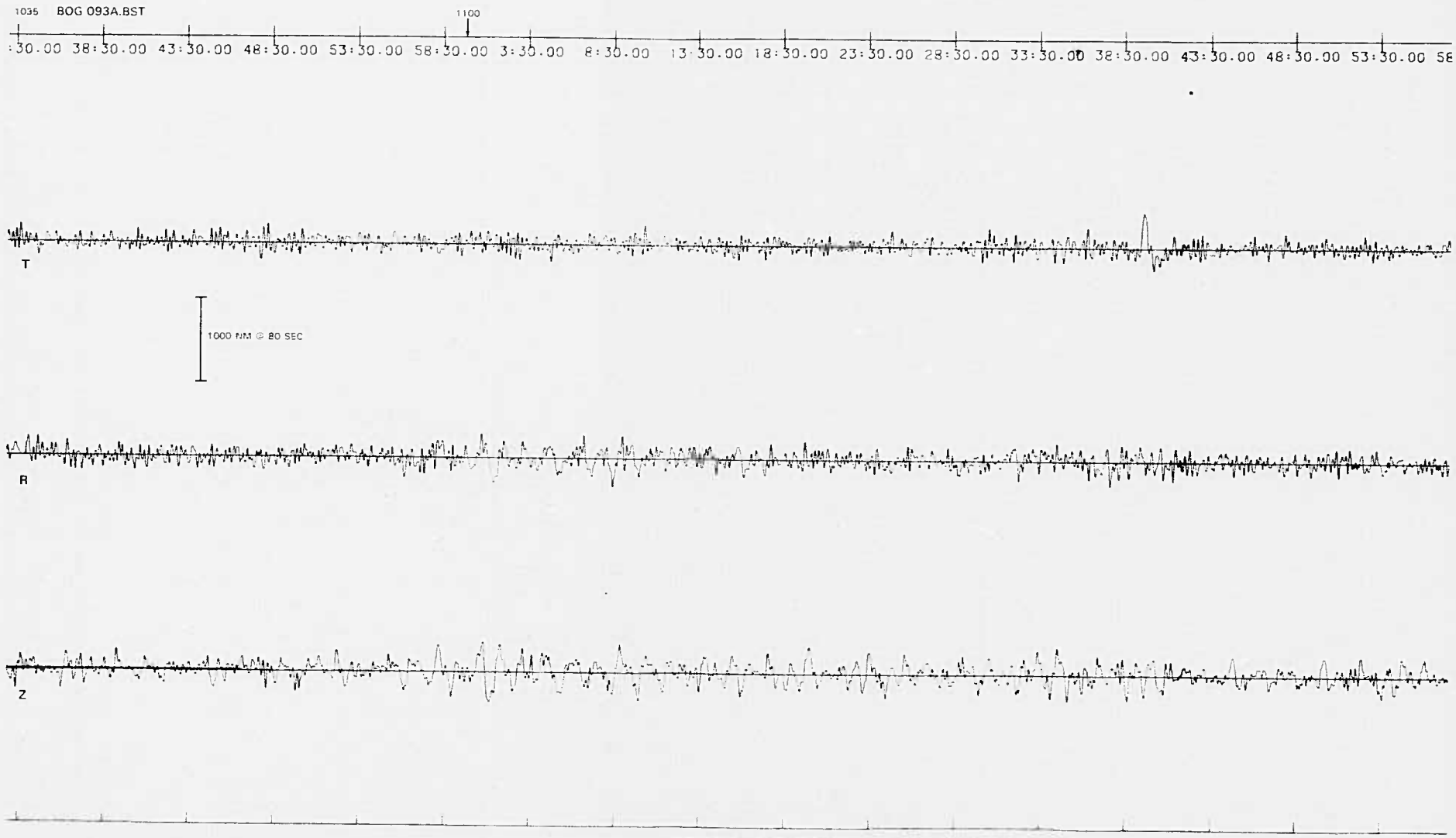

FIGURE 15 EL CHICHON ERUPTION 093A ORIGIN TIME ~ 08:50.
THREE-COMPONENT INERTIAL SEISMOGRAMS BEFORE PURE-STATE FILTERING, RECORDED AT BOCO

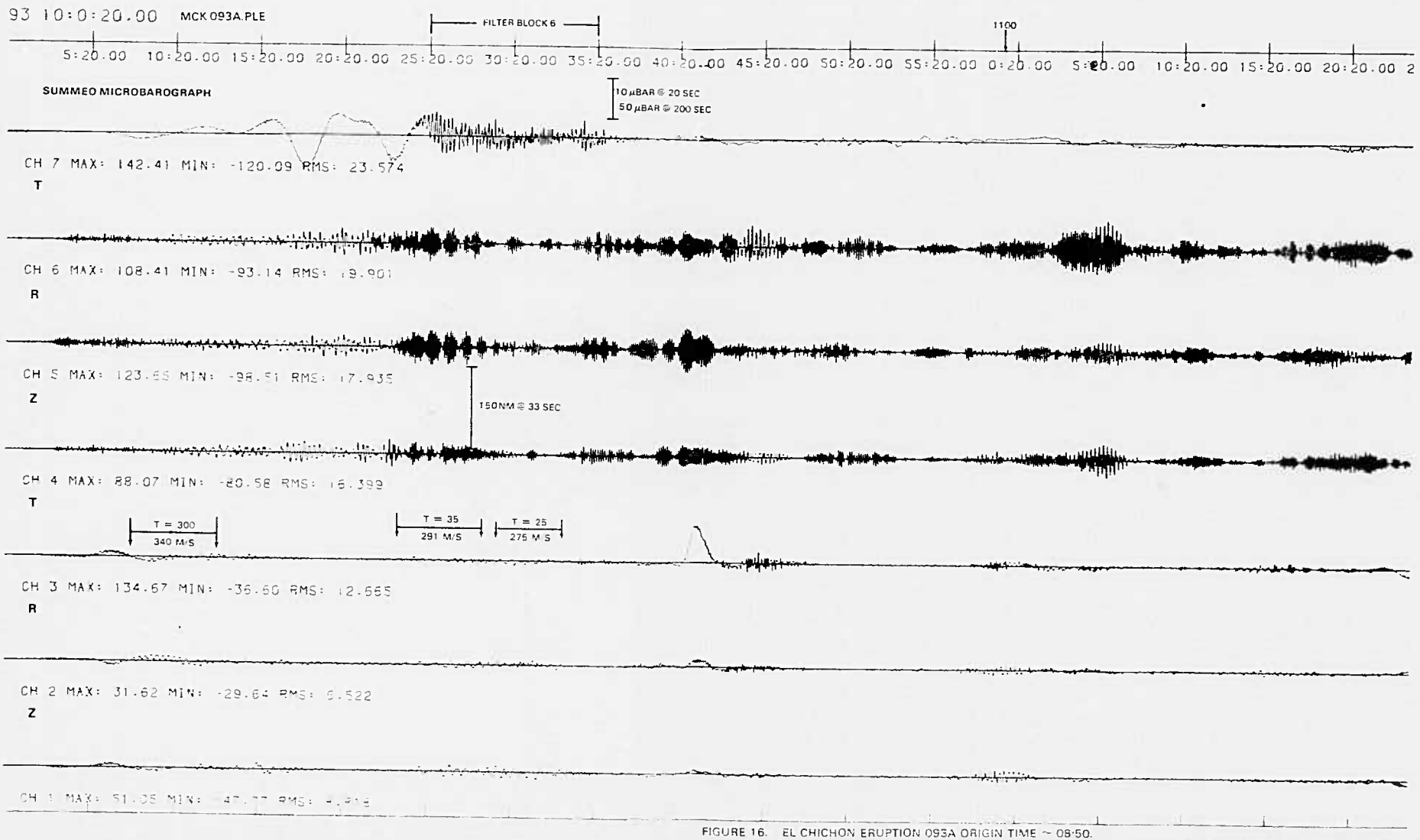

FIGURE 16. EL CHICHON ERUPTION 093A ORIGIN TIME ~ 08:50.
THREE-COMPONENT INERTIAL SEISMOGRAMS AND MICROBAROGRAPH BEAM AFTER PURE-STATE FILTERING.
RECORDED AT McKINNEY.

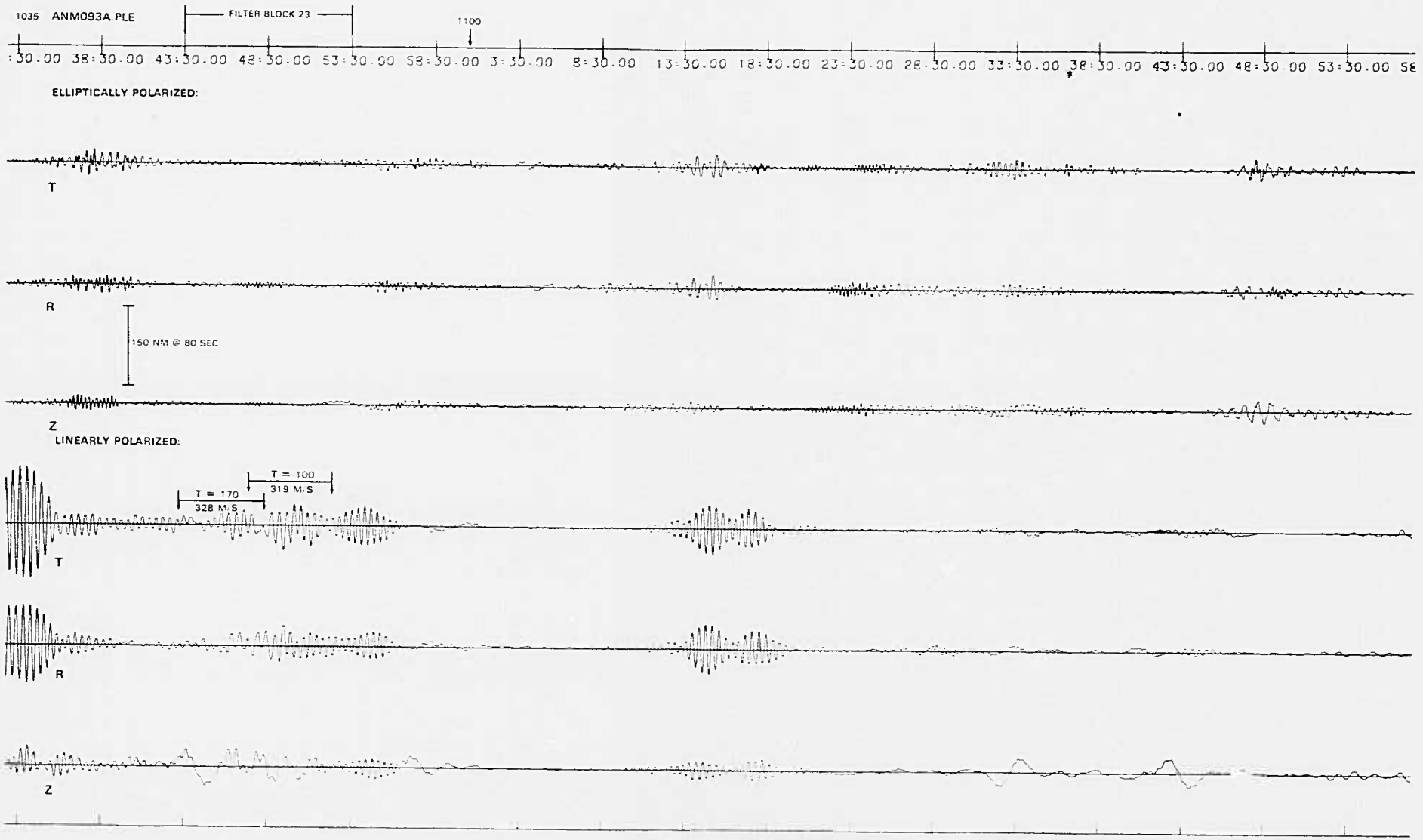

FIGURE 17. EL CHICHON ERUPTION 093A ORIGIN TIME ~ 08.50.
THREE-COMPONENT INERTIAL SEISMOGRAMS AFTER PURE-STATE FILTERING. RECORDED AT ANMO.

G15380

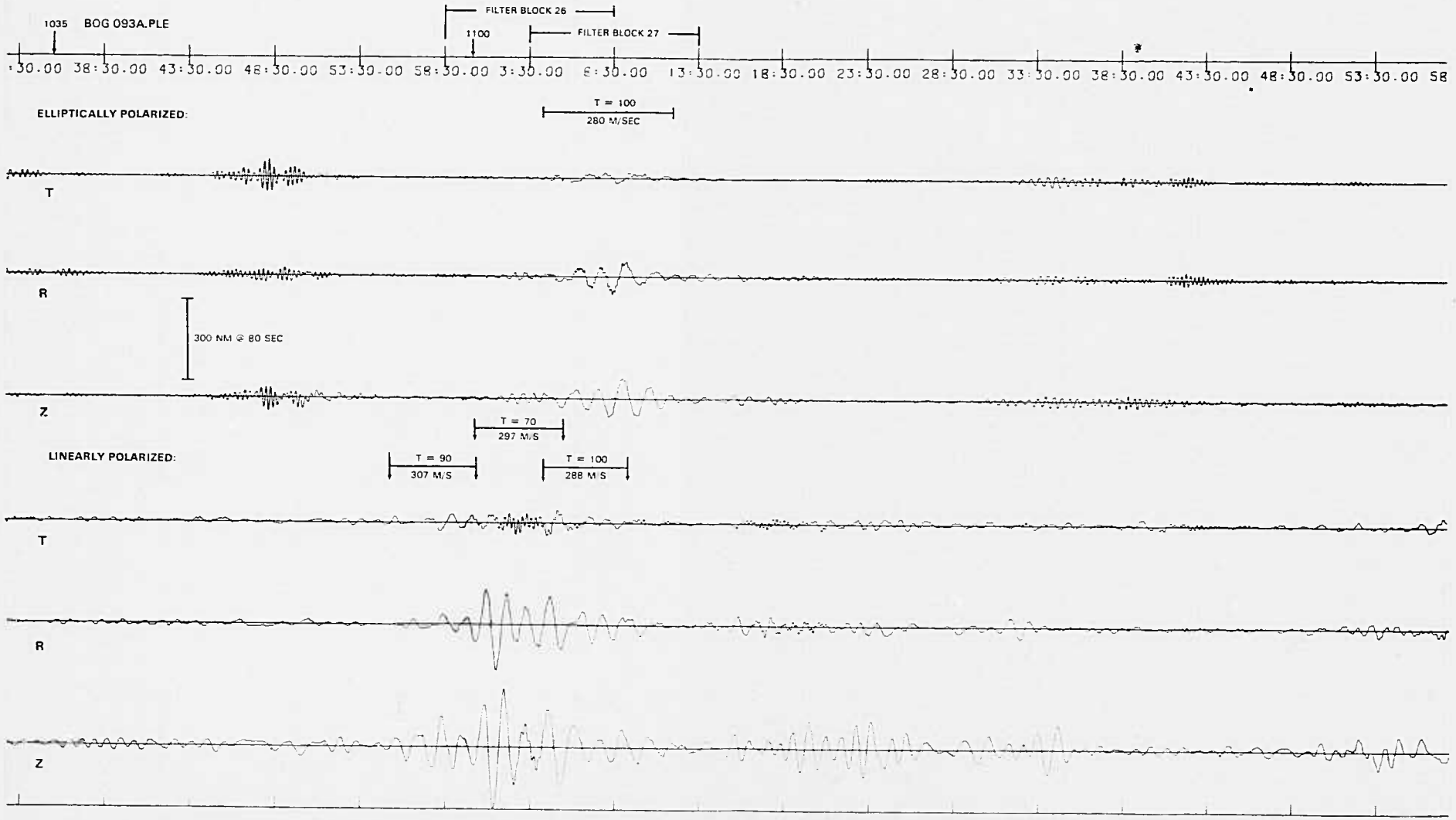

FIGURE 18 EL CHICHON ERUPTION 093A ORIGIN TIME ~ 08:50
THREE-COMPONENT INERTIAL SEISMOGRAMS AFTER PURE-STATE FILTERING. RECORDED AT BOCO.

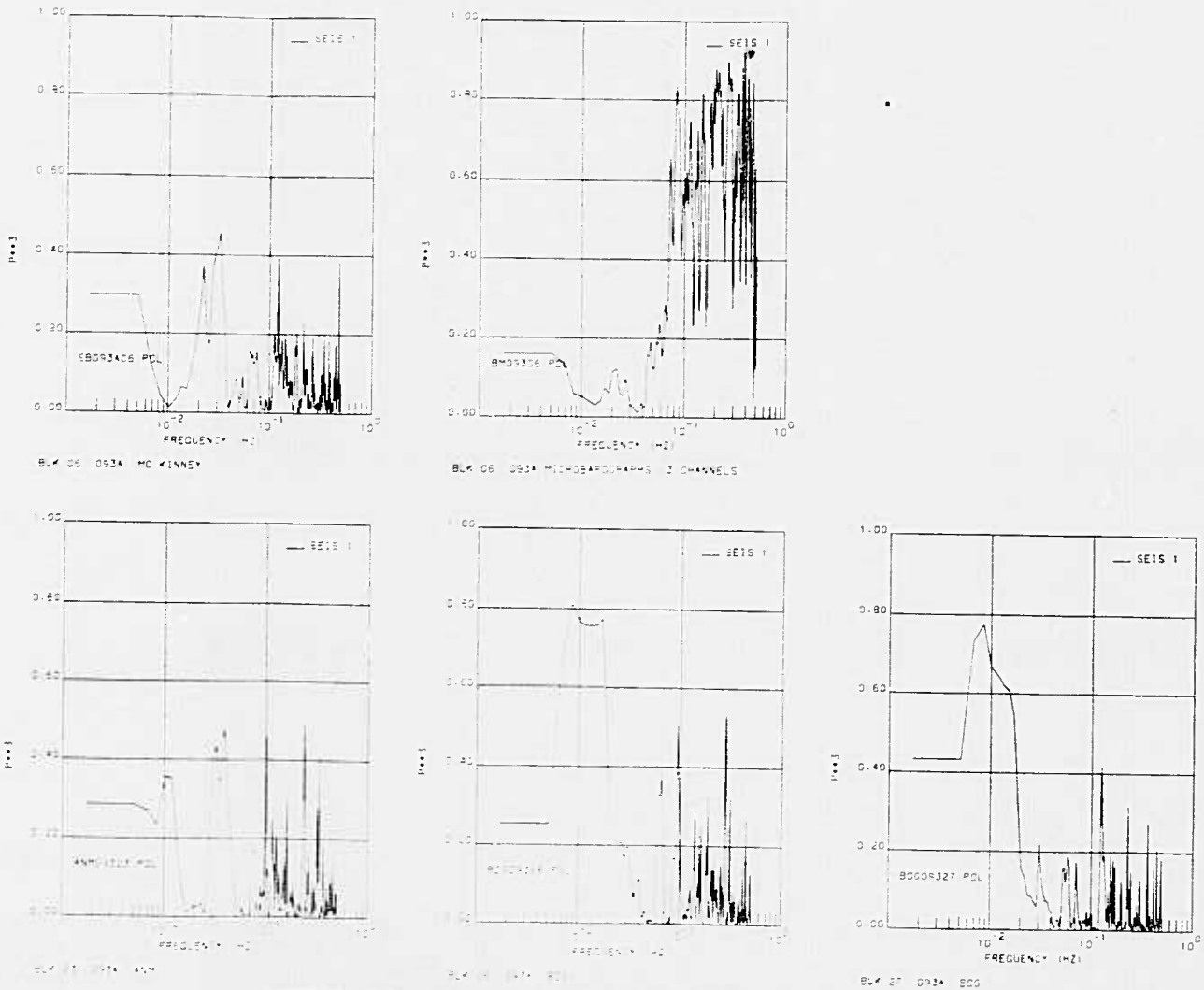

FIGURE 19. EL CHICHON ERUPTION 093A ORIGIN TIME ~ 08.50.
SEISMIC AND MICROBAROMETRIC PURE-STATE FILTERS (P^3) FOR SELECTED FILTER BLOCKS. McKINNEY, ANMO, AND BOCO.

G15382

Results for the second infrasonic event on day 93 (093B) with origin time about 10:03 are shown in figures 20 through 26. The McKinney microbarograph beam (figure 23) shows a clear infrasonic signal, with both gravity and higher modes apparent, beginning at about 11:40:20. The processed seismograms from McKinney (figure 23) show a clear seismic signal during the arrival of the higher-mode acoustic component of the infrasonic signal evident on the microbarograph beam. The seismic signal is composed of two principal components, a narrow-band, linearly polarized arrival with a frequency of 0.035 Hz and a nondispersed, elliptically polarized arrival with a frequency of 0.08 Hz. The microbarometric data for this arrival (figure 26) are strongly polarized at both of these frequencies, as well as at higher frequencies. The state vector for the linearly polarized component has a near-vertical orientation. The plane of polarization for the 0.08 Hz component has a strike of about 165 degrees relative to the radial direction and a near-vertical dip. If this arrival represents an infrasonic signal generated by the El Chichon eruption, the elliptical motion is prograde. This arrival is the only case found in this investigation of a seismically detected arrival in this frequency band that is possibly related to an infrasonic signal. The Rayleigh wave arrival beginning about 11:25:20 is not traveling in the radial direction. The seismic data for this arrival are strongly polarized over a narrow band of frequencies centered at 0.04 Hz, whereas the microbarometric data for this time interval are unpolarized over this bandwidth. This arrival is therefore probably a surface wave from an unidentified earthquake. The processed ANMO seismograms (figure 24) show only a very weak, linearly polarized arrival with a period of about 200 seconds and a weak, elliptically polarized arrival with a period of about 60 seconds, with superposed 15-second microseismic noise. The degree of polarization during this time interval (figure 26) was low for both of these periods; therefore, this arrival is probably not related to the El Chichon eruption. The BOCO processed seismograms (figure 25) show a linearly polarized arrival with a period of about 60 seconds followed by an elliptically polarized arrival with a period of 90 seconds. These two arrivals for event 093B at BOCO are very similar in character to the two arrivals for event 093A at this site. The state vector for the linearly polarized arrival is oriented within 10 degrees of vertical, and the trend of the major axis is 20 degrees from the radial direction. The

plane of polarization for the elliptically polarized arrival strikes 20 degrees from the radial direction with a dip of 75 degrees. If this is an infrasonic arrival at BOCO generated by the El Chichon eruption, the motion is retrograde elliptical.

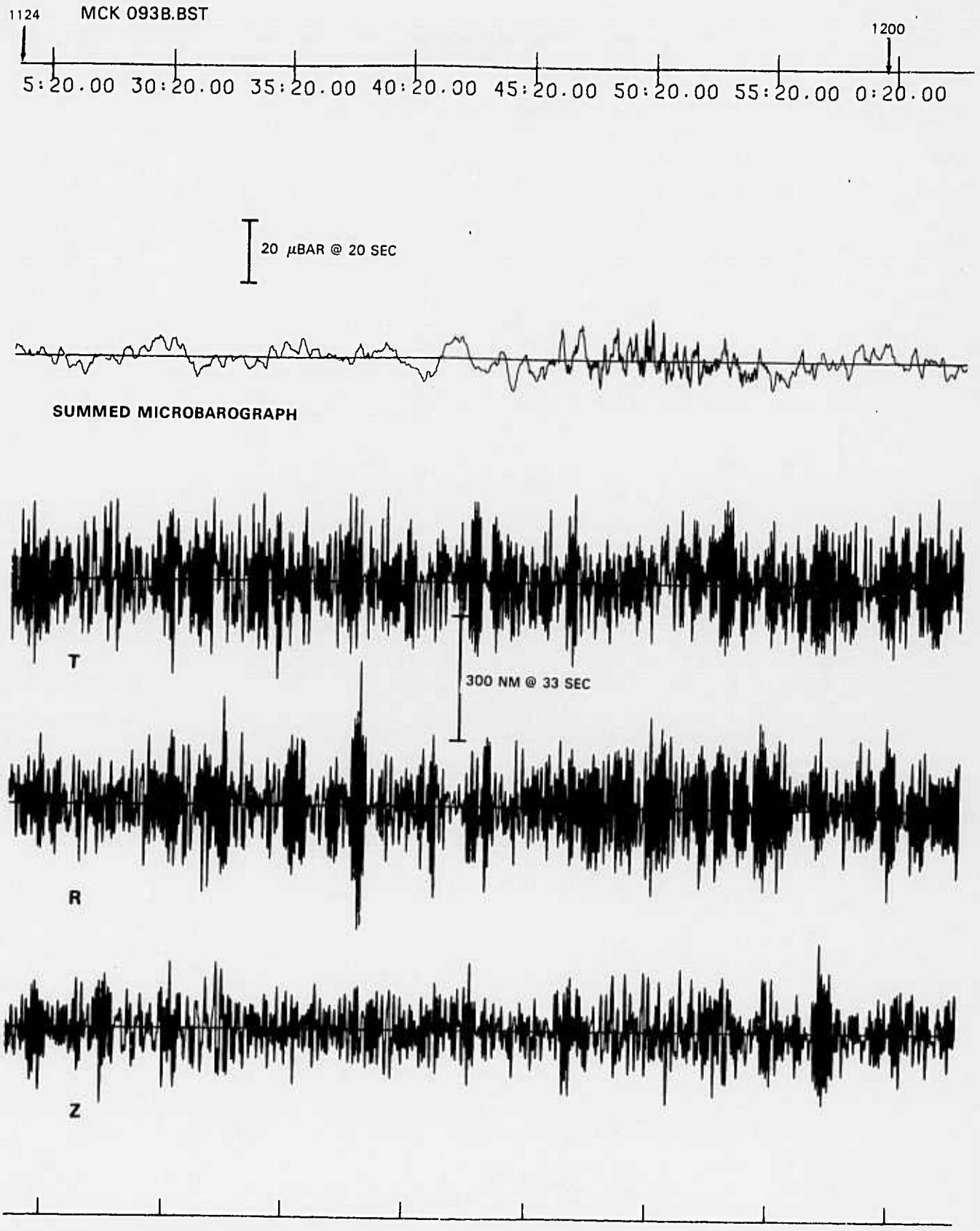

FIGURE 20. EL CHICHON ERUPTION 093B ORIGIN TIME ~ 10:12. THREE-COMPONENT INERTIAL SEISMOGRAMS AND MICROBAROGRAPH BEAM BEFORE PURE-STATE FILTERING, RECORDED AT McKINNEY.

G15383

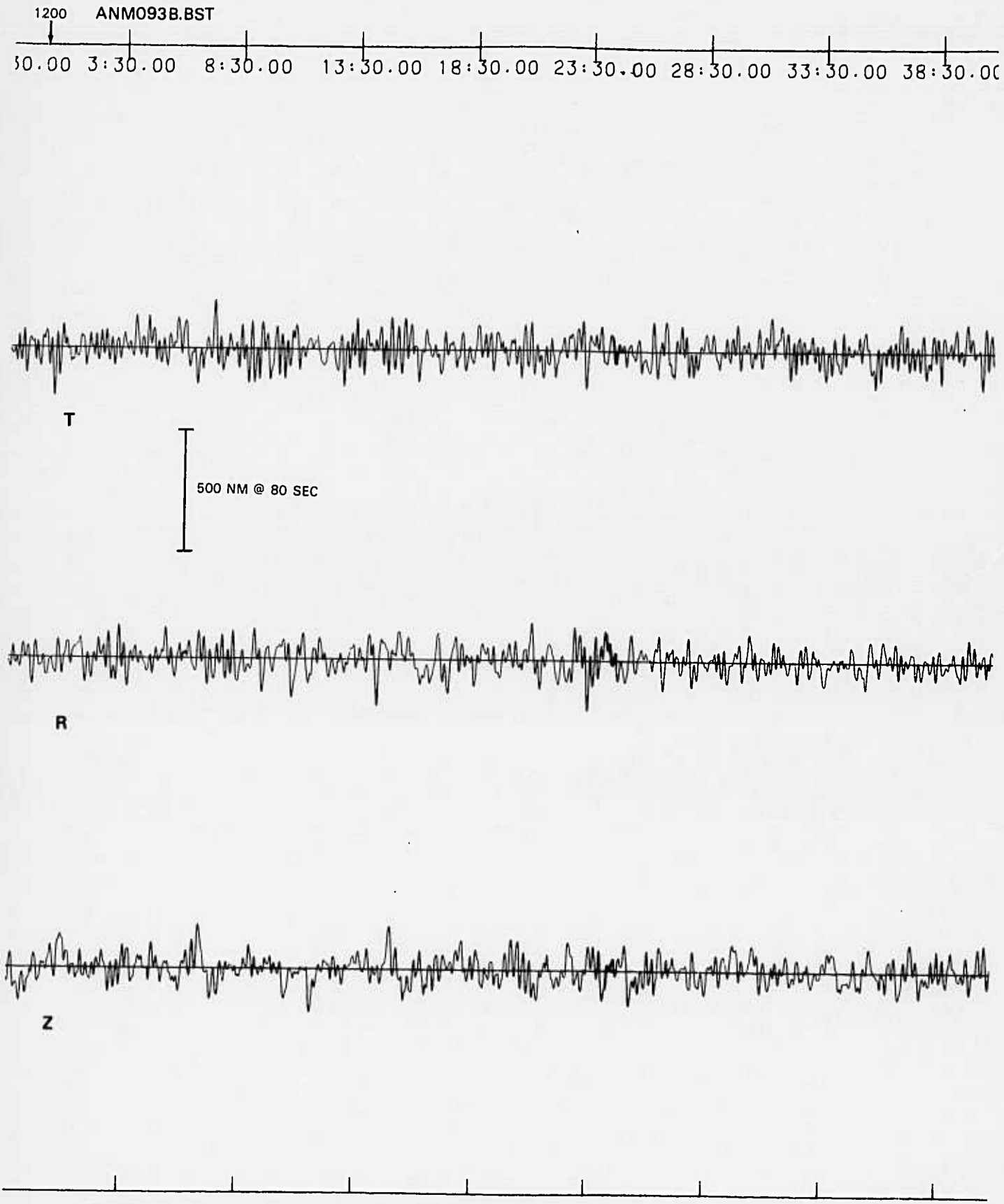

FIGURE 21. EL CHICHON ERUPTION 093B ORIGIN TIME ~ 05:32.
THREE-COMPONENT INERTIAL SEISMOGRAMS BEFORE PURE-STATE FILTERING, RECORDED AT ANMO.

G15384

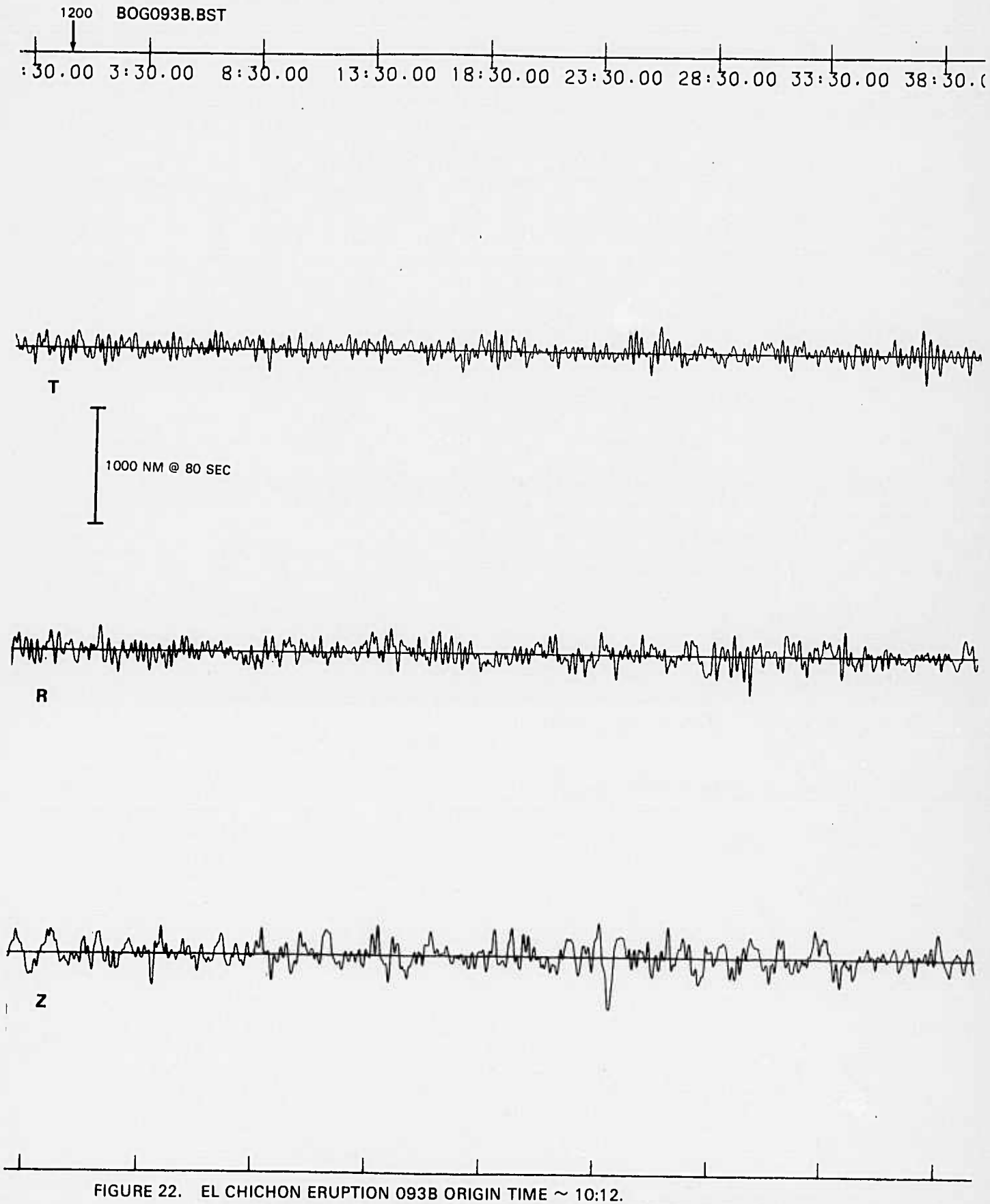

FIGURE 22. EL CHICHON ERUPTION 093B ORIGIN TIME ~ 10:12.
THREE-COMPONENT INERTIAL SEISMOGRAMS BEFORE PURE-STATE FILTERING, RECORDED AT BOCO.

G15385

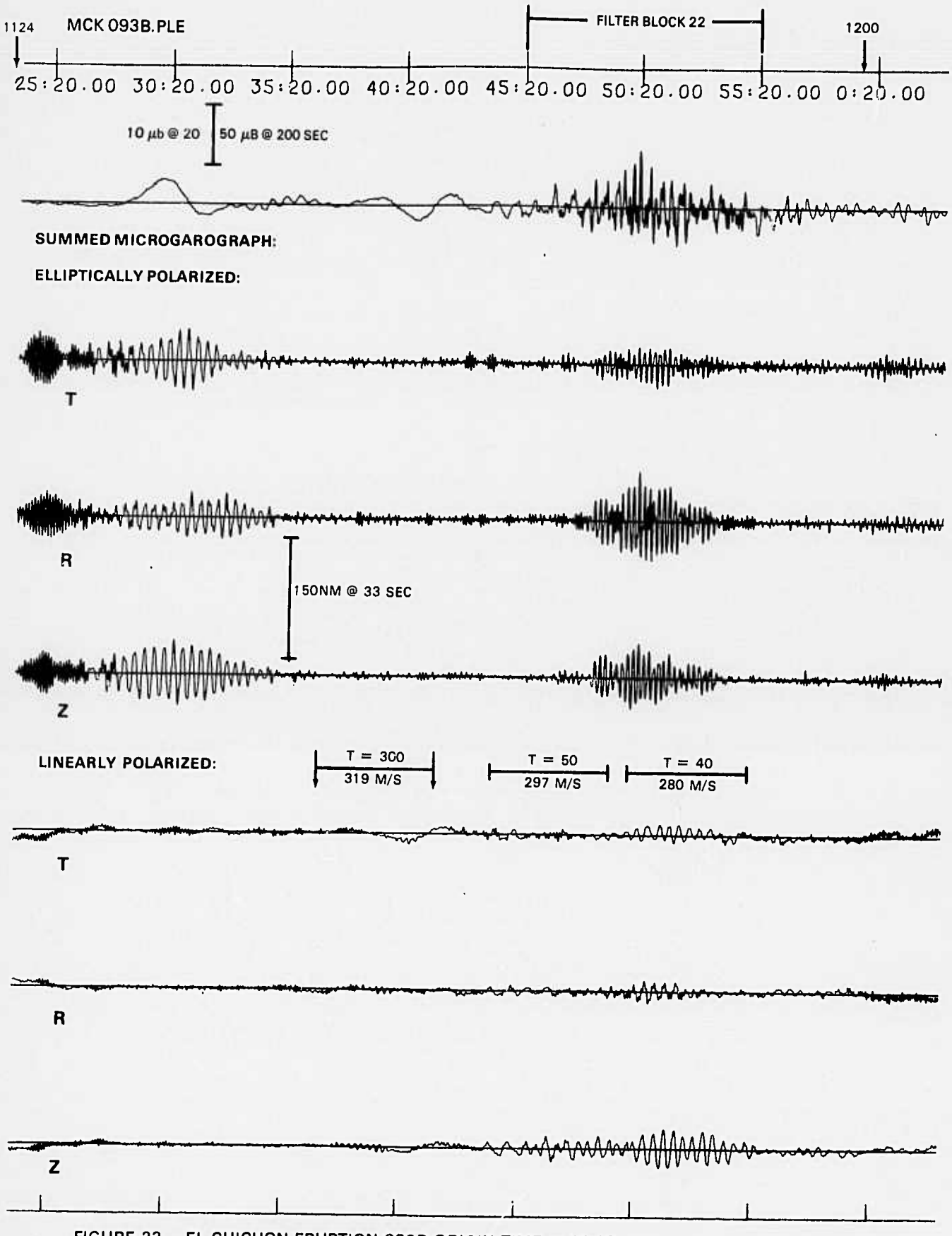

FIGURE 23. EL CHICHON ERUPTION 093B ORIGIN TIME ~ 10:12.
THREE-COMPONENT INERTIAL SEISMOGRAMS AND MICROBAROGRAPH BEAM AFTER PURE-STATE FILTERING, RECORDED AT McKINNEY.

G15386

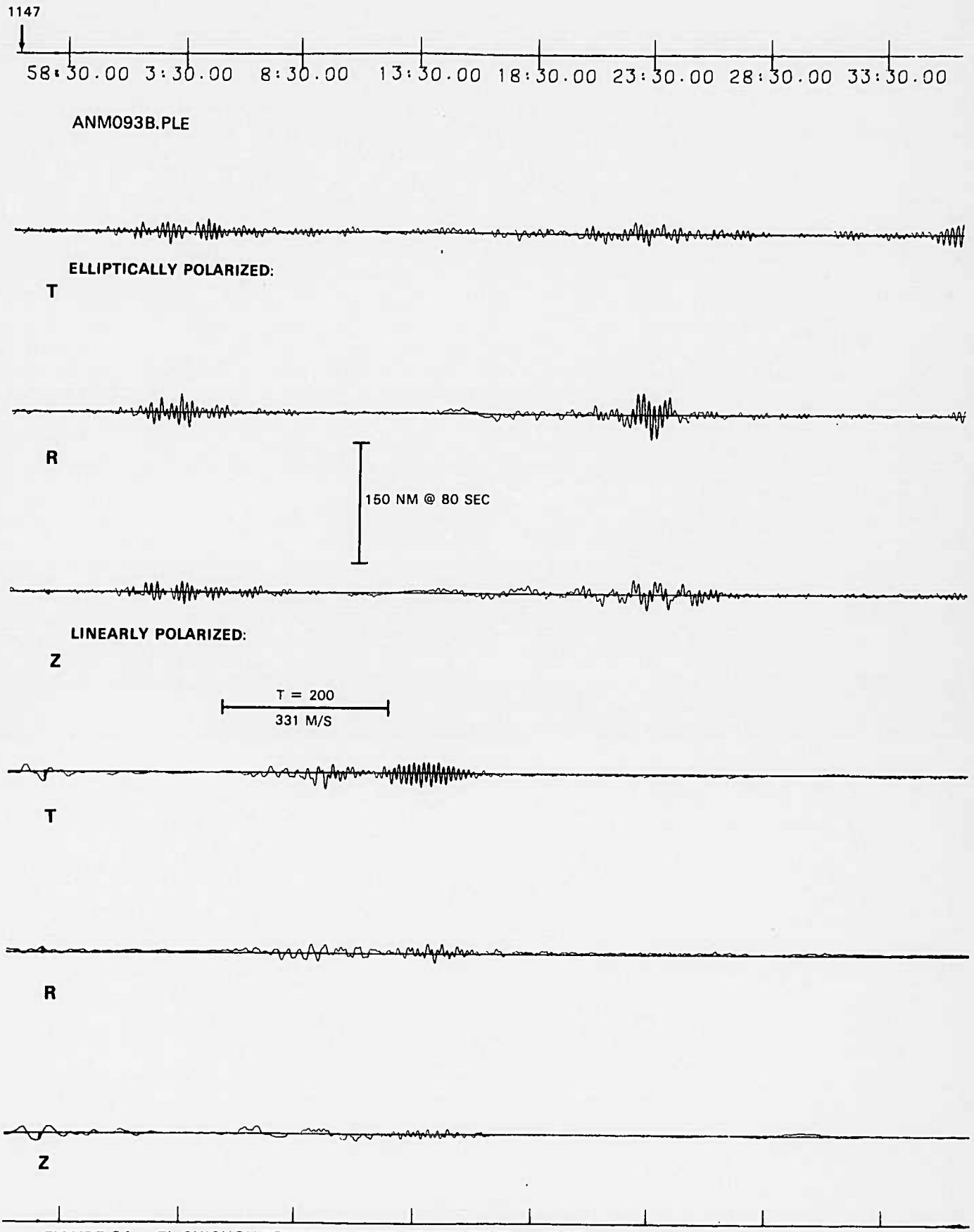

FIGURE 24. EL CHICHON ERUPTION 093B ORIGIN TIME ~ 10:12.
THREE-COMPONENT INERTIAL SEISMOGRAMS AFTER PURE-STATE FILTERING, RECORDED AT ANMO.

G15387

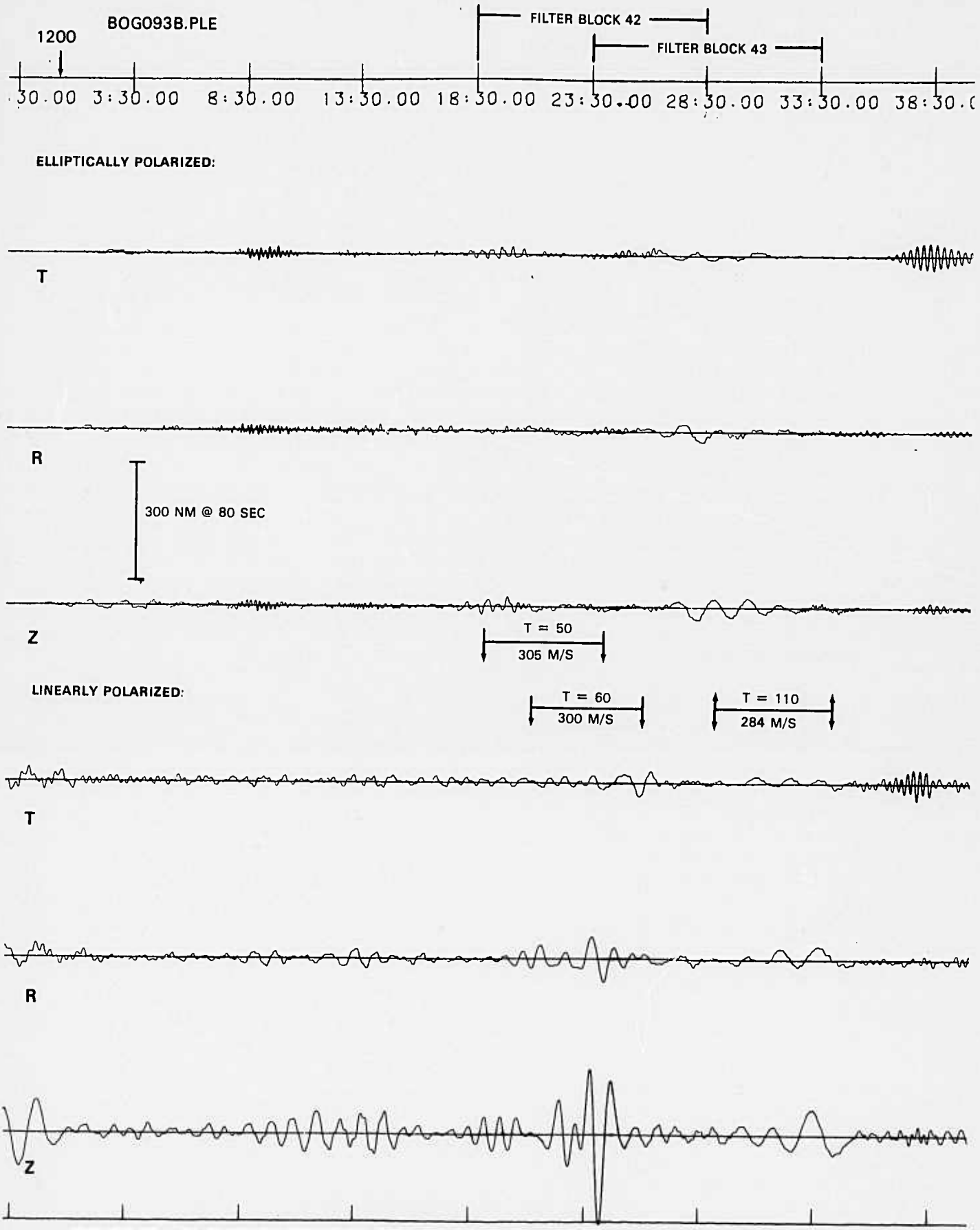

FIGURE 25. EL CHICHON ERUPTION 093B ORIGIN TIME ~ 10:12.
THREE-COMPONENT INERTIAL SEISMOGRAMS AFTER PURE-STATE FILTERING, RECORDED AT BOCO.

G15388

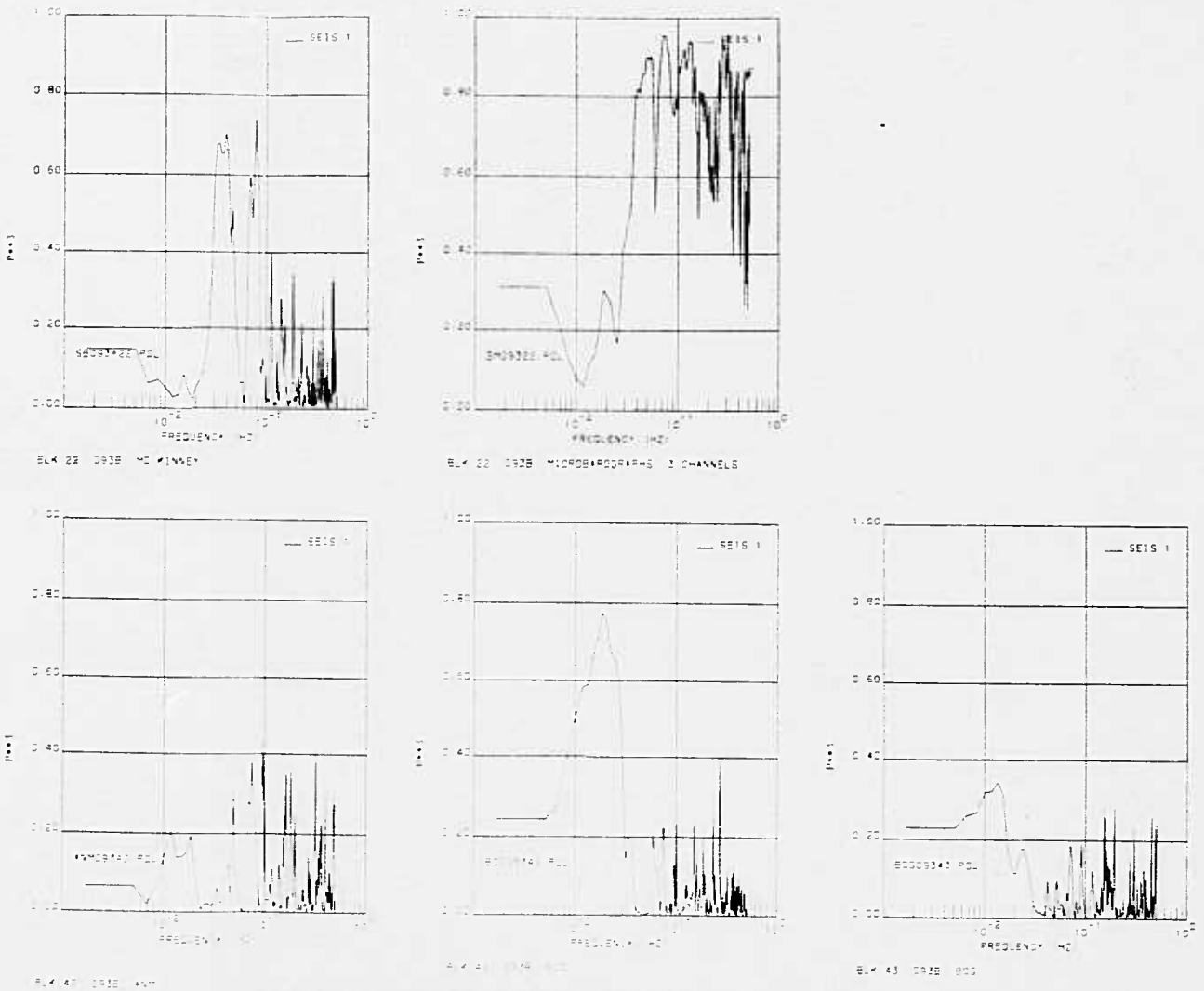

FIGURE 26. EL CHICHON ERUPTION 093B ORIGIN TIME ~ 10:12.
SEISMIC AND MICROBAROMETRIC PURE-STATE FILTERS (P^3) FOR SELECTED FILTER BLOCKS. McKINNEY, ANMO, AND BOCO.

G15389

Results for the infrasonic event on day 094 with origin time about 01:49 are presented in figures 27 through 35. Only the latter part of the signal recorded at McKinney is shown (figures 27 and 31), because the north seismograph component was inoperative during the initial arrival of this signal. Wind speed was low throughout the arrival of this signal, ranging from zero to a maximum of 5.9 mph, with a mean value of 2.3 mph. Under these low-wind conditions, application of a ten-minute, sliding, pure-state filter to the outputs of the microbarographs had very little effect (figures 27 and 31). Application of the pure-state filter to the McKinney seismic data detected a narrow-band, linearly polarized wave train with a dominant period of about 33 seconds during the arrival of the higher-mode acoustics as evidenced by the beamed microbarogram. The degree of polarization for the microbarometric data was very high for most frequencies less than 0.7 Hz (figure 35). The inertial data were highly polarized over only a narrow band of frequencies centered at 0.03 Hz. The state vector for the linearly polarized arrival is oriented within 15 degrees of vertical. The processed seismograms for ANMO (figure 32) show an elliptically polarized arrival with a dominant period of about 50 seconds. The plane of polarization for the elliptically polarized arrival strikes 170 degrees relative to the radial direction with a dip of 80 degrees. The motion is retrograde for a wave traveling from El Chichon toward ANMO. The BOCO processed seismograms (figure 33) show both linearly and elliptically polarized arrivals during the expected arrival time window for an infrasonic signal from this El Chichon eruption. Pure-state filters for the filter blocks beginning at 03:59:30 and at 04:14:30 are given in figure 35. The state vector for the linearly polarized arrival with a period of 90 seconds, arriving at 04:05 is oriented within 15 degrees of vertical; however, the trend of the major axis for this arrival is 30 degrees from the radial direction. Therefore, this linearly polarized arrival is probably not related to the El Chichon eruption. The plane of polarization for the elliptically polarized arrival beginning 04:09:35, with a dominant period of about 50 seconds, strikes 15 degrees from the radial direction with a dip of 65 degrees. For a wave traveling from El Chichon to BOCO, the motion is retrograde. The GRFO processed seismograms (figure 34) show a linearly polarized arrival with a dominant period of about 45 seconds and an elliptically polarized arrival with a dominant period of

about 100 seconds within the expected infrasonic arrival time window. Pure-state filters for filter blocks beginning at 10:46:30 and at 10:51:30 are shown in figure 35. For the 100-second, elliptically polarized arrival, the plane of polarization strikes 175 degrees relative to the radial direction with a dip of 80 degrees. The state vector of the 45-second, linearly polarized arrival is oriented within 5 degrees of vertical; however, the trend of the major axis for this arrival is 70 degrees from the radial direction. Therefore, this linearly polarized arrival may not be related to the El Chichon eruption.

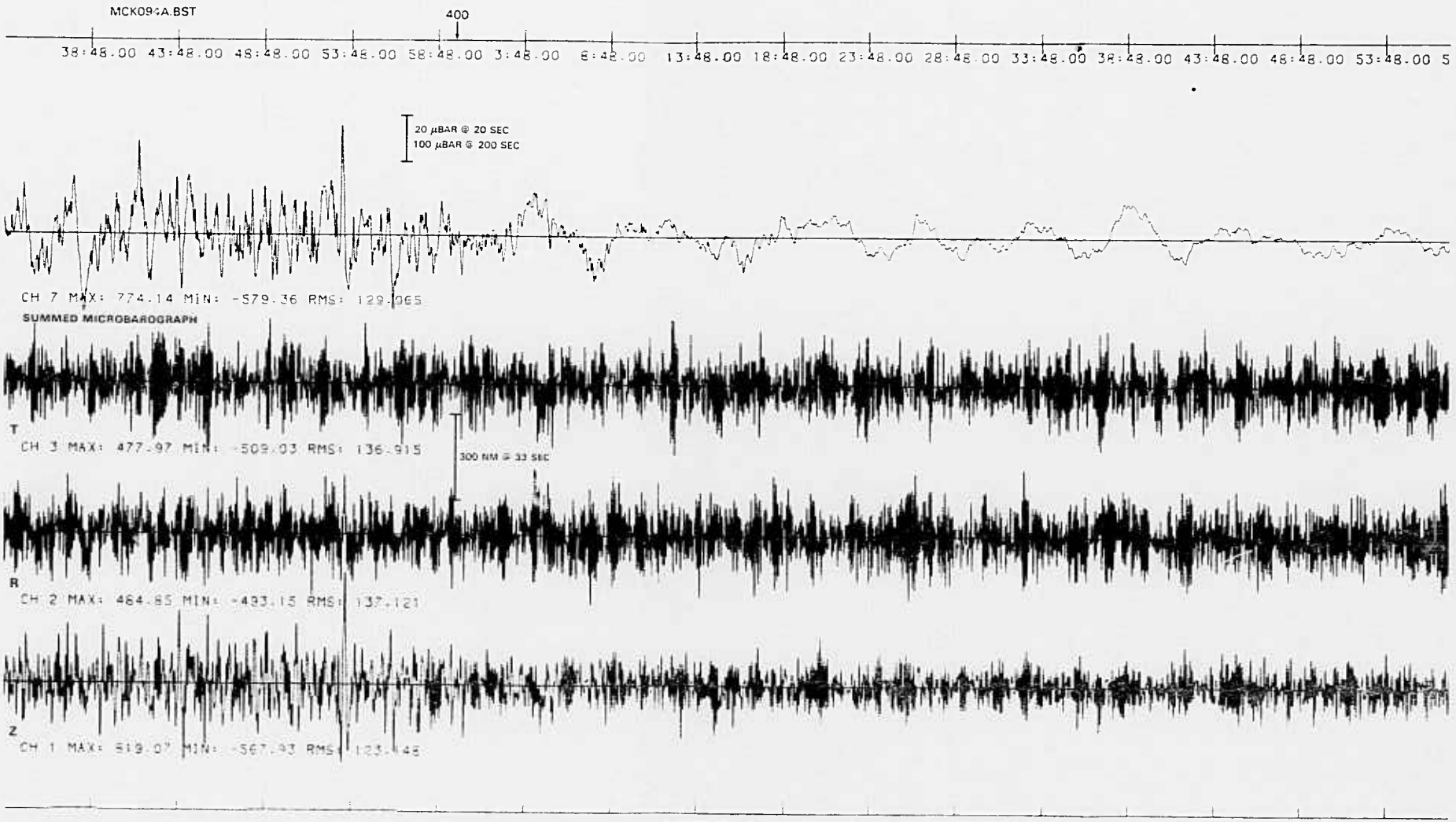

FIGURE 27. EL CHICHON ERUPTION 094A ORIGIN TIME ~ 02:00.
THREE-COMPONENT INERTIAL SEISMOGRAMS AND MICROBAROGRAPH BEAM BEFORE PURE-STATE FILTERING.
RECORDED AT McKINNEY

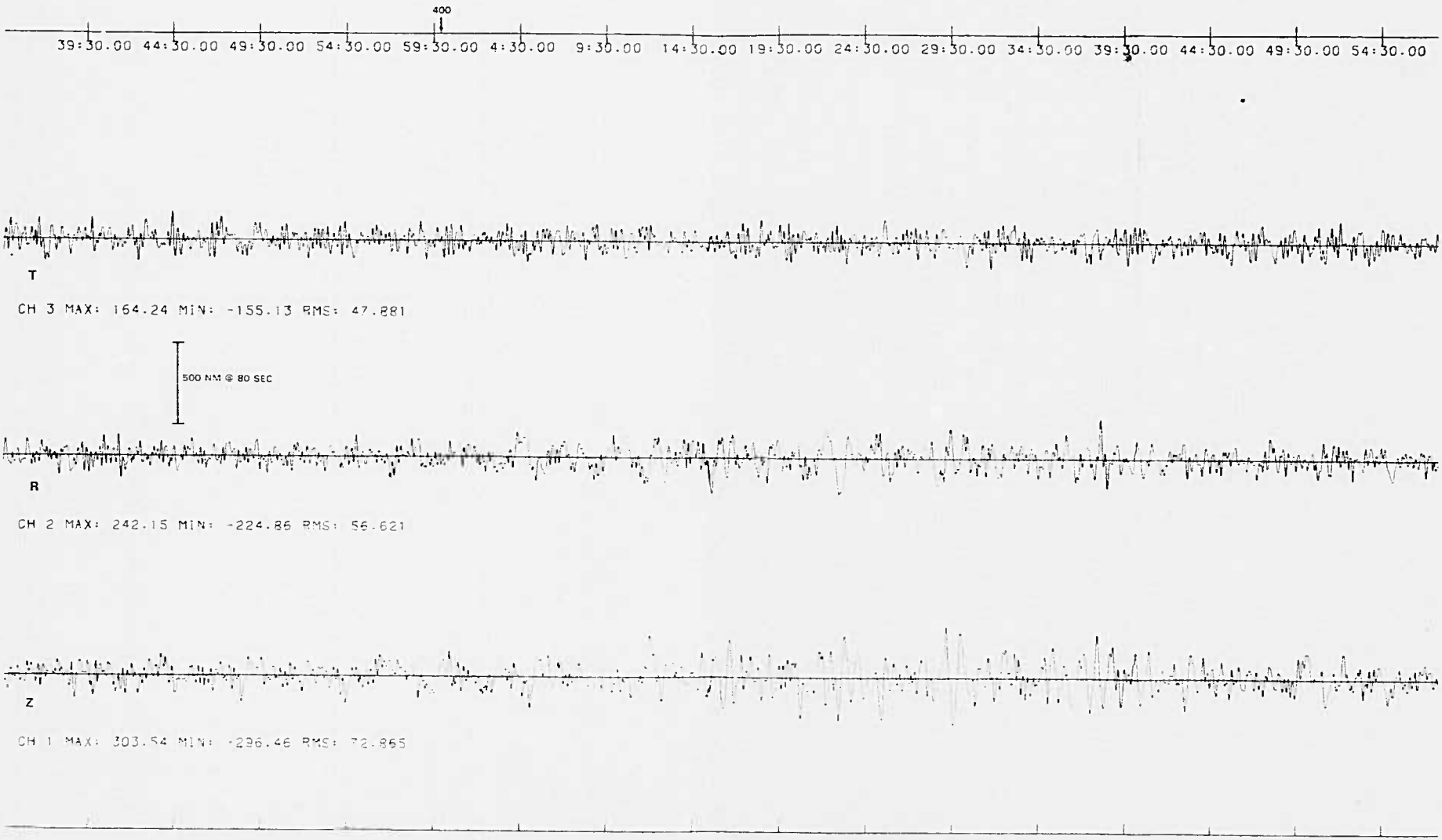

FIGURE 28. EL CHICHON ERUPTION D94A ORIGIN TIME ~ 02:22.
THREE-COMPONENT INERTIAL SEISMOGRAMS BEFORE PURE-STATE FILTERING, RECORDED AT ANMO

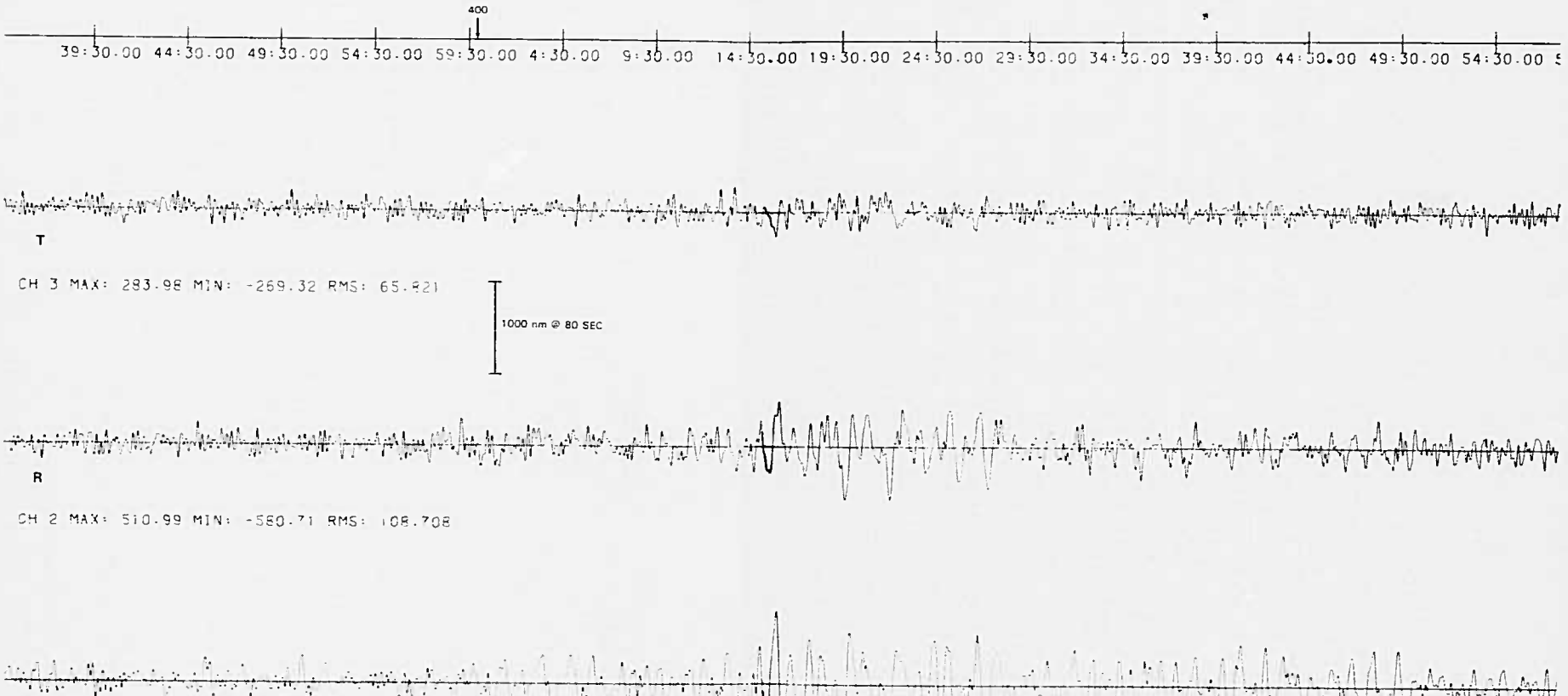

FIGURE 29. EL CHICHON ERUPTION 094A ORIGIN TIME ~ 02:00.
THREE-COMPONENT INERTIAL SEISMOGRAMS BEFORE PURE-STATE FILTERING, RECORDED AT BOCO.

3-63/64

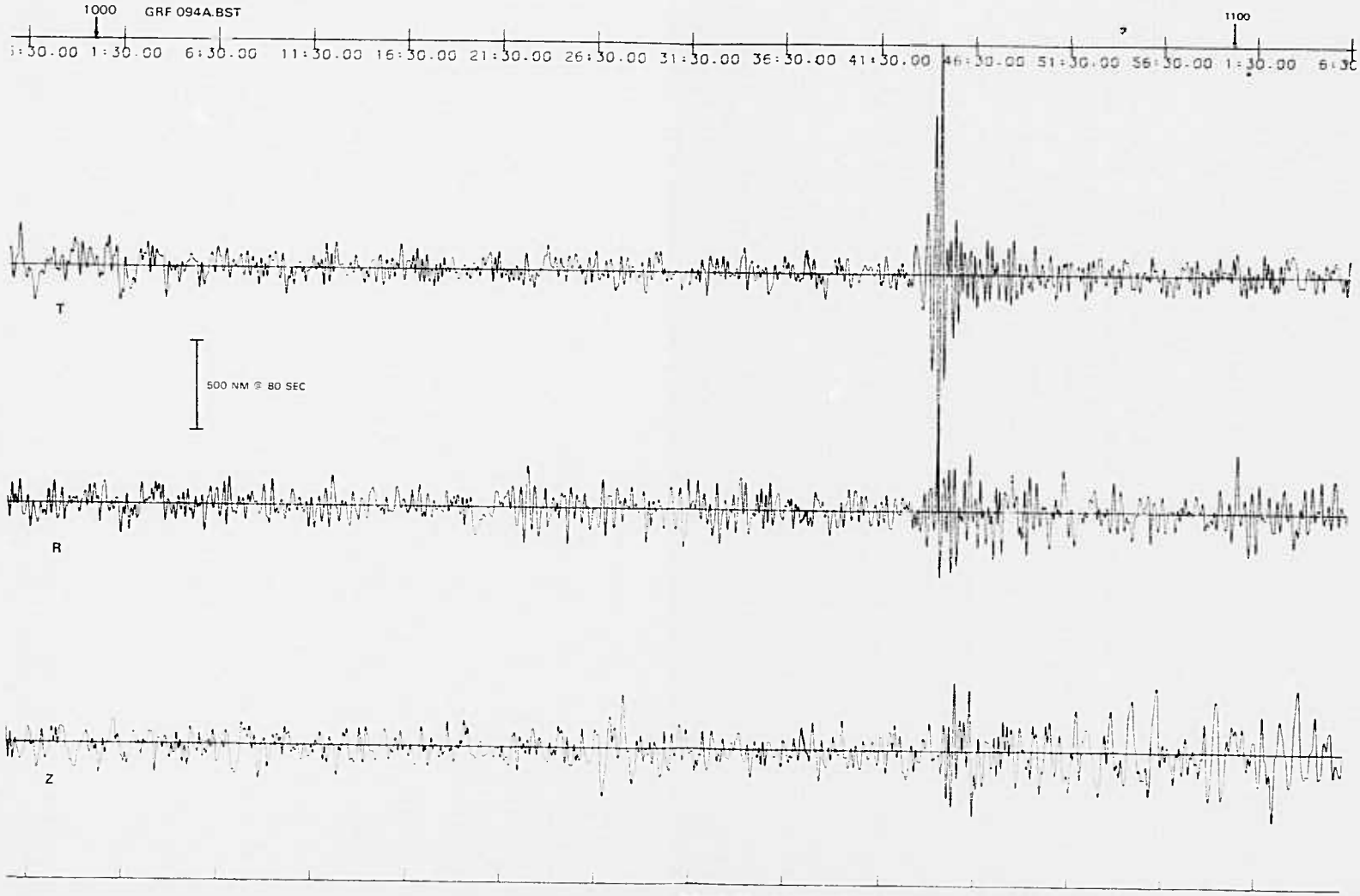

FIGURE 30. EL CHICHON ERUPTION 094A ORIGIN TIME ~ 02:00
THREE-COMPONENT INERTIAL SEISMOGRAMS BEFORE PURE-STATE FILTERING RECORDED AT GRFO.

3-65/66

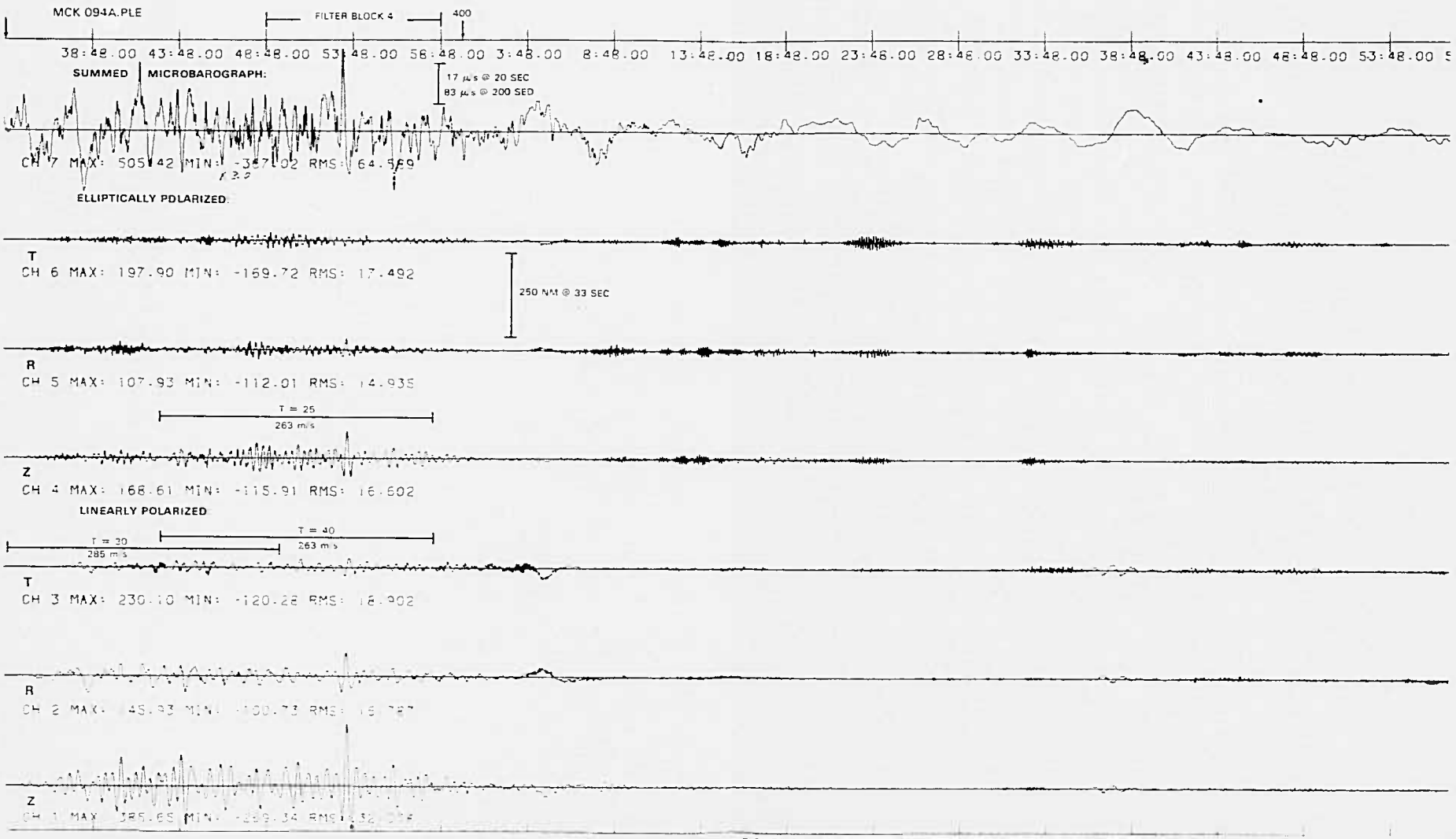

FIGURE 31. EL CHICHON ERUPTION 094A ORIGIN TIME ~ 02:00.
THREE-COMPONENT INERTIAL SEISMOGRAMS AND MICROBAROGRAPH BEAM AFTER PURE-STATE FILTERING.
RECORDED AT McKINNEY

3-67/68

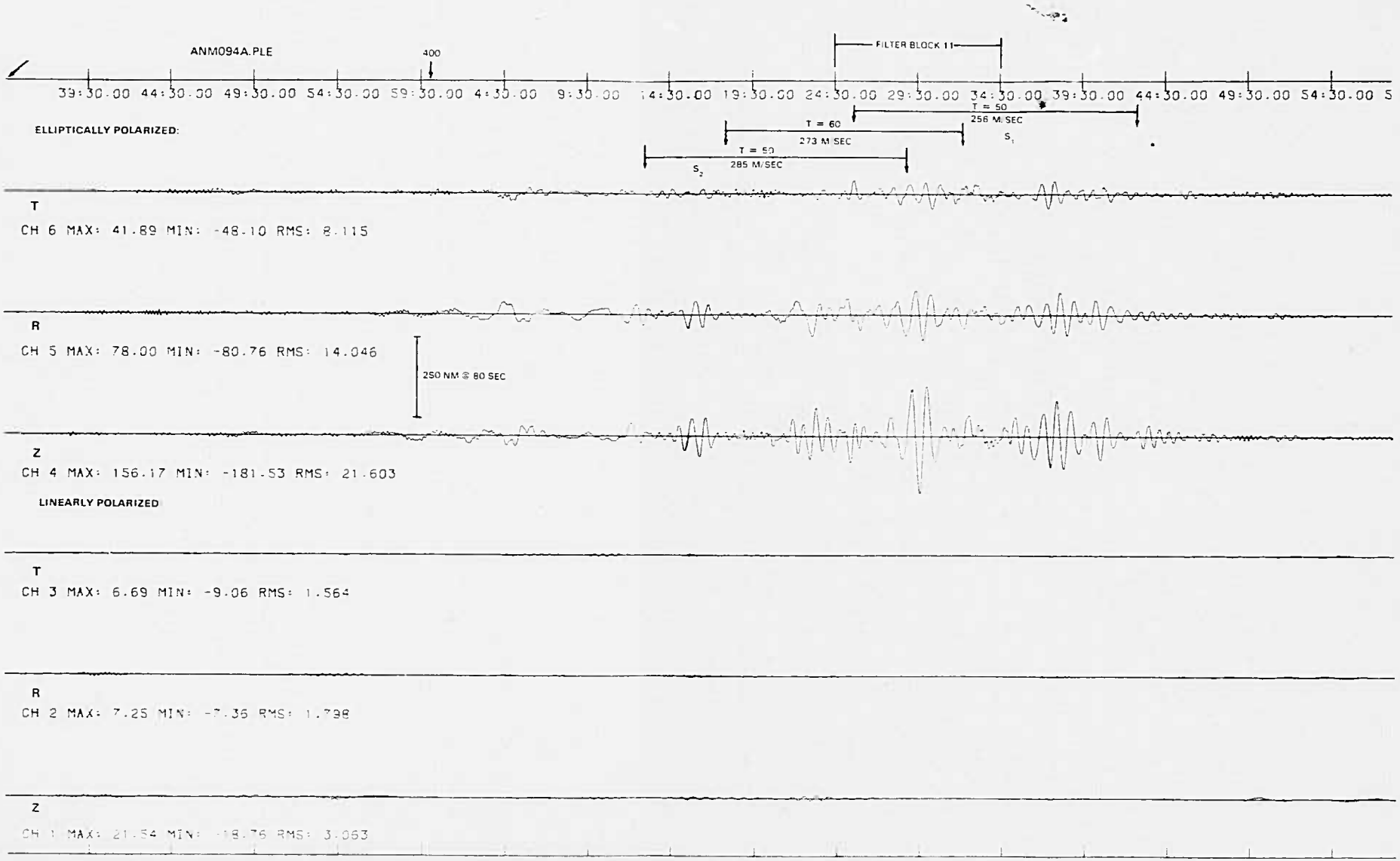

FIGURE 32. EL CHICHON ERUPTION 094A ORIGIN TIME ~ 02:00.
THREE-COMPONENT INERTIAL SEISMOGRAMS AFTER PURE-STATE FILTERING. RECORDED AT ANMO

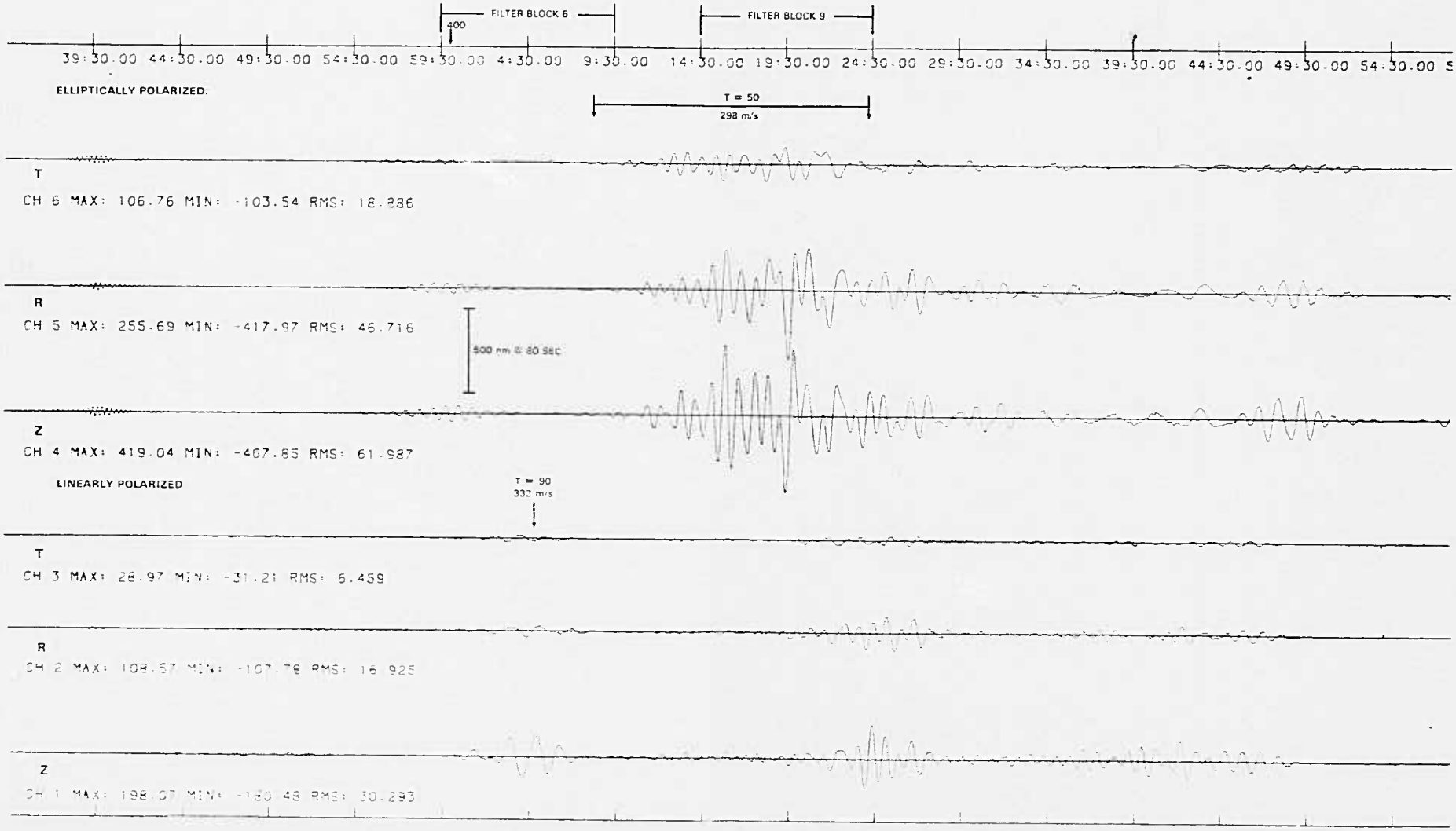

FIGURE 33. EL CHICHON ERUPTION 094A ORIGIN TIME ~ 02 00.
THREE-COMPONENT INERTIAL SEISMOGRAMS AFTER PURE-STATE FILTERING. RECORDED AT BOCO

3-71/72

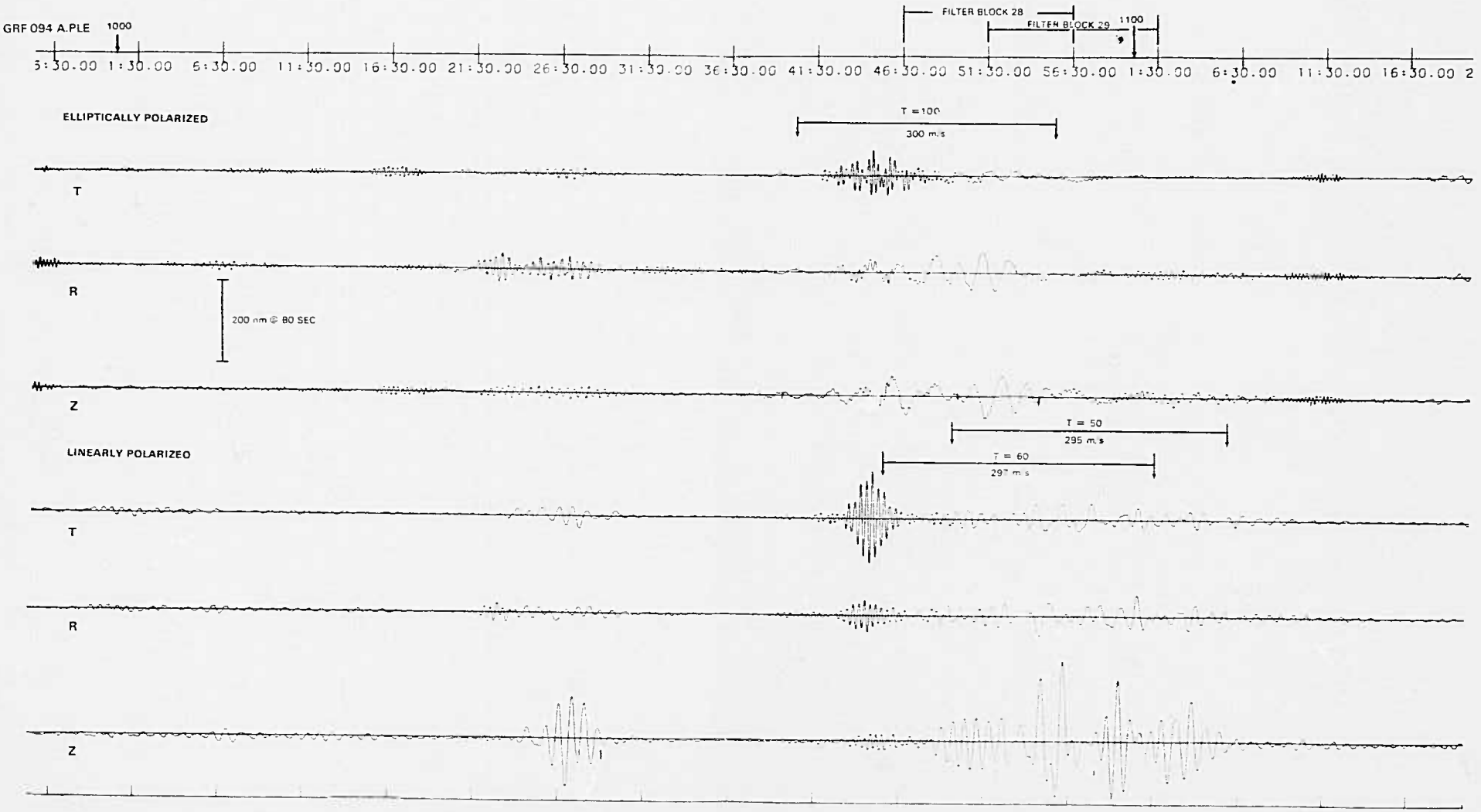

FIGURE 34 EL CHICHON ERUPTION 094A ORIGIN TIME ~ 02 00
THREE-COMPONENT INERTIAL SEISMOGRAMS AFTER FURE-STATE FILTERING RECORDED AT GRFO

3-73/74

TR 84-7

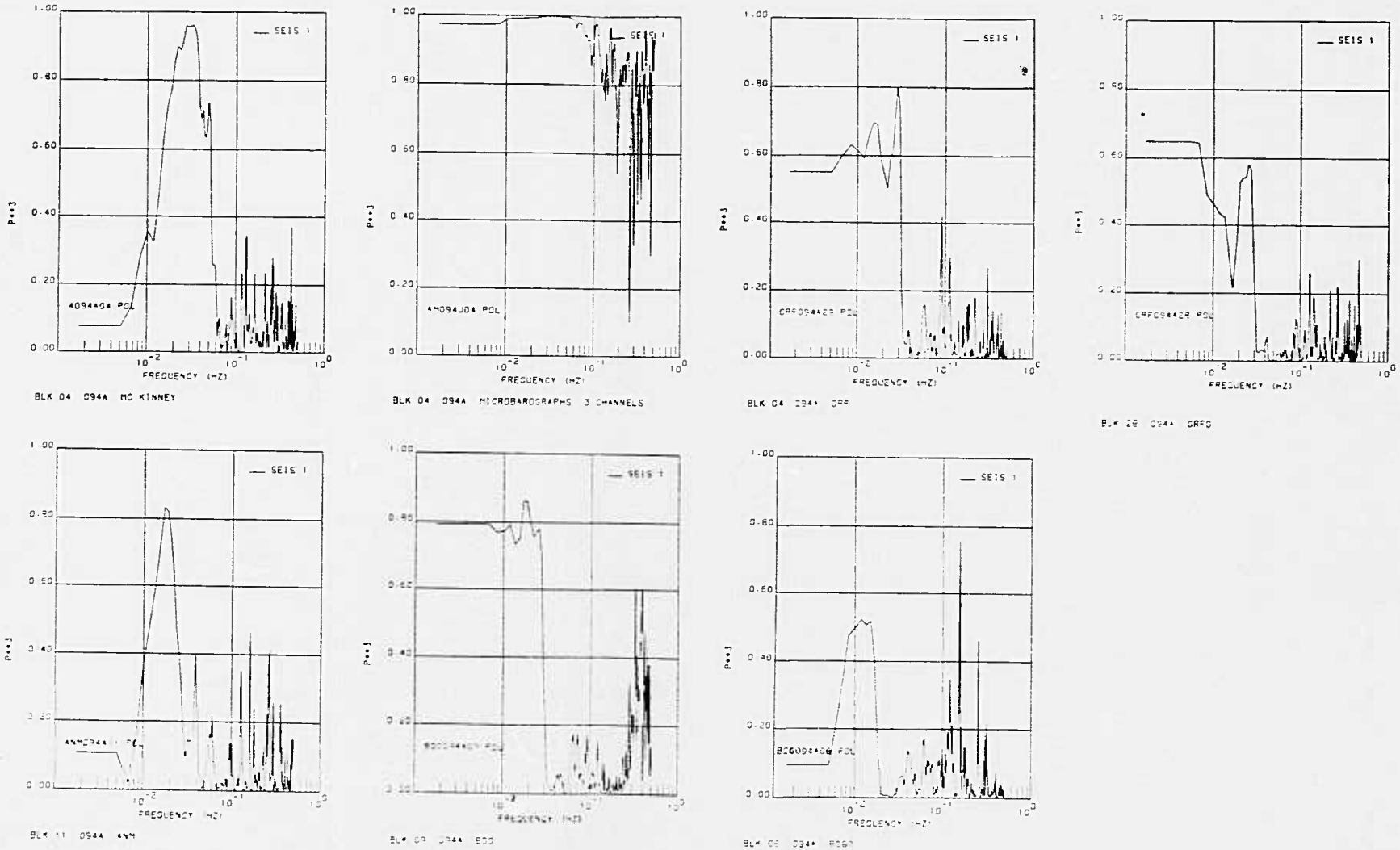

FIGURE 35. EL CHICHON ERUPTION 094A ORIGIN TIME ~ 02:00.
SEISMIC AND MICROBAROMETRIC PURE-STATE FILTERS (P^3) FOR SELECTED FILTER BLOCKS. McKINNEY ANMO, AND BOCO.

Results for the infrasonic event on day 94 with origin time about 11:16 (event 094B) are presented in figures 36 through 46. This eruptive sequence was large and complex with repeated injections into the plinian column. Envelope maxima, indicated by estimated peak origin times on the seismograms, are interpreted to be arrivals from individual explosions within the eruptive sequence. Group velocities for the maxima were computed from origin times of the individual explosions computed from maxima in the envelope of the direct Rayleigh wave. The complexity of this eruptive sequence is evident on the McKinney beamed microbarograms (figures 36 and 41). The sharp spikes on the unprocessd microbarogram (figure 36) result from noise glitches on MKB2 and should be ignored. Application of the pure-state filter to the McKinney seismic data (figure 41) revealed a linearly polarized, narrow-band wave train with a dominant period of about 33 seconds beginning approximately 15 minutes after the arrival of the initial gravity mode recorded on the microbarogram and continuing for more than an hour. Both the seismic and microbarometric data are highly polarized at a frequency of 0.03 Hz for the filter block beginning at 13:25:24 (figure 41). The state vector for the linearly polarized 0.03 Hz arrival is inclined approximately 10 degrees from vertical. The processed seismograms for ANMO (figure 42) show an elliptically polarized wave train lasting approximately 55 minutes. Viewed as a whole, the wave train is normally dispersed, with periods of 200 seconds to 60 seconds. No periods shorter than 50 seconds occur with significant amplitude within the wave train. The pure-state filter for the filter block beginning at 13:50:00 is shown in figure 46. At a period of 60 seconds, the plane of polarization strikes 170 degrees from the radial direction with a dip of 80 degrees. The BOCO processed seismograms (figure 43) show an elliptically polarized wave train lasting approximately 55 minutes. Envelope maxima, corresponding to individual explosions in the eruptive sequence, are better separated on the BOCO seismograms than on the ANMO seismograms. Periods at the maxima range from 60 seconds to 120 seconds. There is no evidence of a dispersed wave train. The pure-state filter for the filter block beginning at 14:04:29 is shown in figure 46. The plane of polarization for the 90-second arrival strikes 165 degrees relative to the radial direction with a dip of 85 degrees. The processed seismograms for GRFO (figure 44) show three distinct maxima within a wave train lasting approximately 55 minutes. The maxima are

interpreted to result from individual explosions within this eruptive sequence. The signal from the first explosion (peak 1121) has a linearly polarized component with a period of about 40 seconds and an elliptically polarized component with a period of about 70 seconds. The signal from the explosion with estimated origin time 11:43 is linearly polarized with a period of 60 seconds. The signal from the last explosion (peak 1205) shows both linear and elliptical polarization because the estimated ellipticity for the dominant period (65 seconds) was between 0.2 and 0.4. The pure-state filter for the filter block beginning at 20:40:30 is shown in figure 46. The state vector of the linearly polarized, 60-second arrival is oriented about 10 degrees from vertical with a trend of 270 degrees relative to the radial direction; therefore, this arrival may not be related to this El Chichon eruption. Results of adaptive beam forming applied separately to the vertical, radial, and transverse components of the seven-element NORSAR long-period array followed by pure-state filtering applied to the resulting three-component system are shown in figure 45. Although the recorded signals are extremely weak, processing of the NORSAR data appears to have detected a linearly polarized arrival, with a a period of 70 seconds, from the explosion with estimated origin time 11:43 of the eruptive sequence, and possibly detected an elliptically polarized arrival from the explosion with estimated origin time 12:05. The state vector for the linearly polarized arrival is oriented about 20 degrees from vertical with a trend of 24 degrees from the radial direction.

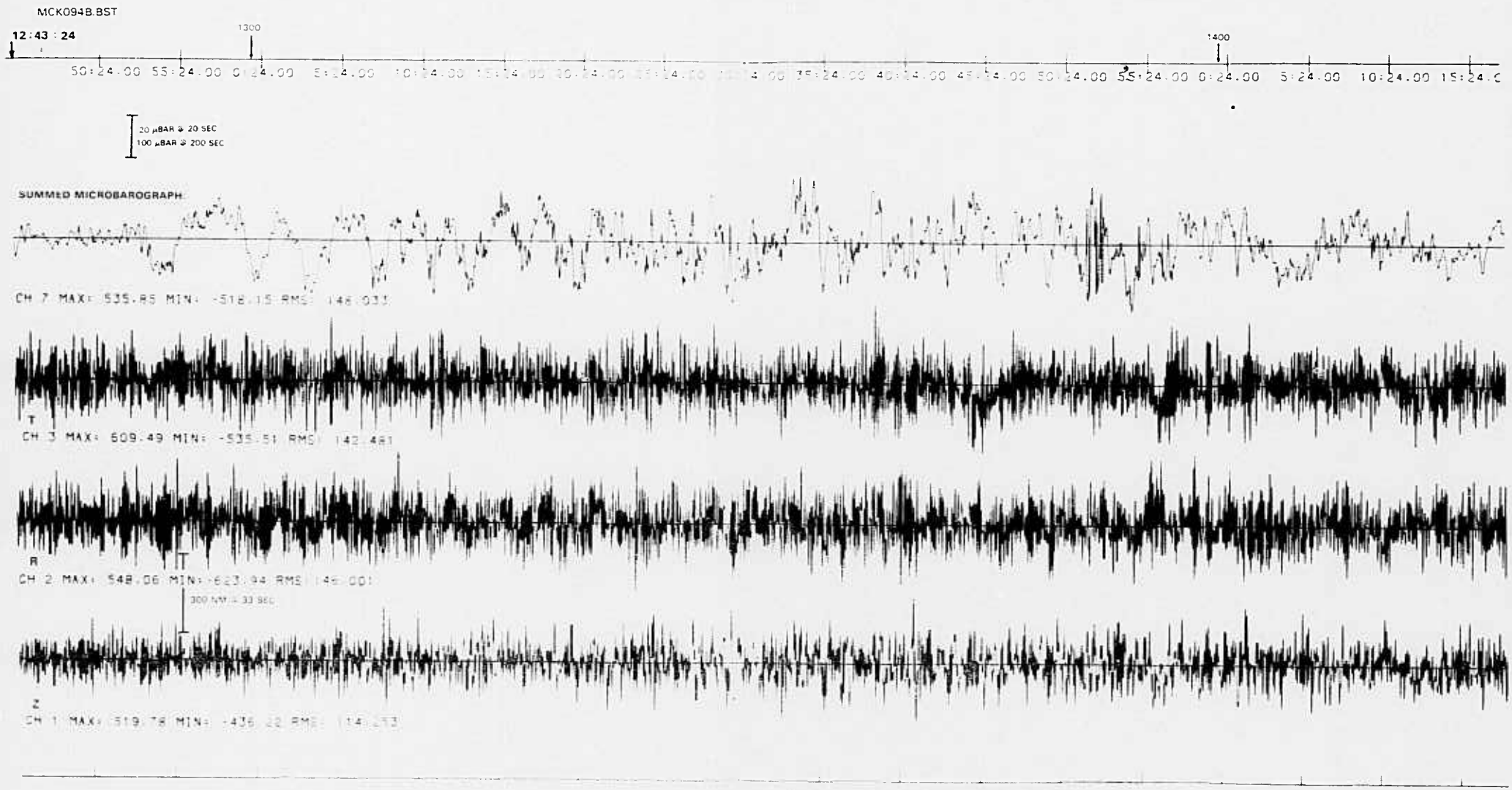

FIGURE 36 EL CHICHON ERUPTION 094B ORIGIN TIME ~ 11:22
THREE-COMPONENT INERTIAL SEISMOGRAMS AND MICROBAROGRAPH BEAM BEFORE PURE-STATE FILTERING.
RECORDED AT McKINNEY

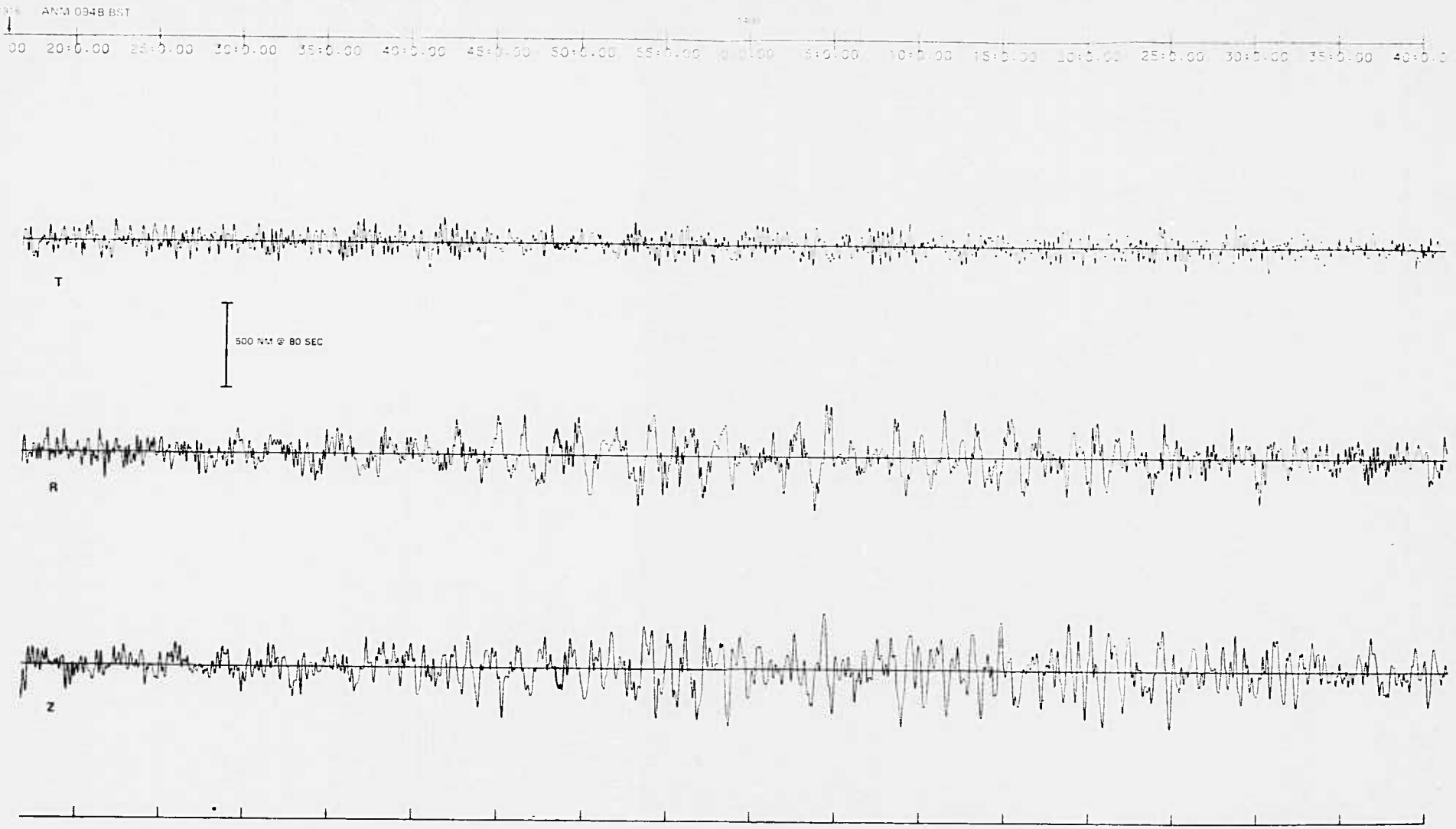

FIGURE 37. EL CHICHON ERUPTION 094B ORIGIN TIME ~ 11:22.
THREE-COMPONENT INERTIAL SEISMOGRAMS BEFORE PURE-STATE FILTERING. RECORDED AT ANMO.

3-81/82

TR 84-7

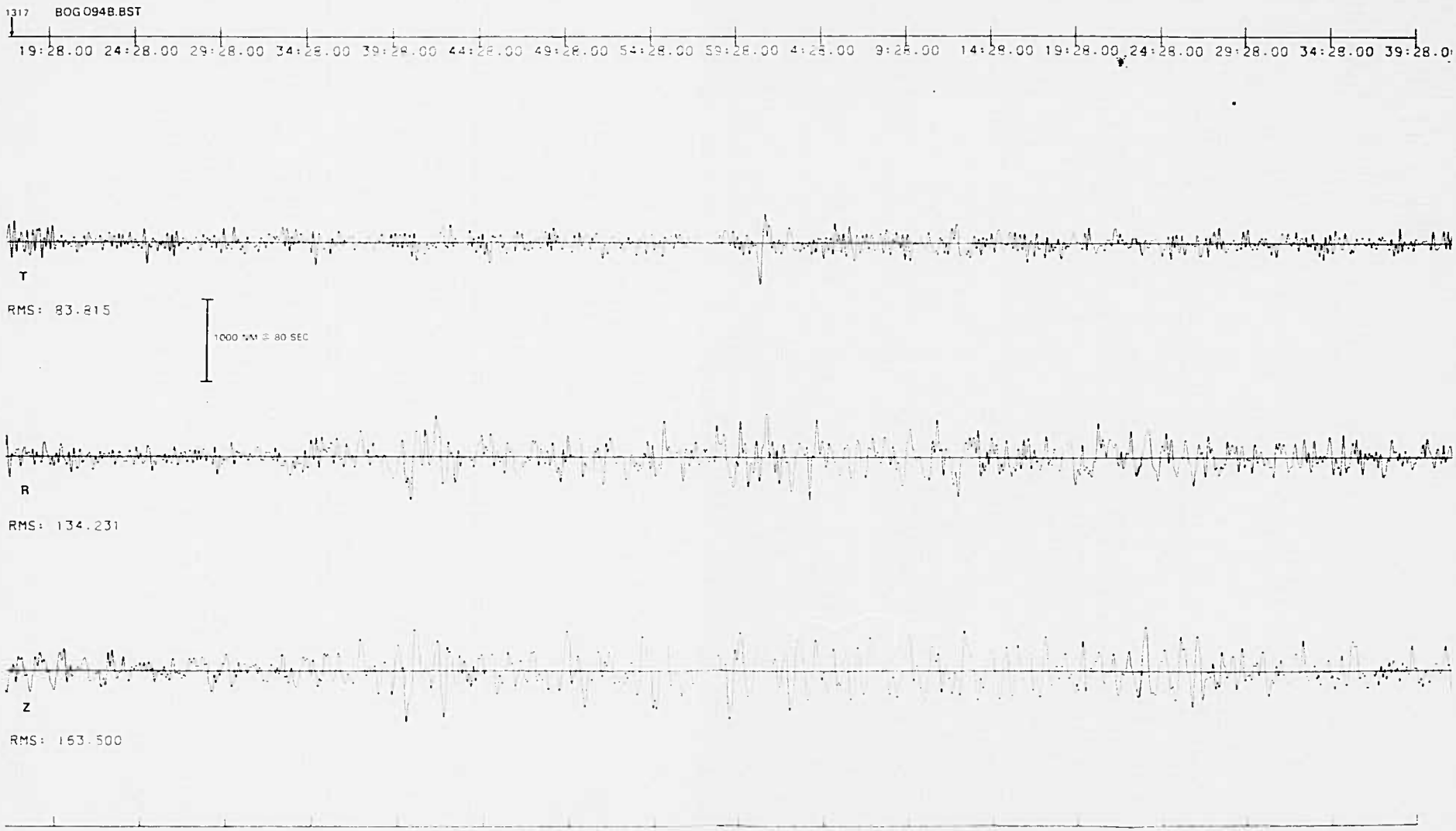

FIGURE 38. EL CHICHON ERUPTION 0948 ORIGIN TIME ~ 11:22
THREE-COMPONENT INERTIAL SEISMOGRAMS BEFORE PURE-STATE FILTERING, RECORDED AT BOCO

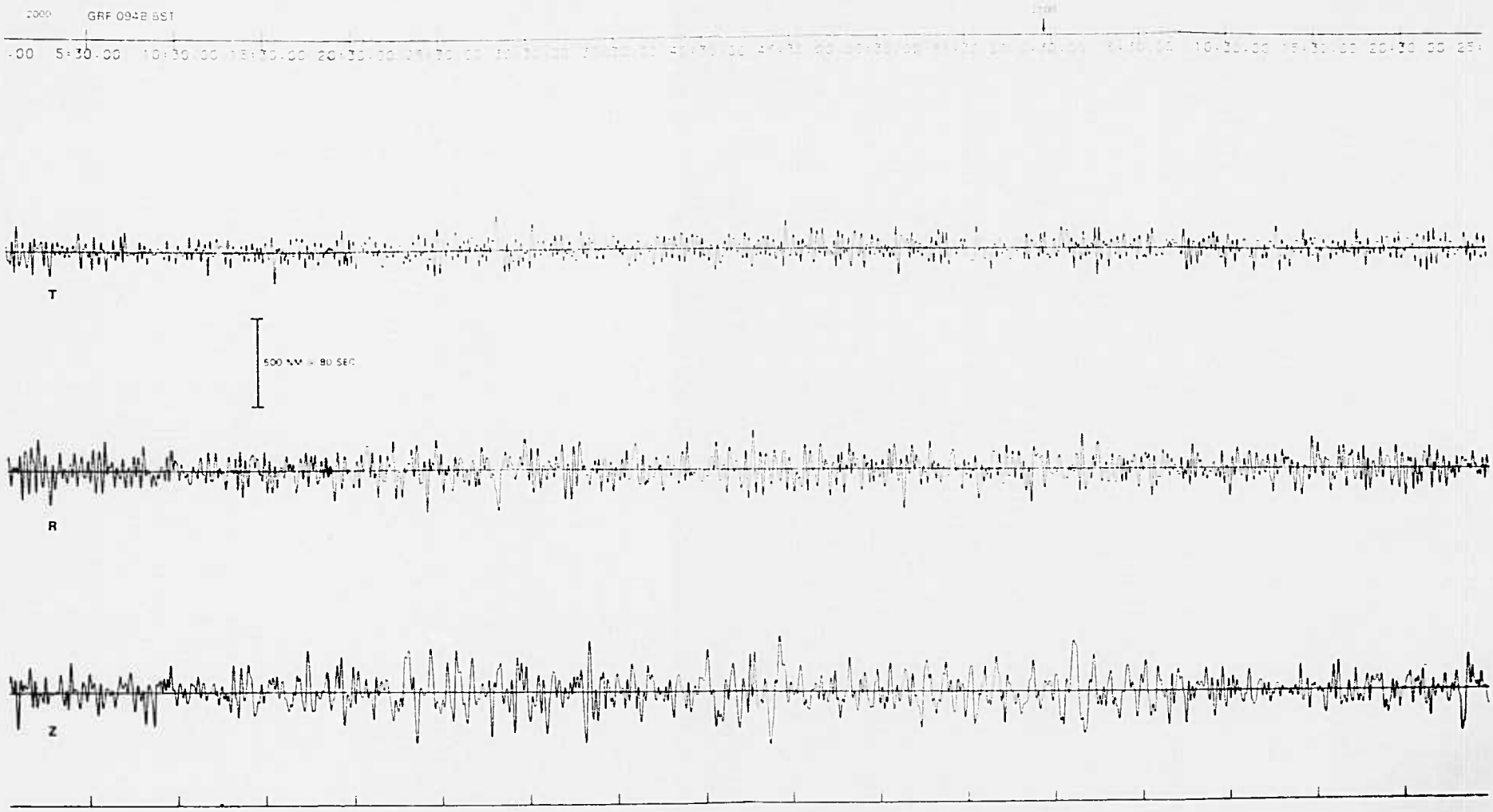

FIGURE 39. EL CHICHON ERUPTION 094B ORIGIN TIME ~ 11:22.
THREE-COMPONENT INERTIAL SEISMOGRAMS BEFORE PURE-STATE FILTERING. RECORDED AT GRFO.

3-85/86

TR 84-7

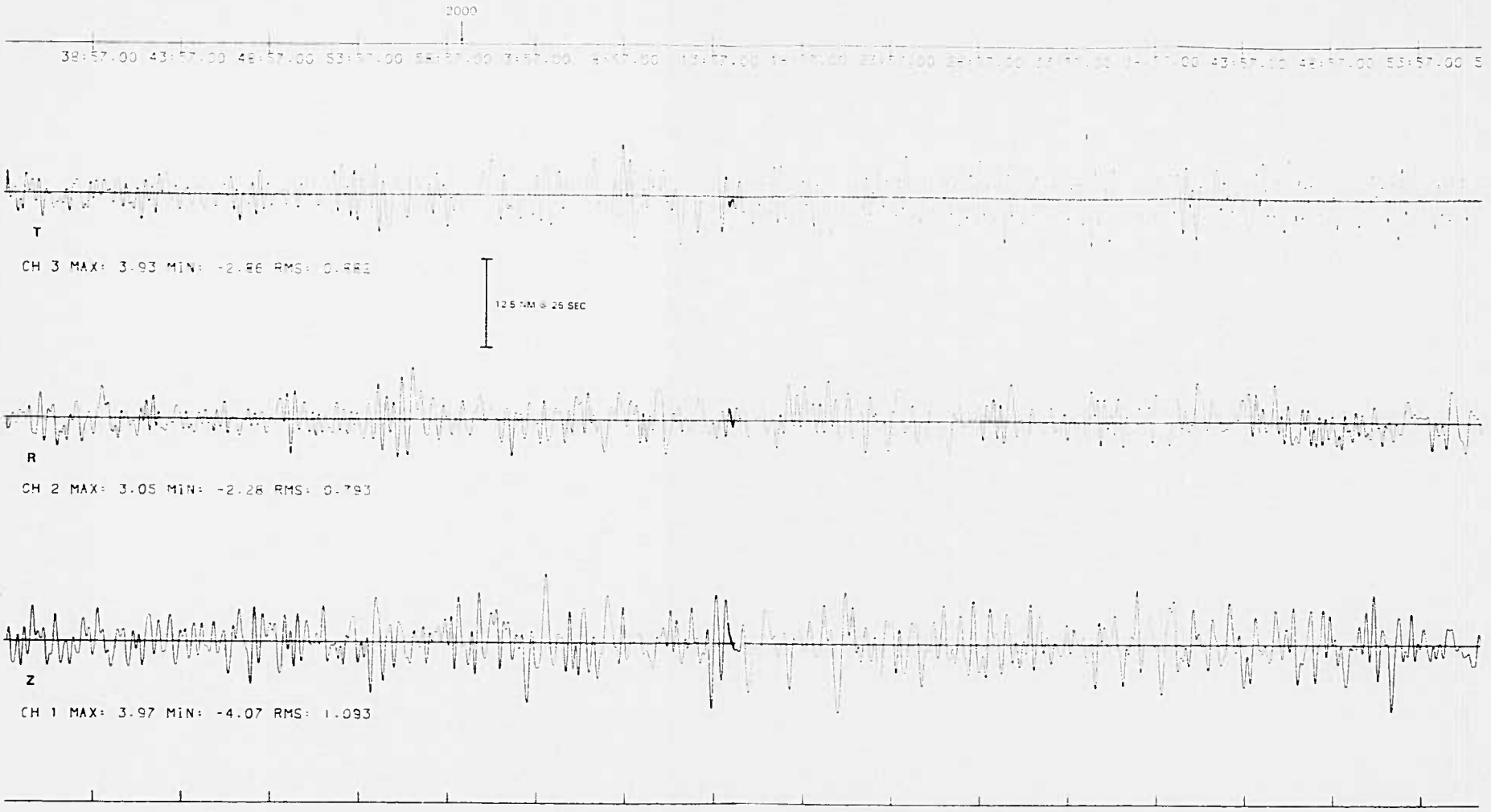

FIGURE 40 EL CHICHON ERUPTION 094B ORIGIN TIME ~ 11:22.
ADAPTIVE BEAM FORMING APPLIED SEPARATELY TO VERTICAL, RADIAL, AND TRANSVERSE COMPONENTS OF NORSAR THREE-COMPONENT, LONG-PERIOD ARRAY.

G1540

3-87/88

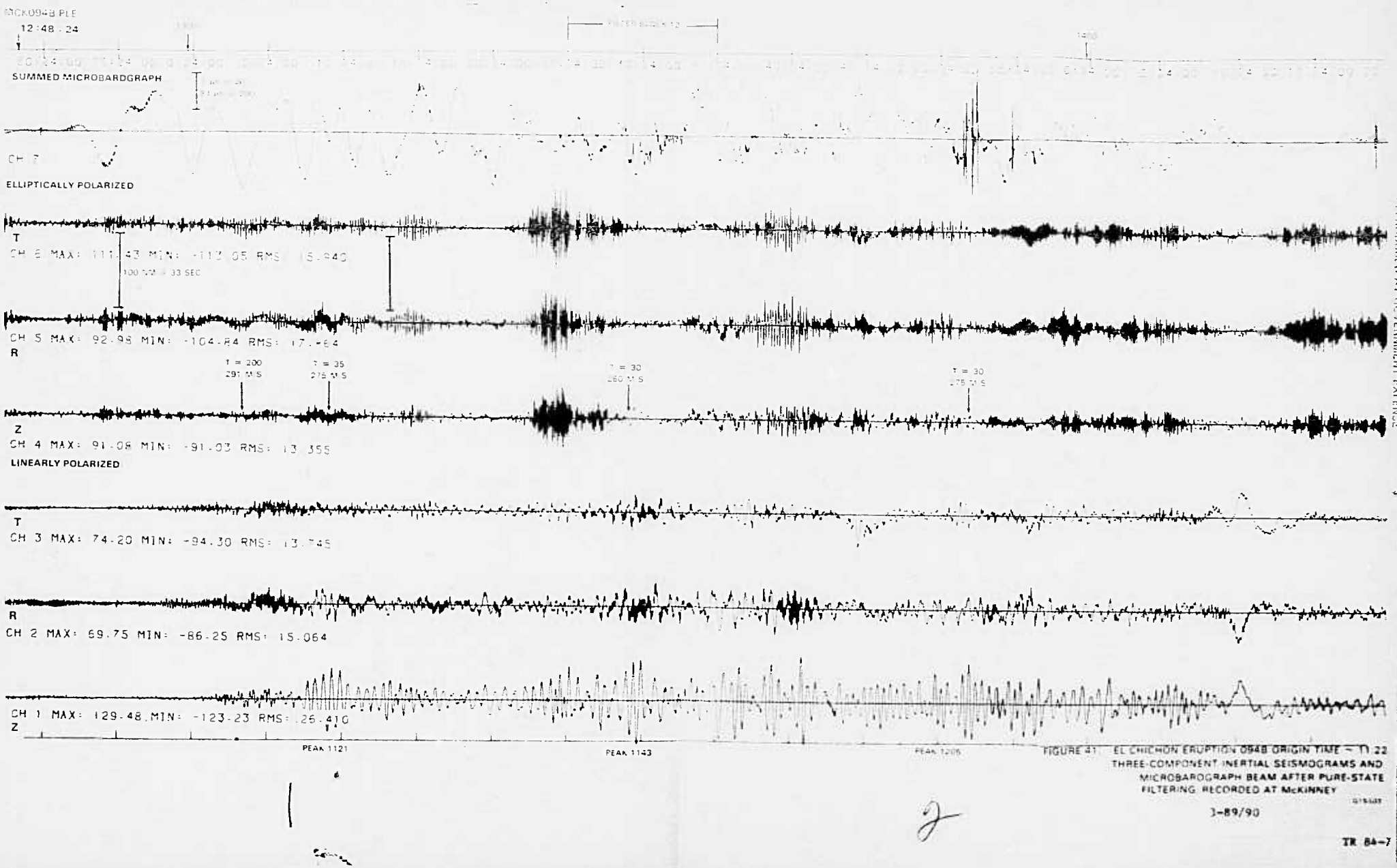

FIGURE 41. EL CHICHON ERUPTION 0948 ORIGIN TIME — 11.22
THREE-COMPONENT INERTIAL SEISMOGRAMS AND
MICROBAROGRAPH BEAM AFTER PURE-STATE
FILTERING. RECORDED AT McKINNEY

3-89/90

TR 84-7

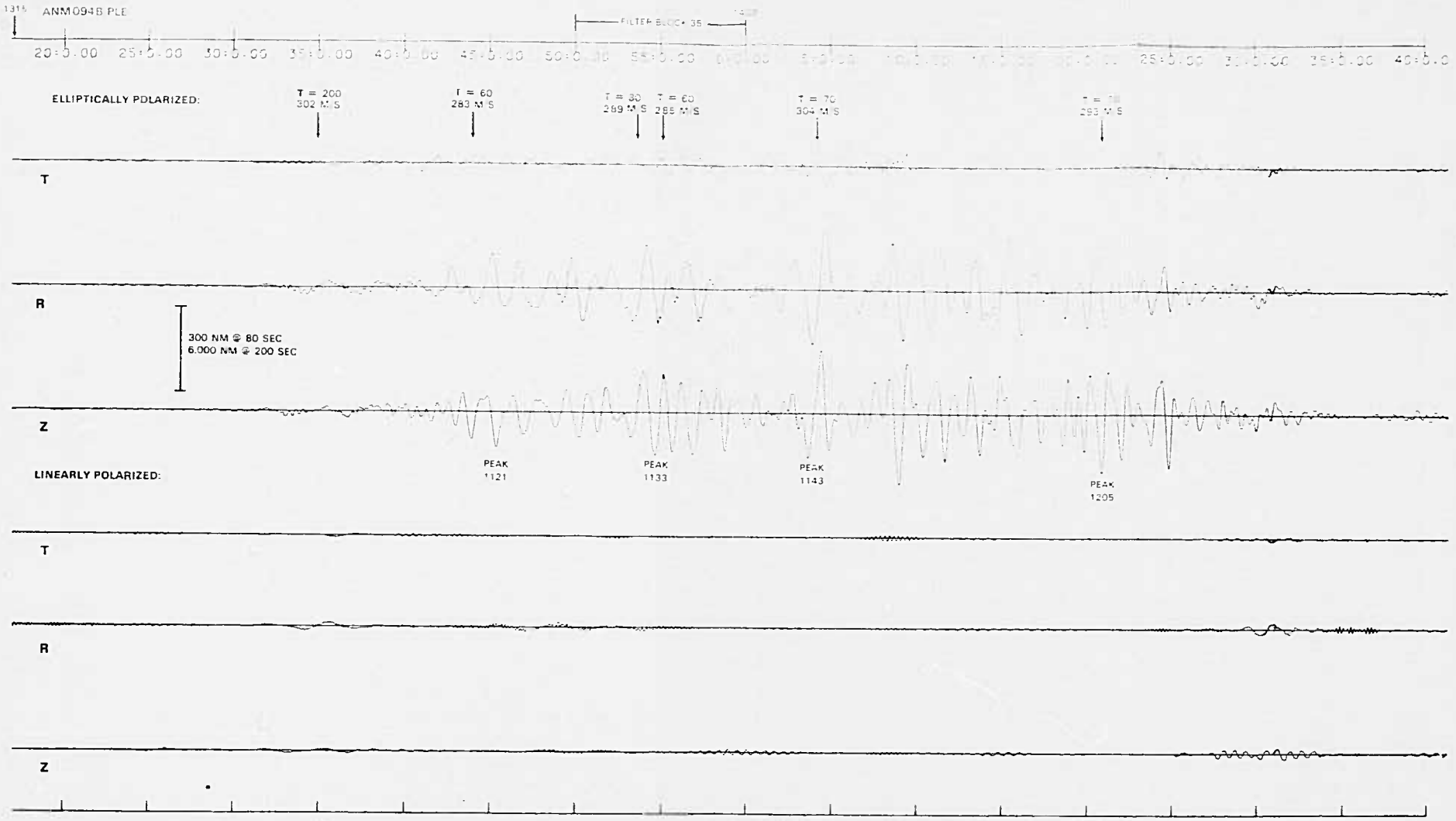

FIGURE 42. EL CHICHON ERUPTION 094B ORIGIN TIME ~ 11:22.
THREE-COMPONENT INERTIAL SEISMOGRAMS AFTER PURE-STATE FILTERING. RECORDED AT ANMO.

G15404

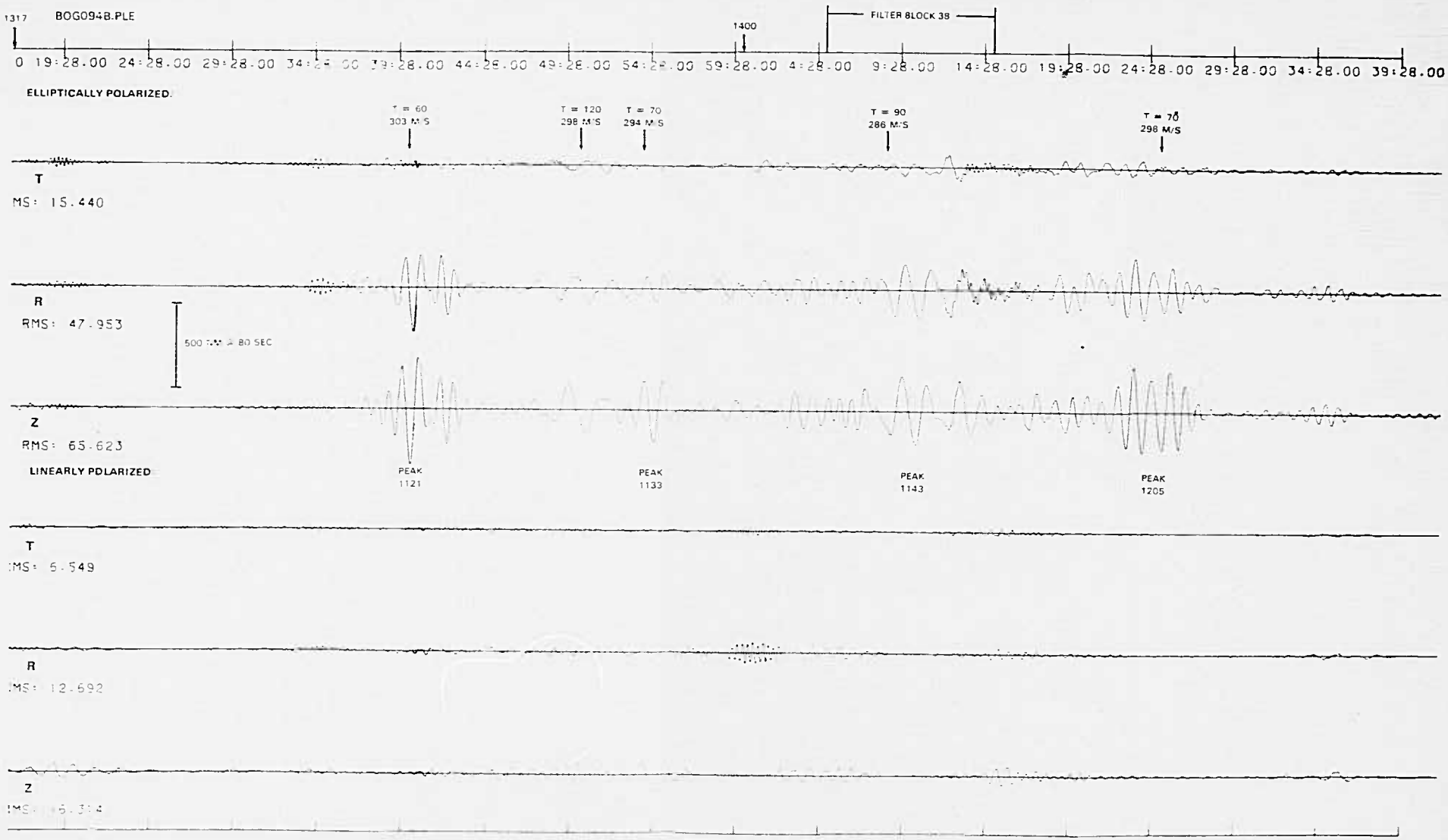

FIGURE 43 EL CHICHON ERUPTION 0948 ORIGIN TIME ~ 11:22.
THREE-COMPONENT INERTIAL SEISMOGRAMS AFTER PURE-STATE FILTERING. RECORDED AT BOCO.

3-93/94

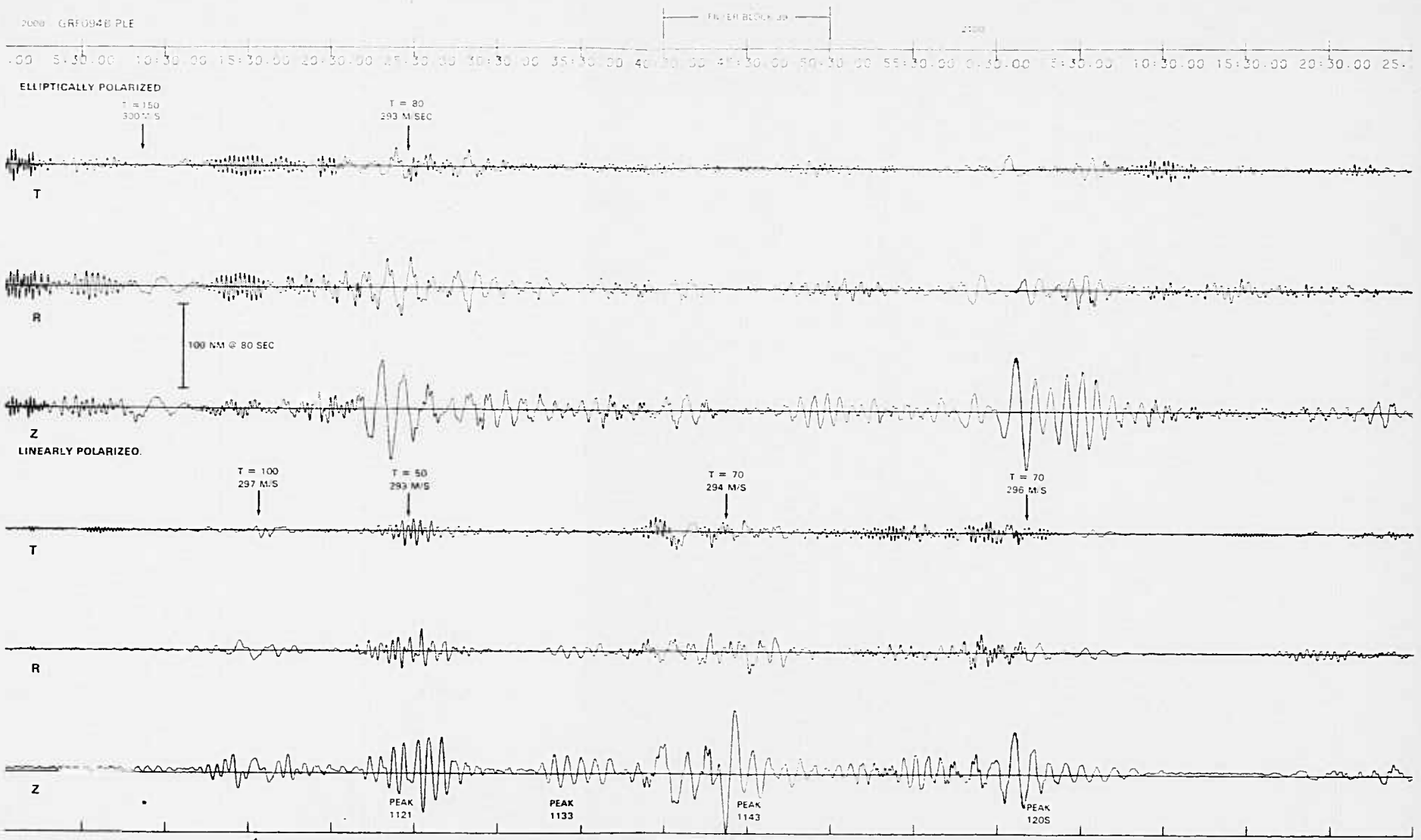

FIGURE 44. EL CHICHON ERUPTION 094B ORIGIN TIME ~ 11:22.
THREE-COMPONENT INERTIAL SEISMOGRAMS AFTER PURE-STATE FILTERING, RECORDED AT GRFO.

G15405

3-95/96

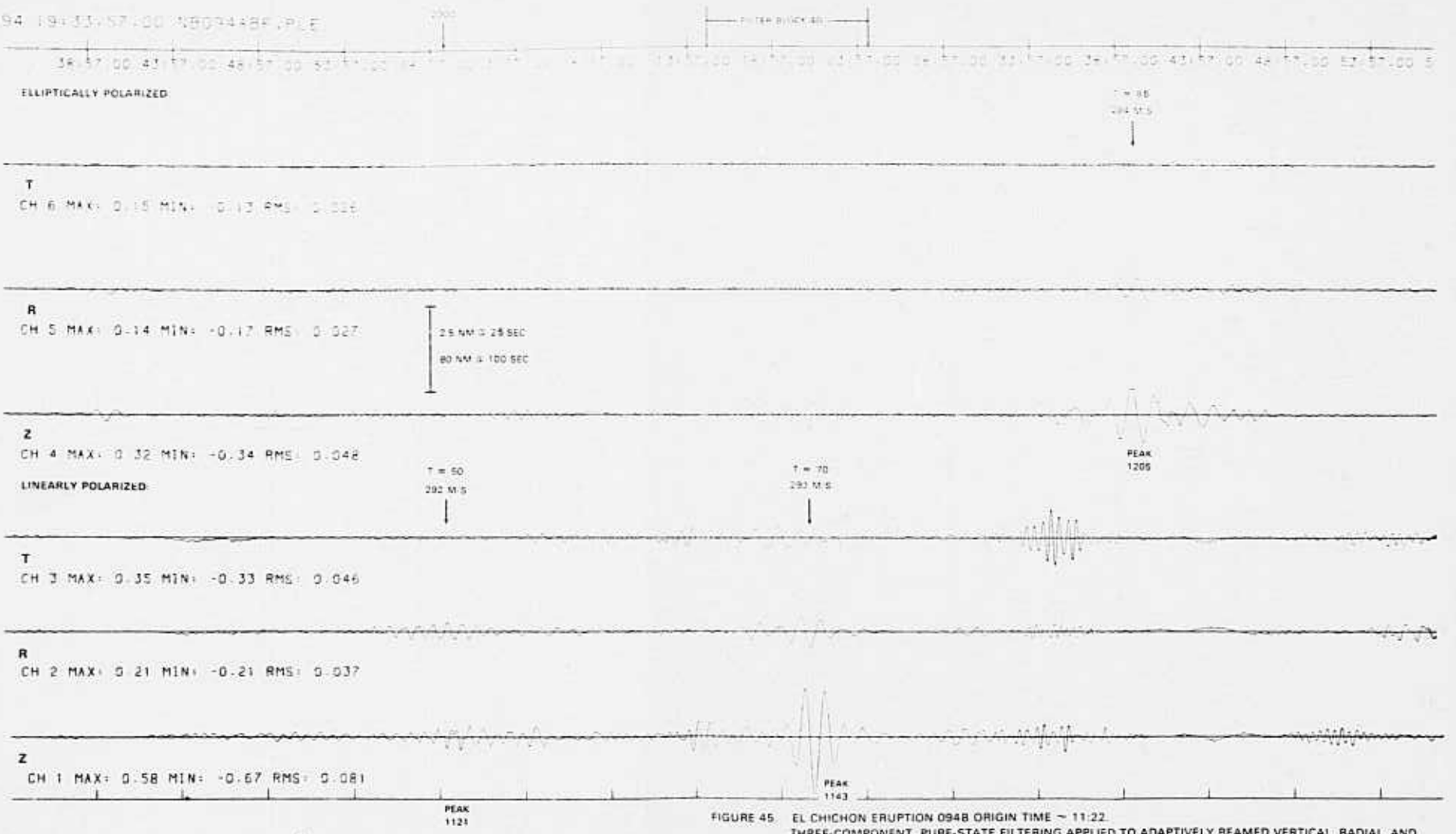

FIGURE 45 EL CHICHON ERUPTION 094B ORIGIN TIME ~ 11:22
THREE-COMPONENT, PURE-STATE FILTERING APPLIED TO ADAPTIVELY BEAMED VERTICAL, RADIAL, AND TRANSVERSE COMPONENTS OF NORSAR THREE-COMPONENT, LONG-PERIOD ARRAY.

G15406

3-97/98

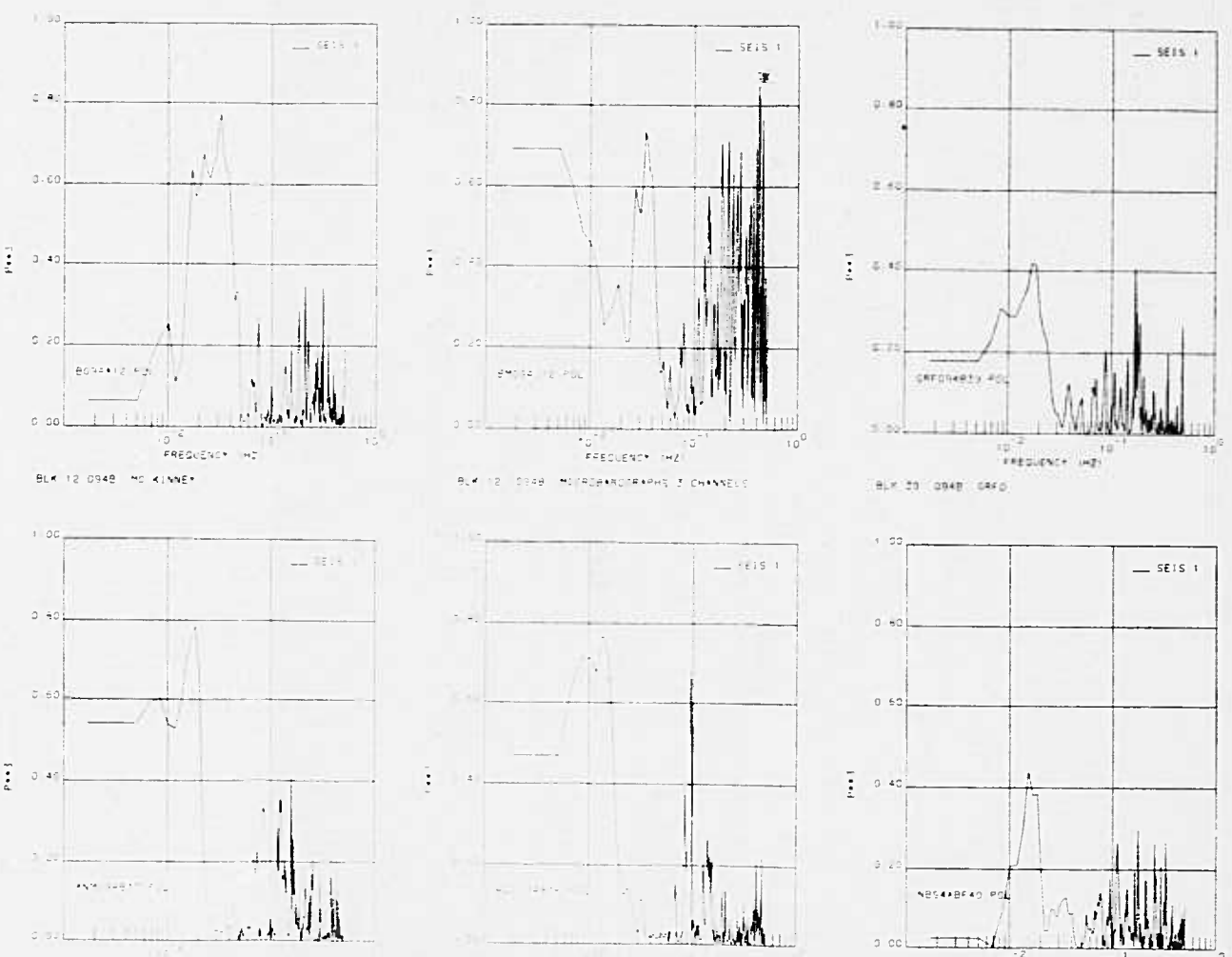

FIGURE 46. EL CHICHON ERUPTION 094B ORIGIN TIME ~ 11:22.
SEISMIC AND MICROBAROMETRIC PURE STATE FILTERS (P^3) FOR SELECTED FILTER BLOCKS. McKINNEY. ANMO. BOCO. GRFO. AND NORSAR.

Calculated group velocities of the observed infrasonic arrivals are shown as a function of period in figure 47, together with a theoretical atmospheric group velocity dispersion curve derived by Pfeffer and Zarichny (1963). The observed infrasonic group velocities range from 256 to 357 m/sec. Residuals of the observed group velocities from theoretical values ranged from -22 m/sec to +48 m/sec. A wind component parallel to the propagation direction could account for this variance and is a critical unknown in identifying specific acoustic modes. Wind velocity will vary with altitude and, hence, with frequency. The drift of ash from El Chichon on day 088 indicates average wind velocity in the middle troposphere was nearly 130 m/sec from the east, while in the upper troposphere it was 100 m/sec from the west. On day 094, the drift was 27 m/sec from the southwest at an unknown altitude. Clearly, without a much more complete model of wind velocity as a function of frequency, wind effects will necessarily contribute to residual errors in velocity calculations.

Fortunately, the two nearest SRO stations, ANMO and BOCO, are at roughly equal distance (21.8° vs 22.4°) and opposite azimuth (329° vs 121°) from El Chichon. One would expect residual velocities to be nearly equal and opposite at the two sites. In fact, just such a wind model was derived by averaging each site's residual velocities for each day of activity over two frequency bands (table 4). Note that residuals at GRFO and NORSAR were small (figure 47), indicating a cancelling of wind effects over a longer path. Corrected group velocities based on this model are shown in figure 48. The variance of the corrected data about the theoretical curves has been reduced substantially. It should be emphasized that this model is crude and highly speculative, but it illustrates that the parallel-to-propagation components of a reasonable wind model can account for much of the difference between observed and theoretical velocities.

The dispersion of acoustic waves is more complex than that of seismic surface waves because of phase velocity lows at 12 and 83 km altitude. The theoretical curve after Pfeffer and Zarichny (figure 47) illustrates this complexity. Velocity increases with period except for group velocity minima around 46 and 70 seconds. The observed infrasonic signals clearly do not have the appearance of deep, crustal surface waves, while they do have a complex

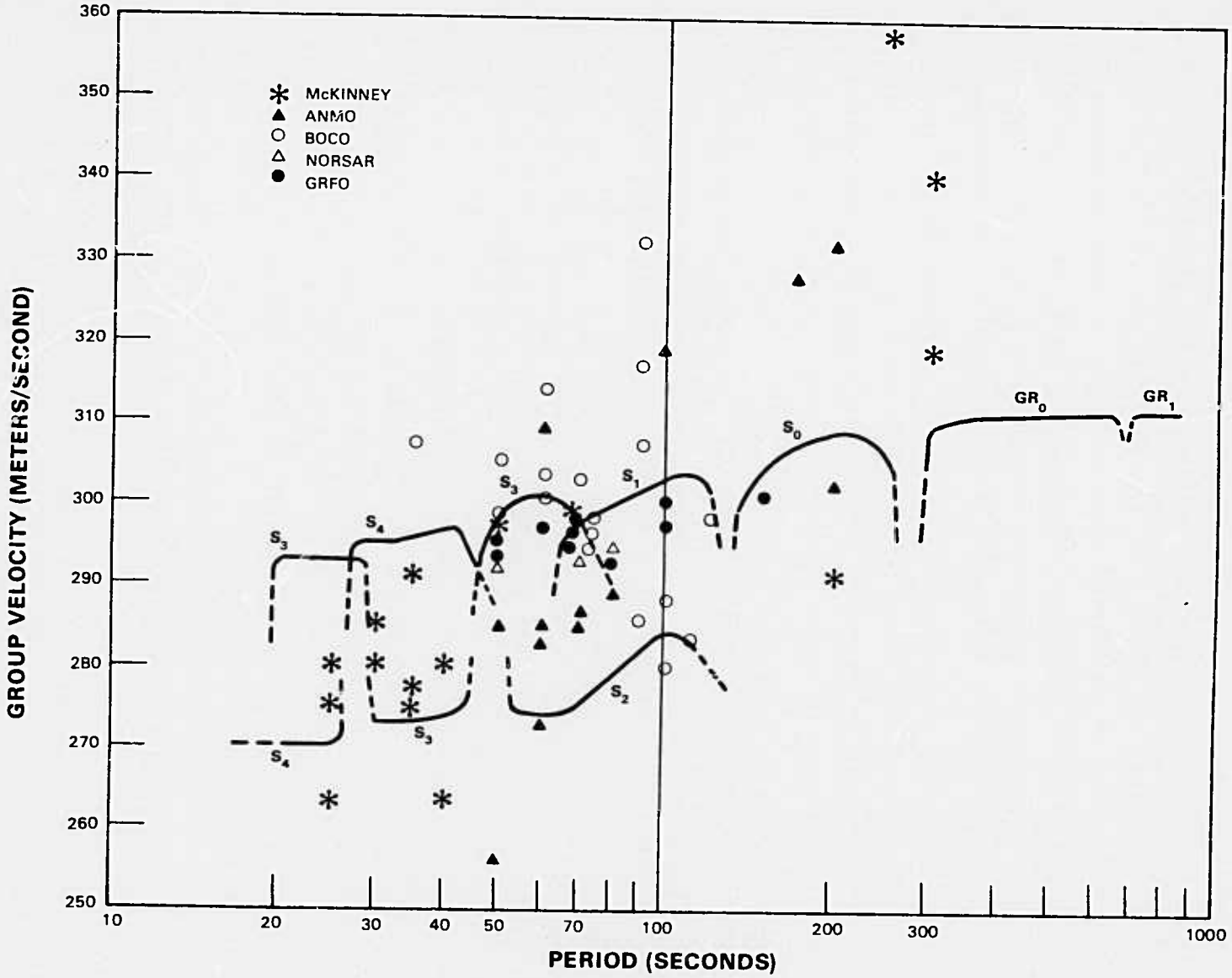

FIGURE 47. THEORETICAL ATMOSPHERIC GROUP VELOCITY DISPERSION CURVE, AFTER PFEFFER AND ZARICHNY (1963), WITH OBSERVED UNCORRECTED VELOCITIES SUPERIMPOSED.

G15363

TABLE 4. WIND MODEL DERIVED FROM MEAN GROUP VELOCITY ERRORS

		0-90 Second Period		100-300 Second Period	
		Mean Residual	Correction	Mean Residual	Correction
Day 088	ANMO	-13 m/s	+13 m/s	-	-
	BOCO	+12	-13	-	-
	McKinney	-18	+18	+48	-48
	Wind Model	18 m/s	180° Az	48 m/s	0° Az
Day 093	ANMO	-	-	+21	-21
	BOCO	+3	-3	-18	+18
	McKinney	+1	0	+20	-19
	Wind Model	4 m/s	90° Az	21 m/s	330° Az
Day 094	ANMO	-13	+13	-7	+17
	BOCO	+10	-10	+16	-16
	McKinney	-13	+13	-18	+18
	Wind Model	13 m/s	160° Az	18 m/s	170° Az
	GRFO and NORSAR	-3	+4	-4	+4
	Wind Model	4 m/s	180° Az	4 m/s	180° Az

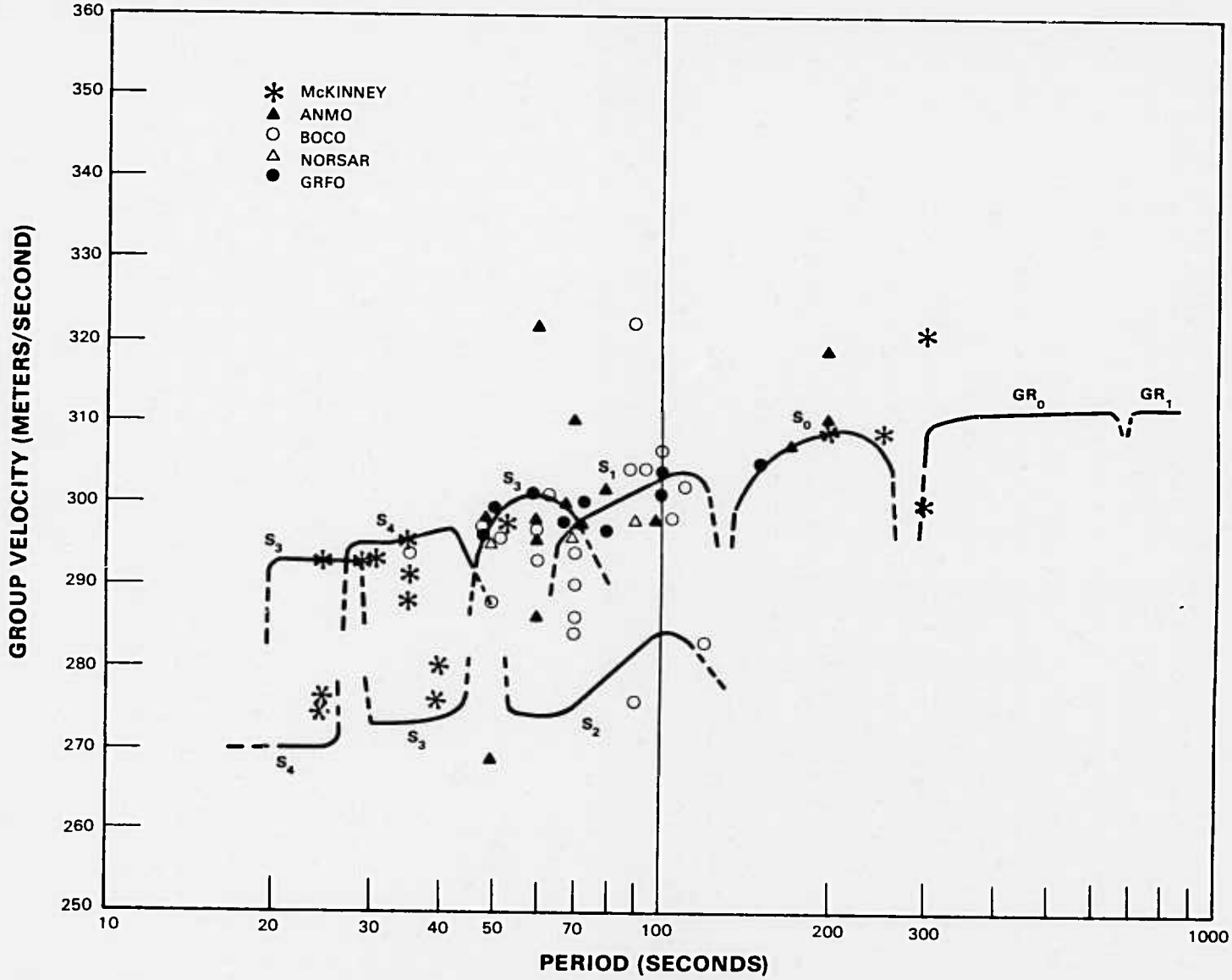

FIGURE 48. THEORETICAL ATMOSPHERIC GROUP VELOCITY, AFTER PFEFFER AND ZARICHNY (1963), WITH OBSERVED WIND-CORRECTED VELOCITIES SUPERIMPOSED.

G15364

dispersion. Accurate measuring of this dispersion was limited by the vector addition of unknown wind velocity and overlapping of dispersed signals from events closely spaced in time. Nevertheless, the velocities measured agree, within the uncertainty due to wind velocity, with theory for the modes and frequencies picked. The various modes observed include the gravity fundamental GR_0, the acoustic fundamental S_0, and four higher modes S_1, S_2, S_3 and S_4 (figure 48).

The character of the infrasonic signals seismically recorded at McKinney was quite different from the character of the infrasonic signals recorded at the SRO's. This difference presumably results from differences in the atmospheric pressure - ground displacement transfer functions at the various sites. For the McKinney data, the dominant feature of the processed seismograms for all five El Chichon events is a narrow-band arrival, with a period of approximately 30 seconds, that persists throughout the higher-mode acoustic arrivals as evidenced by the beamed microbarograms. For the more complex events (088 and 094B), this arrival persists throughout the infrasonic signal recorded by the microbarographs. This arrival is linearly polarized, with a near-vertical orientation of the state vector. The degree of polarization estimated for this arrival at 0.03 Hz was typically 0.75 to 0.98. For signal-free time intervals, the estimated degree of polarization for the same frequency was consistently less than 0.3. The frequency of this arrival falls on a null in the atmospheric pressure-horizontal ground displacement transfer function for the McKinney site (see figure 5, section 3.2), probably accounting for the lack of horizontal ground motion at this frequency. In contrast, the infrasonic signals recorded at the SRO's were of lower frequency, with no frequencies as great as 0.03 Hz. Although the SRO system response had a 6-second notch, the SRO and McKinney system responses were essentially identical for frequencies less than 0.07 Hz (see figure 4, section 3.2). State vector parameters estimated for selected filter blocks are summarized in table 5. The El Chichon infrasonic signals recorded at ANMO were all elliptically polarized, with ellipticities of 0.6-0.7. The infrasonic signals recorded at BOCO typically were composed of both linearly and elliptically polarized components, with ellipticities of 0.15-0.55. GRFO recorded both linearly and elliptically polarized infrasonic signals

TABLE 5. SUMMARY OF STATE VECTOR PARAMETER ESTIMATES

Event	Site	Filter Block Beginning at hr:min:sec	T Second	P^3	Ellipticity	Trend Degrees	Plunge Degrees	Strike Degrees	Dip Degrees	Motion
088	McKinney	07:35:28	30	0.80	0.05	350	15			
	ANMO	08:05:00	60	0.45	0.70			160	80	Retrograde
	BOCO	08:00:00	60	0.85	0.45			10	80	Retrograde
	BOCO	08:00:00	35	0.80	0.20	330	10			
093A	McKinney	10:25:20	33	0.45	0.10	10	10			
	ANMO	10:43:30	no detection							
	BOCO	10:58:30	70	0.77	0.20	345	25			
	BOCO	11:03:30	90	0.65	0.30	345	22	10	80	Retrograde
093B	McKinney	11:45:20	30	0.67	0.20	45	15			
	McKinney	11:45:20	12	0.70	0.70			165	90	Prograde
	ANMO	10:43:30	no detection							
	BOCO	10:58:30	60	0.77	0.15	20	10			
	BOCO	11:03:30	90	0.33	0.35	330	20	20	75	Retrograde
094A	McKinney	03:48:48	33	0.95	0.20	0	15			
	ANMO	04:24:30	50	0.82	0.60			170	80	Retrograde
	BOCO	03:59:30	90	0.50	0.12	310	15			
	BOCO	04:14:30	50	0.85	0.40			15	65	Retrograde
	GRFO	10:46:30	100	0.50	0.50			175	80	Retrograde
	GRFO	10:51:30	45	0.70	0.10	280	5			
094B	McKinney	13:25:24	33	0.77	0.20	350	10			
	ANMO	13:50:00	60	0.78	0.70			170	80	Retrograde
	BOCO	14:04:29	90	0.75	0.55			165	85	Retrograde
	GRFO	20:40:30	60	0.40	0.10	270	10			
	NORSOR	20:15:12	70	0.40	0.20	24	20			

from the two eruptions on day 094, with ellipticities of 0.1-0.5. The dispersion of the infrasonic signals observed at the SRO's was complex, not at all similar to seismic surface-wave dispersion. This signal character, together with arrival time differences at stations of the SRO network, should be sufficient to discriminate infrasonic signals from seismic surface-wave signals.

Several approximations can be used to arrive at orders of magnitude for the expected peak pressure and earth displacement at the stations due to El Chichon eruptions 088 and 094B, and the MARSA explosions. Mauk, et al (1982) estimated the energy release for these two El Chichon eruptions based on maximum cloud height as 1.5×10^{23} ergs = 3600 kt. Ericsson (1962) gives the empirical relation $\Delta p = C\ W^{1/3}/R$ where Δp is peak excess pressure in μbar, C is a constant, W is yield in kt and R is source distance in 1000's of km. Average values of C are 4 upwind and 10 downwind for acoustics. So, at McKinney, Δp = 32-81 μbar depending on wind direction. Observed peaks were 55 and 45 μbar for events 088 and 094B respectively, in good agreement with theory. However, Ericsson also predicts period $T = 2.8\ W^{1/3}$ = 43 sec, while observed dominant periods are 150-700 seconds. Sorrell's and Goforth's (1973) transfer function for McKinney is 11.5 at 43 second period. So, predicted displacements are 368-931 nm at 43 seconds. Observed peak displacement for event 088 is 590 nm at 250 seconds.

If the McKinney transfer function is used for ANMO and BOCO, predicted displacements are about 250-650 nm depending on wind direction. Observed peaks at BOCO are 350 and 325 nm at 60 seconds for events 088 and 094B. At ANMO, event 088 has a peak of 120 nm at 200 seconds, and event 094B has a peak of 470 nm at 200 seconds. The NORSAR predicted range was 70-176 nm. The observed amplitude peak was 110 nm at 170 seconds for event 094B. In each case, amplitude predictions are quite good, but dominant periods are longer than predicted for an atmospheric explosion, which is not surprising.

The largest MARSA events were described as having magnitude M = 5. Based on Herrin (1968), yield may be estimated as $E = 10^{(1.1\ m_b - 4.06)}$ ergs. If the MARSA magnitude is m_b, $E = 1.3 \times 10^{21}$ ergs = 31 kt; then at NORSAR, Δp would be 1.4-3.5 μbar, and period would be about 9 seconds. Using the McKinney transfer function again, peak earth displacements at 9-second period would be 9-21 nm, depending on wind direction. Even if actual periods are much longer than 9 seconds, it can readily be seen why no infrasonic signals from the MARSA explosions were observed at NORSAR.

3.4.2 SNR Enhancement

Signal-to-noise ratios (SNR's) of the infrasonic signals seismically recorded at the different sites are presented in table 6. Because the unprocessed McKinney data were dominated by 6-8 second microseisms, whereas the SRO system response had a 6-second notch, a low-pass filter was applied to the McKinney data before estimating the SNR's. Without the low-pass filtering, signals from only two events (094A and 094B) were at all discernable in the unprocessd McKinney data. None of the events were detectable in the unprocessed NORSAR long-period array data. Application of a pure-state filter, either to individual three-component elements of the array or to the seven vertical elements of the array, failed to detect a signal from any of the five El Chichon eruptions. Application of adaptive beam forming separately to the vertical, radial, and transverse components of the array, followed by pure-state filtering applied to the resulting three-component system, marginally detected the large event on day 094 (094B). Because of the surface installation of the NORSAR long-period array, ambient noise levels were high, particularly on the horizontal components. High noise levels, together with the relatively low gain of the NORSAR seismographs (22 dB below the gain of the SRO seismographs at 0.04 Hz) probably account for the poor results obtained from the NORSAR data. For the McKinney and SRO data, the El Chichon events were undetectable or marginally detectable in the unprocessed data, and clearly detectable after pure-state filtering, except that ANMO failed to detect the two weak events on day 093. The average gain in SNR achieved by pure-state filtering was 14 dB.

TABLE 6. INFRASONIC SIGNAL-TO-NOISE RATIOS BEFORE AND AFTER PURE-STATE FILTERING

Site		Event 088	093A	093B	094A	094B
McKinney	unprocessed	4	3	3	3	3
	processed	30	8	20	25	7
ANMO	unprocessed	2	0	0	3	3
	processed	4	0	0	30	10
BOCO	unprocessed	2.5	1.5	1.5	3	2
	processed	10	12	10	15	15
GRFO	unprocessed				3	2
	processed				14	20
NORSAR	unprocessed					0
	processed					1.5

A four-hour sample of wind-induced noise recorded by the microbarograph array at McKinney was processed with the ten-minute, sliding pure-state filter. Wind speed varied from 2 to 28 mph during this interval, with a mean wind speed of 13 mph. No infrasonic or seismic signals were present in this sample. Microbarograms, both without and with the pure-state filter applied, are shown in figure 49 for a segment of this noise sample. For clarity, the processed microbarograms are displayed at a scale three times that of the unprocessed microbarograms. Summation of the four unprocessed microbarograms attenuated the noise 6 dB relative to the individual microbarograms. The pure-state filter was highly effective in attenuating the wind noise recorded by the microbarograph array. Wind noise recorded by individual microbarographs was attenuated an average of 22 dB. Summation of the processed microbarograms resulted in an additional 5 dB noise attenuation.

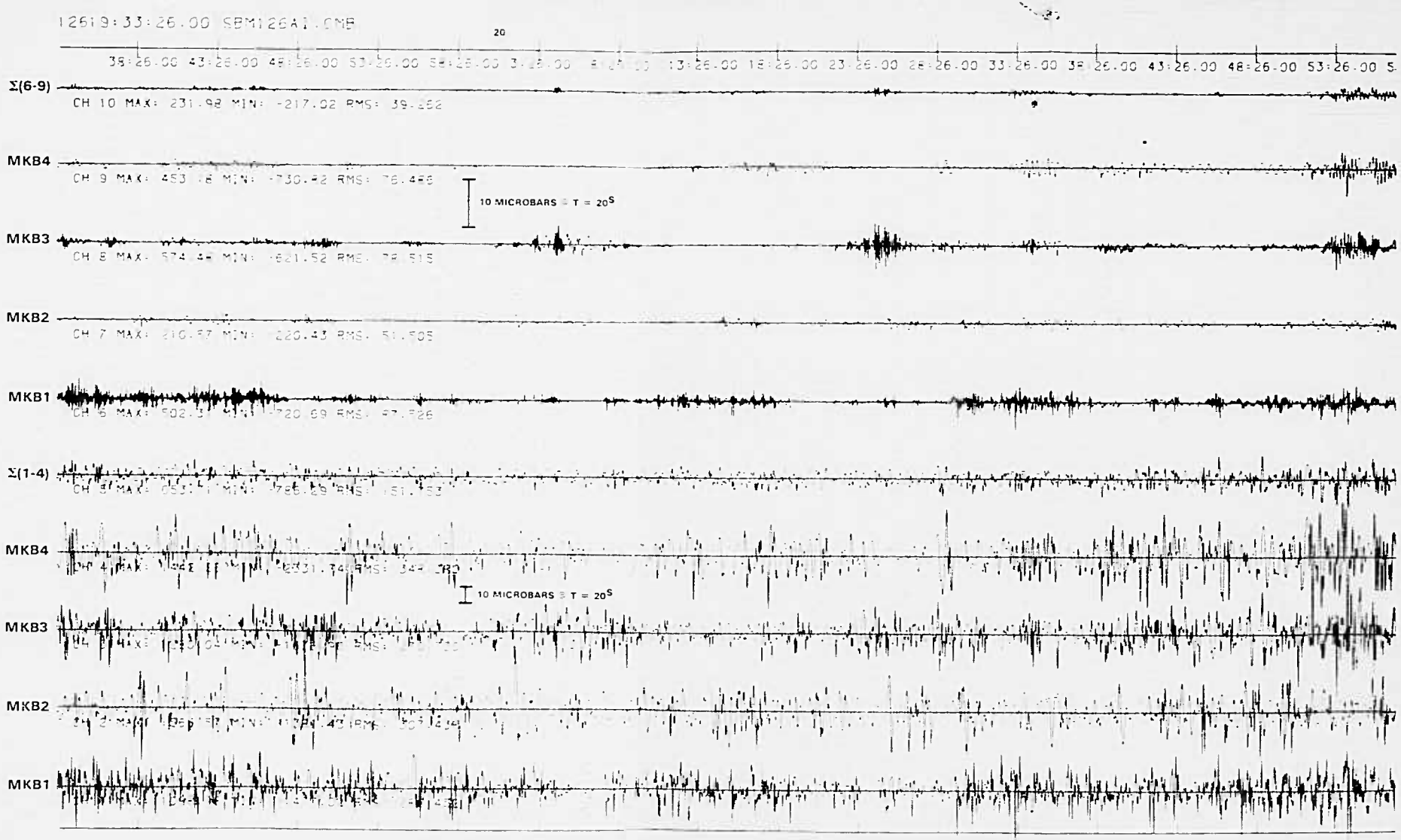

FIGURE 49. WIND NOISE SAMPLE WIND SPEED 2-28 MPH, AVG. 13 MPH MICROBAROGRAMS AND SUMMATION BEFORE AND AFTER PURE STATE FILTERING RECORDED AT McKINNEY, TEXAS

3-113/114

TR 84-7

4. CONCLUSIONS AND RECOMMENDATIONS

The sliding, pure-state filter was highly effective in attenuating wind-induced pressure variations recorded by the microbarograph array.

The sliding, pure-state filter improved the SNR of seismically recorded infrasonic signals at McKinney and the SRO's an average of 14 dB. The character of the infrasonic signals varied significantly among the sites, probably because of differences in atmospheric pressure-ground displacement transfer functions at the different sites.

Oceanic microseisms (0.05-0.25 Hz) at McKinney are mostly elliptically polarized. A noise conditioning technique designed to eliminate polarized noise from the spectral matrix before estimating the degree of polarization was ineffective because of nonstationarity of the microseismic noise.

The observed character of seismically recorded infrasonic signals, after pure-state filtering, together with arrival time differences at stations of the SRO network, should be sufficient to discriminate infrasonic signals from seismic surface-wave signals. To assure accurate interpretation of seismically observed infrasonic signals, atmospheric pressure-ground displacement transfer functions should be determined for each SRO.

5. REFERENCES

Ericsson, V., 1962, Microbarograph waves from nuclear explosions: Ntl. Bur. Stnd. translation from Kosmos, Vol. 40, p.. 187-208.

Frost, O. L. III, 1972, An algorithm for linearly constrained adaptive array processing: Proc. IEEE, Vol. 60, No. 8, p. 926-935.

Herrin, E., 1968, Seismic methods for monitoring underground explosions, Chapter 3, David Davies, Ed.: Stockholm, Sweden, International Inst. for Peace and Conflict Res., p. 82-85.

Mauk, F.J., Sorrells, G.G., Grant, L., and Taylor, K.B., 1982, Seismic methods of infrasonic signal detection, annual report no. 1; TR 82-5, Garland, TX, Teledyne Geotech, 141p.

Pfeffer, R. L, and Zarichny, J., 1963, Acoustic-gravity wave propagation in an atmosphere with two sound channels: Geofisica Pura E Applicata-Milano, Vol. 55, p. 175-199.

Sorrells, G.G., and Goforth, T.T., 1973, Low-frequency earth motion generated by slowly propagating partially organized pressure fields; Bull. Seis. Soc. Amer., Vol. 63, No. 5, p. 1583-1601.

Samson, J.C., and Olson, J.V., 1981, Data-adaptive polarization filters for multichannel geophysical data; Geophysics, Vol. 46, No. 10, p. 1423-1431.

Samson, J.C., and Olson, J.V., 1980, Some comments on the descriptions of the polarization states of waves; Geophys. J.R. Astr. Soc., Vol. 61, p. 115-129.

Sampson, J. C., 1983a, Pure states, polarized waves, and principal components in the spectra of multiple, geophysical time-series; Geophy. J. R. Astr. Soc., Vol. 72, p. 647-664.

Samson, J.C., 1983b, The reduction of sample-bias in polarization estimators for multichannel geophysical data with anisotropic noise; Geophys. J.R. Astr. Soc., Vol. 75, p. 289-308.

Swanson, J. G., 1984, Seismic observation of infrasonic signals, Semi-Annual Technical Report; TR 84-4, Garland, TX, Teledyne Geotech.

END